DEVELOPMENT OF A GAS TURBINE PERFORMANCE SOFTWARE INCLUDING SUB-IDLE REGION AND STARTING PROCESS

RÖLANTİ ALTI BÖLGESİNİ VE BAŞLATMA SAFHASINI KAPSAYAN BİR GAZ TÜRBİNİ PERFORMANS YAZILIMININ GELİŞTİRİLMESİ

BURAK ORHAN GÜNAY

ASSOC. PROF. DR. ÖZGÜR EKİCİ

Supervisor

Submitted to

Graduate School of Science and Engineering of Hacettepe University

as a Partial Fulfillment to the Requirements

for the Award of the Degree of Master of Science

in Mechanical Engineering

June 2022

ABSTRACT

DEVELOPMENT OF A GAS TURBINE PERFORMANCE SOFTWARE INCLUDING SUB-IDLE REGION AND STARTING PROCESS

Burak Orhan GÜNAY

Master of Science , Mechanical Engineering

Supervisor: Assoc. Prof. Dr. Özgür EKİCİ

June 2022, 109 pages

This study aims to develop a computer software to mathematically model a gas turbine engine's design point, steady state off-design and starting phases. Having a computer simulation software is crucial for a engine development project in terms of budget and schedule. In this scope, a component matching based performance code has been developed. Above-idle code results are validated by comparing with commercially available GasTurb13 results. Additionally, by using engine information found open literature, another performance model is created for T700-GE-700 turboshaft engine and results are validated by comparing the code results and open literature data.

For engine starting modeling, sub-idle component performance characteristics are required. Generally, physics based sub-idle performance models cannot be created since computational fluid dynamics solvers and component test rigs cannot produce reliable results for this particular region. Optimisation studies for starting process like fuel scheduling or controlling the maximum temperatures in internal stations are widely performed by the help of engine tests due to the absence of the performance model. In this thesis study, sub-idle performance characteristics are estimated by extrapolating the well-known above-idle characteristics

towards zero-speed point. Additionally, by taking the starter torque-speed characteristic from open literature, a sample starting model was created for T700-GE-700 turboshaft engine. By comparing the obtained results with open literature found engine starting data, it is observed that the map extrapolation method produces very realistic outputs even it has lots of uncertainties.

Keywords: Gas Turbine Engines, Component Matching, Engine Starting, Sub-Idle, Extension

ÖZET

RÖLANTİ ALTI BÖLGESİNİ VE BAŞLATMA SAFHASINI KAPSAYAN BİR GAZ TÜRBİNİ PERFORMANS YAZILIMININ GELİŞTİRİLMESİ

Burak Orhan GÜNAY

Yüksek Lisans, Makina Mühendisliği

Danışman: Assoc. Prof. Dr. Özgür EKİCİ

Haziran 2022, 109 sayfa

Bu çalışma; bir gaz türbini motorunun tasarım noktası, tasarım noktası dışı durağan çalışma noktaları, geçici hal ve başlatma safhalarının matematiksel olarak modellenebileceği bir bilgisayar programı geliştirmeyi amaçlamaktadır. Bir motor geliştirme projesi için, bütçe ve takvim bakımından bir performans modeline sahip olmak oldukça etkilidir. Bu kapsamda; komponent eşleşme metoduna dayalı bir performans kodu geliştirilmiştir. Kodun sonuçları, tasarım noktası ve diğer rölanti üstü hızlar için GasTurb13 ticari yazılımıyla elde edilen sonuçlarla kıyaslanarak doğrulanmıştır. Ek olarak, açık literatürden elde edilen T700-GE-700 motor bilgileri kullanılarak kurulan performans modelinin, durağan hal ve geçici hal analiz sonuçları literatürde bulunan veriler ile karşılaştırılarak doğrulama gerçekleştirilmiştir.

Başlatma modellemesi için, rölanti altı hızlarda komponent performans haritalarına ihtiyaç duyulmaktadır. Bu hızlarda, hesaplamalı akışkanlar dinamiği çözücüleri ve komponent test düzeneklerinde güvenilir sonuçlar alınamadığı için genelde rölanti altı hızlar için modelleme gerçekleştirilememektedir. Başlatma safhası için yakıt miktarının şaft hızına bağlı

düzenlenmesi ya da iç istasyonlarda maruz kalınacak en yüksek sıcaklığın kontrol edilmesi gibi optimizasyon süreçleri, güvenilir bir başlatma modeli kurulamadığı için genellikle motor testleri ile gerçekleştirilmektedir. Bu tez çalışmasında, rölanti üstü hızlar için geçerli olan komponent performans haritaları kullanılarak rölanti altı hızlardaki komponent davranışı tahmin edilmiştir. Ek olarak, başlatıcı ekipmanının tork-hız karakteri literatürden alınarak T700-GE-700 motoru için bir örnek başlatma modellemesi gerçekleştirilmiştir. Elde edilen sonuçlar açık literatürden bulunan veriler ile kıyaslanarak harita uzatma metodu ile oluşturulan bir başlatma modelinin barındırdığı belirsizliklere rağmen oldukça gerçekçi sonuçlar sunduğu gözlemlenmiştir.

Anahtar Kelimeler: Gaz Türbinli Motorlar, Komponent Eşleşme Metodu, Motor Başlatma, Harita Genişletme

ACKNOWLEDGEMENTS

I would like to express my deepest gratitude to my supervisor Assoc. Prof. Dr. Özgür EKİCİ. Without his patience and guidance throughout my study, I could not have undertaken this journey. I would like to extend my sincere thanks to my thesis defense committee members for their guidance and invaluable comments.

I am also deeply indebted to Asst. Prof. Dr. Sıtkı USLU for all his teaching throughout my Bachelor's degree and attracting my attention to the gas turbine engines. His contributions for my education cannot be forgotten.

Special thanks goes to my dear friends and colleagues Mert ERK and Ayşe BAY for their precious technical and moral supports in this work. Their contributions solved lots of major problems that were faced during this study. I am also thankful to my dear friend and former colleague Emre GÜMÜŞSU for encouraging me to apply for this program at the first place and his continuous support.

Words cannot express my gratitude to my lovely wife Melike BOZ GÜNAY and to my family for always believing in me and endlessly supporting me during difficult times. Your trust means everything to me. I would not be able to achieve anything without every single one of you.

CONTENTS

Page

TABLES

FIGURES

ABBREVIATIONS

DP	:	**D**esign **P**oint
EPR	:	**E**xhaust **P**ressure **R**atio
FAR	:	**F**uel **A**ir **R**atio
FHV	:	**F**uel **H**eating **V**alue
GE	:	**G**eneral **E**lectric
HPT	:	**H**igh **P**ressure **T**urbine
ISA	:	**I**nternational **S**tandard **A**tmosphere
ITD	:	**I**nter-**T**urbine **D**uct
LHS	:	**L**eft **H**and **S**ide
LPT	:	**L**ow **P**ressure **T**urbine
NGV	:	**N**ozzle **G**uide **V**ane
NPR	:	**N**ozzle **P**ressure **R**atio
POT	:	**P**ower **O**fftake
PR	:	**P**ressure **R**atio
PSFC	:	**P**ower **S**pecific **F**uel **C**onsumption
PT	:	**P**ower **T**urbine
RHS	:	**R**ight **H**and **S**ide
RNI	:	**R**eynolds **N**umber **I**ndex
SAS	:	**S**econdary **A**ir **S**ystem
SAE	:	**S**ociety of **A**utomotive **E**ngineers
SLS	:	**S**ea **L**evel **S**tatic **C**ondition

1. INTRODUCTION

Gas turbine engines are used for many years in aircraft propulsion/power, marine propulsion, land-based power generation and mechanical drive applications of gas and oil pipelines [6]. Gas turbines are based on the Brayton thermodynamic cycle and basically consist of an inlet, compressor(s), a combustion chamber, turbine(s) and a nozzle, depending on the configuration. An inlet diffuses the free stream air to provide uniform air flow to the compressor with minimum possible loss in total pressure. Compressor consumes the power generated by the turbine to pressurize the air. Then, the fuel is introduced to the pressurized air in combustion chamber in order to add energy. The turbine component expands the high energy flow and extracts energy from it. While single spool turboshaft or turboprop engines use the same turbine to drive both the compressor and the load of rotor or propeller, multi-spool applications may employ a power turbine just to drive the load. In thrust engines, remaining energy after driving the compressor is used for thrust generation. Nozzle is basically responsible to increase the velocity of the fluid to increase the amount of thrust. In power engines, nozzle is required for providing a safe, low-noise exhaust of gases and not meant to increase the velocity for thrust producing, since the turbines are extracted most of the energy to produce shaft power.

Mathematically modeling the engine behavior is of great importance. Having a chance to understand the performance characteristics of the engine before production creates an opportunity to predict aircraft performance characteristics, evaluate if there is a component performance deficit or find out if a design change is required. During performance modeling, station numbering is critical and should be given clearly to avoid any possible confusion. SAE AS755 [1] describes the internationally accepted station numbering as given in Figure 1.1. Given standard convention is also accepted and applied in this study. Details can be found in Table 3.2.

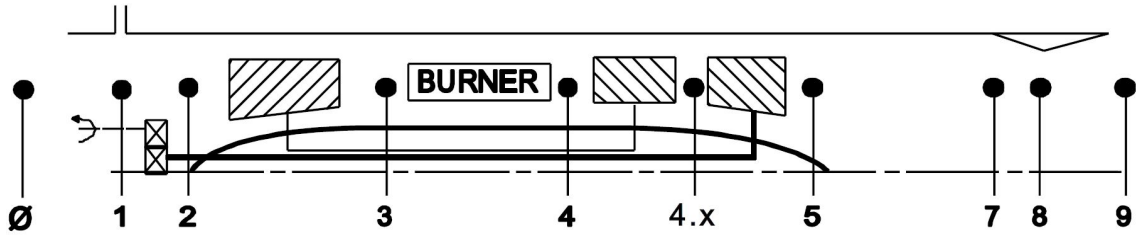

Figure 1.1 Station Numbering for a Turboshaft/Turboprop with a free turbine [1]

There are several methods to create steady-state and transient engine performance models. Component-matching based engine performance models offers a high accuracy with a reasonable complexity, and use component performance characteristics (maps) which are obtained by numerical studies or component test rigs. Nonetheless, due to their complex nature, these maps generally do not involve low speed performance characteristics of components. Mostly, the maps represent the component behavior over the idle speed. However, sub-idle operation which includes engine starting and restarting/relighting capability is a substantial part of certification requirements because it is simply an indicator of flight safety. In case of a malfunction or flameout, engine needs to be restarted, immediately. To evaluate or optimize the engine starting phase, a component-matching based starting model can be created if the component performance maps include their working characteristics in this region.

This study introduces a gas turbine performance software which is capable of modeling the starting process. Above-idle component characteristics are extended towards lower speeds for starting modeling purpose. In order to create a starting model, steady-state and transient performance models are created firstly. Section 2., reviews modeling methodologies for gas turbine performance, commercial performance software, T700-GE-700 modeling studies and map extension methods given in open literature. Theory and modeling details used for creating the software are presented in Section 3. Component map extension methodology is also given in the same section. Results of the performed studies for design, off design and transient modes are given in Section 4. Commercially available GasTurb13 gas turbine performance software is used as reference for validation of the steady-state and transient modes of the software. GasTurb13's 2 Spool Demo Turboshaft

model was selected for comparison and validation. Mark G. Ballin's work [7] shares the compressor performance map and other useful information along the steady-state and transient behavior of T700-GE-700 engine, which are also used as a comparison reference to validate T700-GE-700 above-idle models, after validating the software itself. Rhoden's technical evaluation report [9] presents the reaching times to starter cutout and idle speeds for T700-GE-700 engine. Given times set the reference for starting model validation. His work also includes the starter torque and engine drag characteristics which are crucial for engine starting studies. Conclusion, discussions and possible improvements can be found in Section 5.

2. LITERATURE REVIEW

Gas turbine performance models are required and used in order to decrease engine development test costs and speed-up the development process by gaining insight of engine behavior. Effect of alternative designs can be observed before actually manufacturing and integrating the engine with a robust performance model. Aircraft development process also depends on the engine performance prediction to a great extent. This section summarizes the main studies in the field which were beneficial for this thesis study.

2.1. Performance Model Types

Sanghi et al. [12] gives a comprehensive literature survey about gas turbine simulation approaches from the initiation of gas turbine modeling until state-of-art practice. It discusses detailed thermodynamic modeling and simulation technology, real-time simulations, and simulation applications to the design and development of gas turbines, its controls and diagnostic systems. Reference [13] reviews performance based gas turbine diagnostics while summarizing alternative methods to predict off design performance of gas turbine.

Suraweera [14] also reviews the available gas turbine off design performance simulation methods, both for performance prediction and diagnostics. Author classifies the simulation methods into component-matching, stage stacking, variants of gas path analysis, artificial intelligence, fuzzy logic and computational fluid dynamics-based methods and discusses these techniques. Additionally, Thirunavukarasu [2] combines the information from References [14] and [13] and presents the available modeling alternatives for digital computers in terms of accuracy and complexity as can be seen in Figure 2.1. As the figure shows, complexity extremely increases to ensure the same accuracy level with Component Matching method. Relation between accuracy and complexity for component matching method seems favorable.

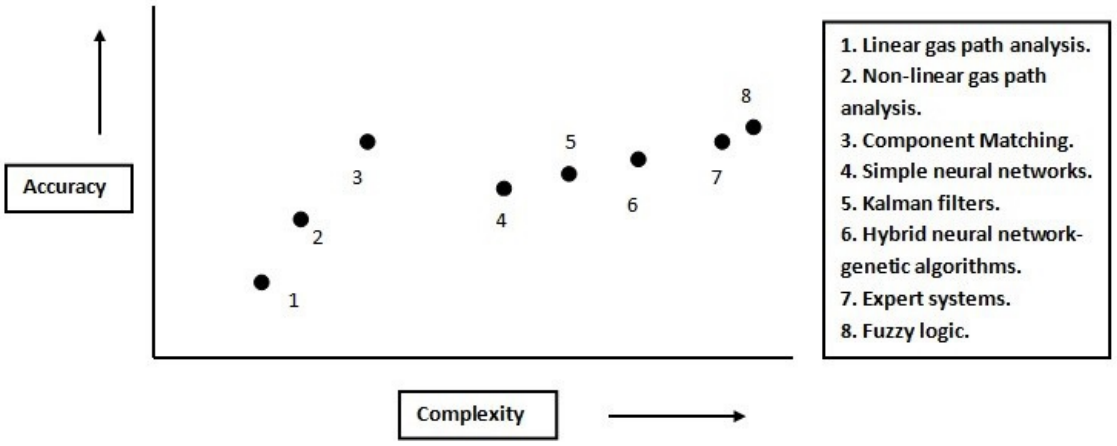

Figure 2.1 Gas Turbine Performance Simulation Models [2]

Walsh and Fletcher [6] defines the component matching method as the almost universal form of off design model and handles it under two main headings as serial nested loops and matrix iteration. Saravanamutto et al. [15] utilize serial nested loops, while Kurzke prefers matrix iteration [3, 16] for his commercial software GasTurb [4]. Serial nested loops pairs the iteration guesses and constraints, and solve in a nested structure for each component but becomes inefficienct for more than five nested loops [6]. Matrix iteration simultaneously changes iteration guesses by using Newton-Raphon method to reduce the error and meet convergence criteria. Component matching method, as will be given in Section 3.4., considers flow and work compatibility between the components. In order to use this method, component performance characteristics should be known for operating range.

2.2. Commercial Performance Software

Kurzke published his performance software GasTurb [16] which was capable to perform both cycle design and off design steady-state and transient calculations. Even inlet distortion effect modeling was included in the software by using parallel compressor model. Kurzke also developed two software named as SmoothC and SmoothT, which are used in this study for smoothing and extending the compressor and turbine maps, respectively [17, 18]. They can be used to convert component performance data measured in a rig or calculated by CFD

calculations into a table format for a performance software. Quality of the generated maps can be checked by using various plots available in these software.

NASA Glenn Research Center engineers developed an object-oriented C++ based software which is called Numerical Propulsion System Simulation (NPSS) and can also be used for liquid rocket engines, refrigeration cycles, multi-phase heat transfer systems, vehicle emission analyse, engine control systems additional to air breathing propulsion systems [19, 20].

Another commercial software named Gas turbine Simulation Program (GSP) has been developed by Visser et al. [21, 22]. Authors reported that steady-state and transient simulation of any gas turbine configuration including lift-fan STOVL propulsion systems can be performed due to GSP's flexible object-oriented architecture. Deterioration and malfunctions of control system can be analysed, as well.

2.3. Sub-Idle Studies

Apart from all the above-idle performance prediction, Chapell and McLaughlin [23] performed one of the first studies with component matching method to simulate the engine operation from near static conditions to maximum engine power with windmill starting, spooldown starting and starter assisted starting options. Relationship between component pumping capacity and and efficiency at above-idle speeds were expanded until zero-speed line. Authors stated they used a streamline curvature program to estimate compressor performance for low speeds. Results were validated by using engine test data.

Agrawal and Yunis [24] decribed a generalized mathematical method in order to extrapolate the operating line towards starting region and estimating the gas turbine performance during starting, by using similarity laws and empirical coefficients obtained from a broad engine database. This study not only included turbomachinery behavior in sub-idle region, but also included the combustor performance and parasitic losses in that region, as well. However, the study did not aim to extrapolate the component maps. Main objective is to extrapolate the operating line of the components. Validation of the method also carried out by comparing the

model predicted starting times and drag torques with available engine test results, for three different engines.

Sexton [25] developed a methodology based on Agrawal and Yunis' work. Sexton's work describes manipulating process of the similarity laws' exponents in order to include compressibility effect while extrapolating the component maps towards zero-speed. His method was validated by comparing obtained results with manufacturer's data and observing well agreement. Only drawback about Sexton's method is that the extrapolation procedure involves a trial-and-error process while selecting the exponents of the similarity laws by using the two lowest available speed line.

Gaudet and Gauthier [26] improved Sexton's study and eliminated the trial and error steps to manipulate the exponents of similarity laws for extrapolated speed line. Authors managed to produce a general procedure applicable to any performance map, but they could not manage to obtain pressure ratio below unity. Hence, windmilling studies cannot be performed by this method. The results of the study were not experimentally validated, yet it is stated that they can be used to get a general sense on engine behavior during starting and provide preliminary estimations for engine starting system.

Riegler et al. [27] discusses methods of modelling compressors in performance calculations. Based on Mach number similarity, basic methodologies by including some second order effects are summarized. The operating points in the map are located for untested region like sub-idle or windmilling. They suggested to use specific work or specific torque parameters for such lower speeds, instead of efficiency. Additionally, it is mentioned that usual parameters like work coefficient (Ψ) and flow coefficient (Φ) are not suitable for zero-speed by definition since their denominator is shaft speed. Instead, usage of corrected torque is recommended. Map extrapolation by using SmoothC software, based on similarity laws is proposed. This study remarks that map extrapolation procedure is not fully reproducible, due to not using mathematical algorithm but using a sophisticated drawing tool.

Zachos et al. [28] quote that using purely mathematical extrapolation methods does not result in sufficient accuracy levels. In order to figure the accuracy problem out, authors performed

a study to obtain a better low speed region definition by a study of locked rotor condition to derivate zero speed line in order to perform interpolation, instead of extrapolation. As an advantage, this study provides a physical background for such lower speeds. However, blade row geometry is needed for this method. After performing a numerical study for half stage, entire compressor characteristic is obtained by using stage stacking method. This study shares the sub-idle compressor map obtained with three different methodologies; extrapolating using Φ, Ψ parameters, extrapolation using torque parameter and physically enhanced interpolation. Main objective of the study is not comparing them, however the interpolation method provided smoother and more accurate than others. Results of the study could not be experimentally validated due to lack of insufficient data available.

Jia and Chen [29] managed to validate Zachos' Physically Enhanced Sub Idle Compressor Map Extrapolation Method (PECME). Zachos' method requires knowledge about locked-rotor condition and authors deduced zero-speed line from Hönle's study in 2013 [30], which includes experimentally measured locked rotor data for Allison 250 engine. By using that, sub-idle map was created by Zachos' PECME method. Results of the sub-idle model for Allison 250 engine are then validated by using engine test data, with minor differences in shaft speeds.

Catana et al. [31] examined two different type of engine starting process for TV2-117 turboshaft engine. One configuration is power turbine speed controller by the connected to dynamometer and the second configuration is without dynamometer connection. Power turbine speed is controlled by the engine itself. Results of this study show power turbine speed has a negligible impact on starting time, core engine speed and temperatures.

Kurzke [10, 32] proposed a map extension method for compressor and turbine components by using his map editing software SmoothC and SmoothT [17, 18]. In these studies, $Trq/\dot{W}$ and $\dot{W}$ correlation is shown to be linear, independently from shaft speed and the same relation is used to obtain zero-speed line characteristic. He delivers that after deducing zero-speed line, sub-idle characteristics can be created by interpolation, instead of extrapolation. Also, compressibility effect is taken into account. Obtained maps can be used both for starting

and windmilling studies. His methods and software are used in this thesis to obtain sub-idle characteristics for T700-GE-700 engine and further information can be found in following sections.

2.4. T700-GE-700 Related Studies

Ballin's study [7] is one of the most cited studies for T700-GE-700 engine. The engine performance is modeled with a real-time simulation by using described engine specific correlations and results are validated by using results of manufacturer supplied engine performance models. Many details like compressor performance map, secondary air network information, heat sink model details, combustor efficiency and exhaust pressure loss can be found in this study. Moreover, both steady-state and transient engine behavior are available and used in this thesis as comparison reference for above-idle studies.

Duyar et al. [33] developed a simplified open-loop dynamic model for T700 turboshaft engine for control system design, model-based fault detection and diagnostics purposes. Ballin's real-time simulation results are used in this study as basis. Piecewise linear state space perturbation models at different operating points are used to create the model. Results of linear simplified model are validated in the normal operating range by comparing with nonlinear simulation model.

Uzol [34] developed an aerothermal model for T700-GE-700 engine to simulate critical transient manoeuvres. A multi-layer neural network represented the compressor map and a set of differential equations and non-linear algebraic equations represented each engine component. Gas properties in each engine station are calculated by empirical relations. Open-loop and closed simulation results are validated by comparing with engine results from Ballin's work.

Rhoden [9] evaluated pressurized air start system alternatives for T700-GE-700 and TSE1035 engines. Engine drag and starter torque characteristics are presented for both engines. Engine acceleration times for starter cutout and idle speeds are also shared. Valuable information given for T700-GE-700 engine are extensively used for this thesis study both for

creating the starting model and comparing the results, although the starting fuel schedule is missing.

As a result of the literature survey, component-matching method is decided to be used for this study due to accuracy and complexity levels. Availability of literature data in both above-idle and sub-idle regions lead to T700-GE-700 engine selection for modeling. Found data enables performing comparison for engine model validation purpose in above-idle steady-state and transient behavior. To obtain component characteristics in lower speeds for starting simulation, Kurzke's map extension method is preferred due to utilization of interpolation instead of extrapolation and easy implementation by his map smoothing software, SmoothC and SmoothT. This study proposes a computer software which can be modified and used to simulate any kind of gas turbine engine configuration behavior in steady-state and transient operation including engine starting, with a physics based approach.

3. THEORY & MODELING

The first law of thermodynamics implies total energy of a closed system is conserved unless there is a heat/mass transfer or work input. In other words, energy can be neither created nor destroyed during a process, it can only change forms [35]. With heat transfer or work input/output, total energy of a system can be changed. However, net change of a system's energy should be equal to the gap between entering and leaving total energy, as given with equation (1). This energy balance is also valid for gas turbine components that will be mentioned in this section.

$$E_{in} - E_{out} = \Delta E_{system} \tag{1}$$

Additional to the the total energy, mass should also be conserved for a control volume (CV). Equation (2) implies that the difference between entering and leaving mass flow rate to a control volume should be equal to the net rate of change of mass for a certain time interval.

$$\dot{W}_{in} - \dot{W}_{out} = \frac{dm_{CV}}{dt} \tag{2}$$

All of the engine components are assumed to be steady-flow equipments. As a result, rate of change of mass in equation (2) is ignored and balance between entering and leaving mass flow rate is conserved as given with equation (3).

$$\dot{W}_{in} = \dot{W}_{out} \tag{3}$$

In addition, the second law concerns about both the quality and quantity while the first law only takes the quantity into the account. It requires processes to take place in a certain direction. For instance, electricity supply through a resistor can increase the temperature of a room. However, heat addition to a resistor can not produce the same amount of electrical energy. In order to convert heat to work requires engineers to use some special devices called heat engines. Gas turbines are an example of the heat engines and a turboshaft engine converts fuel's chemical energy into the shaft power, for instance.

Properties of working fluid in a gas turbine is critical to perform rigorous calculations. Simplified representation of fluid properties do not reflect the engine performance accurately. Hence, used relations for dry air and combustion products will be presented in Section 3.1.

3.1. Gas Model

Developed software uses the functions given in this section to define related properties of working fluid through engine stations. Instead of these rigorous equations, simplified versions can be used for quick hand calculations. However, for professional engineering purposes, these given equations are closer representation of the reality.

International Standard Atmosphere (ISA) defines ambient air properties up to 30000 m. ISA definition does not include humidity. Equations (4) to (6) and (7) to (9) provides the effect of altitude on temperature and pressure, respectively. ISA temperature [K] and pressure [kPa] formula changes according to the altitude [m], as it can be seen from below equations.

if $altitude < 11000$ m:

$$T_{ISA} = 288.15 - 0.0065 * Altitude \tag{4}$$

if $altitude \geq 11000$ m and < 24994 m:

$$T_{ISA} = 216.65 \tag{5}$$

if $altitude >= 24994$ m and < 30000 m:

$$T_{ISA} = 216.65 + 0.0029892 * (alt - 24994) \tag{6}$$

if $alt < 11000$ m:

$$P_{ISA} = 101.325 * (288.15/T_{ISA})^{-5.25588} \tag{7}$$

if $alt \geq 11000$ m and < 24994 m:

$$P_{ISA} = \frac{22.632530}{10^{0.000157689*(alt-10998.1)}} \tag{8}$$

if $alt >= 24994$ m and < 30000 m:

$$P_{ISA} = 2.5237 * (216.55/T_{ISA})^{11.8} \tag{9}$$

Gas constant (R) is difference between c_p and c_v, by definition. Equation (10) shows the calculation for R [J/(kg*K)], including the effect of Kerosene. For alternative fuels, different formulas can be found in Ref [6].

$$R = 287.05 - 0.00990 * FAR + 1e^{-7} * FAR^2 \tag{10}$$

In performance calculations, c_p, γ or total enthalpy (H) and entropy (S) differences across a component are widely required. In simpler calculations, c_p and γ can be taken as constant numbers for hot or cold parts of the engine. This approach may be acceptable and illustrative for simple hand calculations but in engineering level, a more rigorous method should be applied. For this purpose, (12) provides a highly accurate c_p [kJ/kg*K)] definition as a function of temperature and fuel to air ratio, FAR by using the constants A and B given in Table 3.1. This definition can be used both for dry air and combustion products, since it takes FAR into account.

Table 3.1 Constants A and B for Air Property Calculations

	Dry air	**O2**	**N2**	**CO2**	**H2O**		
A0	0.992313	1.00645	1.075132	0.408089	1.937043	**B0**	-0.71887
A1	0.236688	-1.04787	-0.2523	2.027201	-0.96792	**B1**	8.747481
A2	-1.85215	3.729558	0.341859	-2.40555	3.338905	**B2**	-15.8632
A3	6.083152	-4.93417	0.523944	2.039166	-3.65212	**B3**	17.2541
A4	-8.89393	3.284147	-0.88898	-1.16309	2.33247	**B4**	-10.2338
A5	7.097112	-1.0952	0.442621	0.381364	-0.81945	**B5**	3.081778
A6	-3.23473	0.145737	-0.07479	-0.05276	0.118783	**B6**	-0.36111
A7	0.794571	—	—	—	—	**B7**	-0.00392
A8	-0.08187	—	—	—	—	**B8**	0.055593
A9	0.422178	0.36979	0.443041	0.36674	2.860773	**B9**	-0.00161
A10	0.001053	0.000491	0.001262	0.001736	-0.00022	—	—

It should be noted that temperature input for Equation (12) and the latter enthalpy and entropy equations, (14) and (15), "TZ" is defined in (11).

$$TZ = T/1000 \tag{11}$$

$$\begin{aligned} cp = A0 + A1 * TZ + A2 * TZ^2 + A3 * TZ^3 + A4 * TZ^4 + A5 * TZ^5 \\ + A6 * TZ^6 + A7 * TZ^7 + A8 * TZ^8 + FAR/(1 + FAR) \\ * (B0 + B1 * TZ + B2 * TZ^2 + B3 * TZ^3 + B4 * TZ^4 \\ + B5 * TZ^5 + B6 * TZ^6 + B7 * TZ^7) \end{aligned} \tag{12}$$

Now that the c_p is calculated rigorously, γ also can be calculated accurately as given with equation (13).

$$\gamma = \frac{cp(T, FAR)}{cp(T, FAR) - R(FAR)} \tag{13}$$

Enthalpy represents relative energy to an arbitrary reference for unit mass flow of gas. Reference point does not matter since the change in enthalpy matters for gas turbine

performance, not the exact value of it. Equation (14) gives the total enthalpy per unit mass flow rate [kJ/kg] calculation relative to an arbitrary reference.

$$\begin{aligned} H = {} & A0 * TZ + A1/2 * TZ^2 + A2/3 * TZ^3 + A3/4 * TZ^4 + A4/5 * TZ^5 \\ & + A5/6 * TZ^6 + A6/7 * TZ^7 + A7/8 * TZ^8 + A8/9 * TZ^9 + A9 \\ & + (FAR/(1 + FAR)) * (B0 * TZ + B1/2 * TZ^2 + B2/3 * TZ^3 \\ & + B3/4 * TZ^4 + B4/5 * TZ^5 + B5/6 * TZ^6 + B6/7 * TZ^7 + B8) \end{aligned} \tag{14}$$

Change in entropy during compression or expansion processes, represents the lost thermal energy due to friction. Again, change in entropy is main concern for performance calculation. Owing to that reason, equation (16) is used to calculate specific entropy relative to an arbitrary reference point. In order to calculate entropy difference between two points, formula can be used for both points and change can be observed.

$$\begin{aligned} FT2 = {} & A0 * ln(TZ) + A1 * TZ + A2/2 * TZ^2 + A3/3 * TZ^3 \\ & + A4/4 * TZ^4 + A5/5 * TZ^5 + A6/6 * TZ^6 + A7/7 * TZ^7 \\ & + A8/8 * TZ^8 + A10 + (FAR/(1 + FAR)) * (B0 * ln(T2) \\ & + B1 * TZ + B2/2 * TZ^2 + B3/3 * TZ^3 + B4/4 * TZ^4 \\ & + B5/5 * TZ^5 + B6/6 * TZ^6 + B7/7 * TZ^7 + B9) \end{aligned} \tag{15}$$

$$S = FT2 - R(FAR) * ln(P) \tag{16}$$

3.2. Utility Function Functions

A number of utility functions are created to be used repetitively in performance calculations. Details of these functions are given in Subsections 3.2.1. and 3.2.2.

3.2.1. Reynolds Correction

Component performance maps reflects their charateristics with nondimensional parameters which represent Mach number. Maps hold compressibility information but the effect of varying Reynolds number is missing. This secondary effect becomes noteworthy at high altitudes or flight velocities due to high Reynolds numbers take place under these conditions. To represent its effect on turbomachinery performance, Reynolds Number Index (RNI) should be calculated first by using equation (17). RNI is defined as actual Reynolds Number's ratio to the reference condition Reynolds number for the same Mach number.

$$RNI = \frac{P}{P_{ref}} * \sqrt{\frac{T_{ref} * R(0)}{T * R(FAR)}} * \frac{vis(T_{ref})}{vis(T)} \tag{17}$$

Reference conditions are ISA sea level static conditions. Figure 3.1 shows the RNI variation among the flight envelope for a fighter jet aircraft.

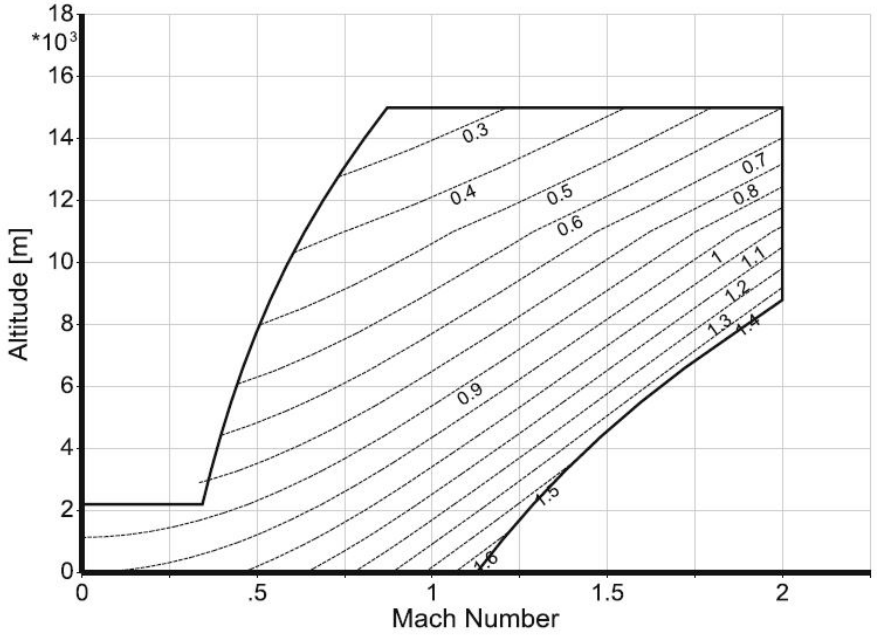

Figure 3.1 Reynolds Number Index in Flight Envelope [3]

Figure 3.2 shows the Reynolds correction factors with logarithmic RNI axis.

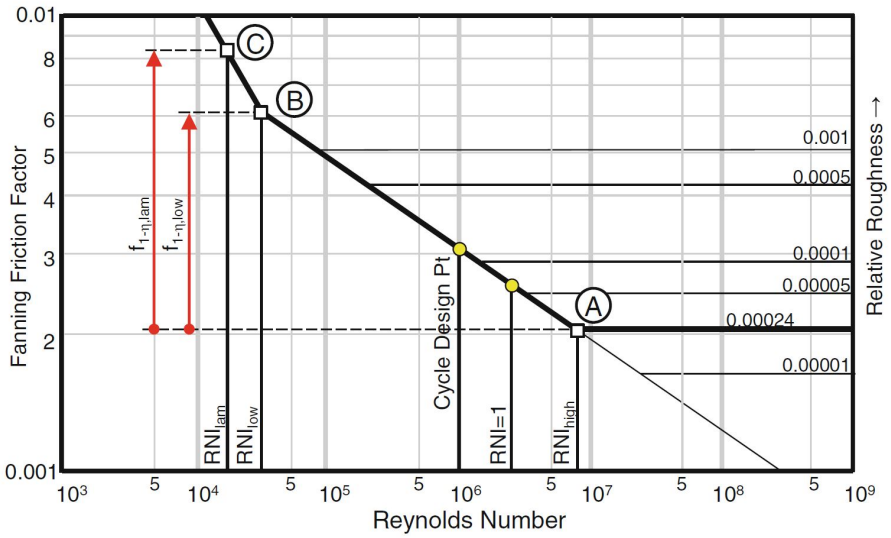

Figure 3.2 Reynolds Correction Factors [3]

For off design points, correction factor $f_{1-\eta}$ can be found by interpolating logarithmically. Efficiency correction method is given with equation (18).

$$\eta = \eta_{map} * (1 - f_{1-\eta}(1 - \eta) \tag{18}$$

Example Reynolds correction on Efficiency and Flow can be seen from Figure 3.3.

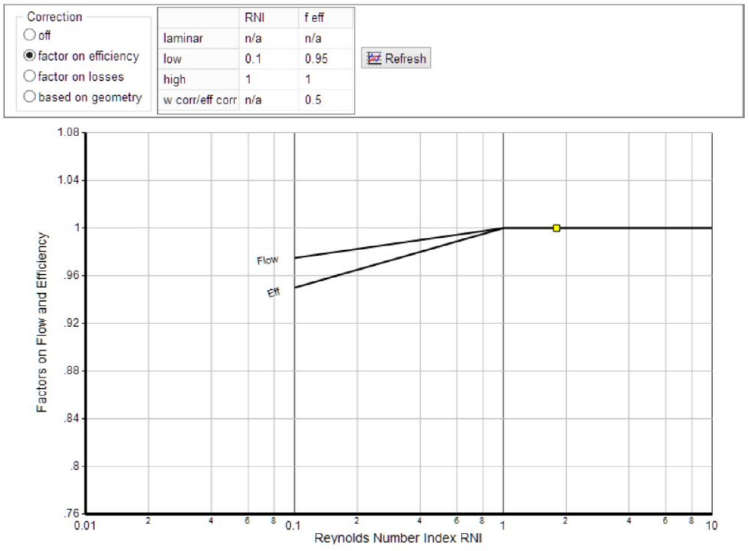

Figure 3.3 Reynolds Correction Factors and RNI Relation [4]

Equations (19) and (20) indicate limitation of Reynolds correction factor on efficiency, in case of extreme RNI values.

if $\log_{10}(RNI) < \log_{10}(RNI_{low})$:

$$factor_{eff} = factor_{low} \tag{19}$$

else if $\log_{10}(RNI) > \log_{10}(RNI_{high})$:

$$factor_{eff} = factor_{high} \tag{20}$$

For cases between minimum and maximum RNI limits, equation (21) gives the logarithmic interpolation formula. Factor on mass flow rate then can be calculated as given in equation (22). Relationship between efficiency and flow correction factors can be different. Given relationship only shows the default value in GasTurb13 software.

$$factor_{eff} = 1 - (factor_{high} - factor_{low}) * \frac{\log_{10}(RNI)}{\log_{10}(\frac{RNI_{low}}{RNI_{high}})} \tag{21}$$

$$factor_{flow} = \frac{1 - factor_{eff}}{2} + factor_{eff} \tag{22}$$

3.2.2. Thermodynamic Transition Functions

Created gas model successfully predicts enthalpy and entropy for temperature, pressure and FAR inputs. However, sometimes it is required to backwardly calculate temperature from enthalpy and FAR, or pressure from entropy, pressure and FAR. An example for obtaining temperature from enthalpy and FAR by using Newton-Raphson method, (H2T) is given below. Iterative process starts with a guess temperature and continues until the error between the input enthalpy and guessed temperature based enthalpy is lower than $1e^{-5}$. Equations (23) to (33) exemplifies the iteration process.

$$T_{guess} = 1000K \tag{23}$$

$$error = 1 \tag{24}$$

while $error > 1e^{-5}$:

$$H_{guess} = H(T_{guess}, FAR) \tag{25}$$

$$error = \frac{H - H_{guess}}{H} * 100 \tag{26}$$

$$step = 1 \tag{27}$$

$$T_{guess,new} = T_{guess} + step \tag{28}$$

$$H_{guess,new} = H(T_{guess,new}, FAR) \tag{29}$$

$$error_{new} = \frac{H - H_{guess,new}}{H} * 100 \tag{30}$$

$$J = \frac{error_{new} - error}{step} \tag{31}$$

$$\Delta T_{guess} = \frac{-error}{J} \tag{32}$$

$$T_{guess} = T_{guess} + \Delta T_{guess} \tag{33}$$

Same procedure is used to obtain temperature and pressure by using entropy function (SP2T and ST2P).

3.3. Design Point Calculations

Engine design point can be chosen in two ways[6]:

- Most time spending point
- Important high power condition

Engine performance requirements, which can be given for both of these conditions, should be fulfilled in cycle design point. Requirements basically define the engine configuration, cycle

parameters, component performance targets and sizes. Fulfillment of these criteria can be evaluated by parametric studies. By alternating engine design parameters like compressor pressure ratio or combustor outlet temperature, effects on outcome can be observed and fulfillment can be checked for each requirement. Thermodynamic calculation in cycle design point is straight-forward. After defining the component performance parameters, all thermodynamic properties can be calculated in order. For these calculations, a proper gas model and utility funtions are created as mentioned in Sections 3.1. and 3.2.

All components of the engine are modeled with separate functions in the developed software. Different engine configurations can be developed by adding or removing components. Details of all components will be given in following Subsections from 3.3.1. to 3.3.9. General schematic of the component and their connection can be seen from Figure 3.4.

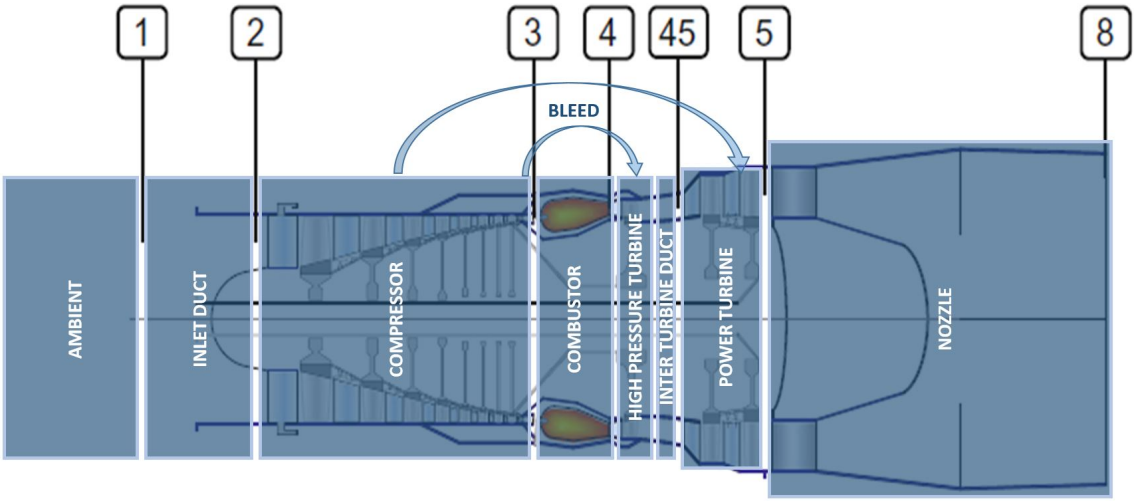

Figure 3.4 Components and Their Connections for a Turboshaft engine with a Power Turbine

These components are used to calculate thermodynamic properties for all of the internal engine stations. Station numbering is given with Figure 1.1 and details are presented herein with Table 3.2

Table 3.2 Thermodynamic Station Numbering

	Definition
0	Ambient
1	Aircraft/Engine Interface
2	Compressor Inlet
3	Compressor Outlet
31	Combustor Inlet
4	Combustor Outlet / HPT NGV Inlet
41	HPT NGV Outlet/Rotor Inlet
43	HPT Rotor Outlet
44	HPT Rotor Cooling Addition / Inter-turbine Duct Inlet
45	Power Turbine Inlet
49	Power Turbine Outlet
5	Power Turbine Rotor Cooling Addition / Exhaust Duct Inlet
6	Exhaust Duct Outlet / Nozzle Inlet
8	Nozzle Outlet

3.3.1. Ambient

Functions T_{ISA} and P_{ISA} are used for finding standard day static ambient properties as given in equations (34) and (35). Deviation from standard day temperature (ΔT) needs to be considered, as well.

$$Tamb = T_{ISA}(alt) + \Delta T \tag{34}$$

$$Pamb = P_{ISA}(Tamb, alt) \tag{35}$$

Forward speed condition creates a dynamic pressure at the engine inlet. Total temperature and pressure at inlet are calculated with equations (36) and (37) by taking flight Mach number into account. In both equations, γ is calculated for T_{amb} and $FAR = 0$ but for simplicity these information is not given there.

$$T_1 = Tamb * (1 + (\frac{\gamma - 1)}{2}) * M^2) \tag{36}$$

$$P_1 = Pamb * (1 + (\frac{\gamma - 1)}{2}) * M^2)^{\frac{\gamma}{\gamma - 1}} \tag{37}$$

3.3.2. Duct

All ducts in the engine are accepted as constant temperature ducts. Minor temperature changes due to heat transfer or friction are neglected and outlet temperature is accepted as equal to the inlet temperature as given in equation (38). At design point definition phase, each duct in the engine is assigned to a target/design pressure loss. Pressure loss in a duct due to wall friction and changes in flow direction defines the outlet pressure. Equation (39) shows the specified relation.

$$T_2 = T_1 \tag{38}$$

$$P_2 = P_1 * PR_{\text{Inlet,DP}} \tag{39}$$

3.3.3. Compressor

Another cycle design parameter is inlet corrected mass flow rate ($\dot{W}_{2,corr}$). This parameter simply dictates the size of the engine because the axial air velocity has a limit and frontal area should match the mass flow rate. Actual mass flow rate can be calculated by using compressor inlet temperature and pressure T_2, P_2, and sea level ISA temperature and pressure, T_{ref} and P_{ref} as given in equation (42).

$$T_{ref} = 288.15 \tag{40}$$

$$P_{ref} = 101.325 \tag{41}$$

$$\dot{W}_2 = \frac{\dot{W}_{2,corr} * \frac{P2}{Pref}}{\sqrt{\frac{T2}{Tref}}} \tag{42}$$

Compressor exit pressure depends on Compressor Pressure Ratio and inlet pressure and can be calculated by equation (43).

$$P_3 = P_2 * CPR_{DP} \tag{43}$$

Compression in a gas turbine engine is not an isentropic process as can be seen in Figure 3.5, on the contrary to ideal Brayton cycle. However, to find the real outlet properties, isentropic outlet properties should be calculated first. For an isentropic process, there is not any entropy difference between inlet and outlet. Accordingly, isentropic outlet temperature can be calculated by using inlet entropy as given in equation (44).

$$T_{3,isen} = sp2t(s_{inlet}, P_3, FAR) \tag{44}$$

After finding isentropic outlet temperature, isentropic outlet enthalpy can be calculated by enthalpy function, as given in equation (45).

$$H_{3,isen} = H(T_{3,isen}, FAR) \tag{45}$$

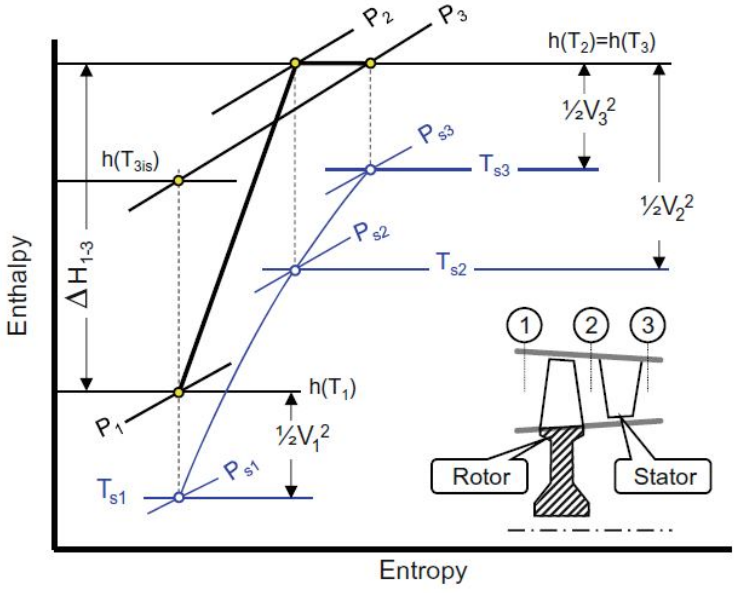

Figure 3.5 Compression process in an Enthalpy-Entropy diagram[3]

Figure 3.5 shows the changes in enthalpy and entropy during the compression process for isentropic and real cases. It should be noted that this figure notates stator inlet with number "2", however, in standard convention, station number "2" is used for rotor inlet and in equation (46) H_2 represents rotor inlet enthalpy. P_1 in Figure 3.5 represents compressor rotor inlet pressure, which is P_2 in standard convention and calculated by Equation (39). Equation (46) gives the definition of isentropic efficiency for a compressor.

$$\eta_{is,comp} = \frac{H_{3,isen} - H_2}{H_3 - H_2} \tag{46}$$

Equation (46) can be rearranged and written as given in equation (47) in order to find H_3.

$$H_3 = \frac{H_{3,isen} - H_2}{\eta_{is,comp}} + H_2 \tag{47}$$

Thermodynamic transition function H2T given in Subsection 3.2.2. is required to calculate T_3 from obtained H_3 as shown in equation (48).

$$T_3 = H2T(H_3, FAR) \tag{48}$$

Compressor inlet mass flow rate should be conserved and be equal to exit mass flow at non-bleeding cases. But usually, some inter-stage compressor bleeds are used to condition cabin air, pressurize seals and bearings, and low pressure turbine cooling purposes. Compressor exit mass flow rate is calculated by equation (49).

$$\dot{W}_3 = \dot{W}_2 - \dot{W}_{LP_{bleeds}} \tag{49}$$

Compressor power is another substantial parameter since it defines the working point of the compressor driver High Pressure Turbine (HPT). Calculation for compressor power is given with equation (50).

$$Power_{Compressor} = \dot{W}_3 * (H_3 - H_2) + \dot{W}_{LP_{bleeds}} * (H_{LP_{bleeds}} - H_2) \tag{50}$$

3.3.4. Bleed Out

There may be another bleed extraction port between compressor outlet and combustor inlet. Inter-stage bleed air pressure is not enough for every bleed operation in engine. For instance, HPT inlet pressure is considerably high compared to inter-stage bleed air pressure. Thus, bleed extraction from compressor outlet is mandatory for HPT cooling. Considering that, Bleed Out element is created and holds all the information about secondary air system network. It both calculates the outlet mass flow rate $\dot{W}_{31}$ by using the $\dot{W}_3$ and $\dot{W}_{HPbleeds}$ inputs as given in equation (51) and holds all secondary air system network's enthalpies to be used later in "Bleed In" element for energy balance calculations in turbine cooling studies.

$$\dot{W}_{31} = \dot{W}_3 - \dot{W}_{HPbleeds} \tag{51}$$

All the other thermodynamic properties like temperature, pressure, enthalpy, and entropy are accepted as the same with Station 3. Other held information can be given as

- $\dot{W}_{cooling,HPTNGV}$ & $H_{cooling,HPTNGV}$
- $\dot{W}_{cooling,HPTRotor}$ & $H_{cooling,HPTRotor}$
- $\dot{W}_{cooling,PTNGV}$ & $H_{cooling,PTNGV}$
- $\dot{W}_{cooling,PTRotor}$ & $H_{cooling,PTRotor}$
- $\dot{W}_{Overboard}$ & $H_{Overboard}$

3.3.5. Combustor

After finding combustor inlet parameters, combustor calculations can be performed. For design point calculations, combustor outlet temperature and fuel heating value (FHV) are inputs. Regarding T_4 input, there is a unique FAR value which ensures the equality given in

equation (52). This FAR value can be calculated iteratively. For a more rigorous calculation, reference temperature for air and fuel will also be taken into the account.

$$\begin{aligned}(H(T_4, FAR) - H(T_{ref}, FAR)) * (1 + FAR) = FAR * FHV * \eta_{combustor} \\ +H(T_3, FAR) - H(T_{ref}, FAR) + FAR * (H_{fuel}(T_{fuel}) - H_{fuel}(T_{ref}))\end{aligned} \tag{52}$$

Hereupon, fuel mass flow rate can be calculated as given in equation (53) since FAR and $\dot{W}_{31}$ are known.

$$\dot{W}_{fuel} = FAR * \dot{W}_{31} \tag{53}$$

Combustor outlet mass flow rate is equal to sum of combustor inlet air mass flow rate and fuel mass flow rate as can be seen from equation (54).

$$\dot{W}_4 = \dot{W}_{31} + \dot{W}_{fuel} \tag{54}$$

In ideal Brayton cycle, fuel/heat addition is a constant pressure operation. Yet, in application it is not the case. A certain amount of pressure loss takes place in combustor, due to the friction, compressor diffuser dump, cooling the flame tubes and turbulent mixing in the dilution zone. Equation (55) gives pressure decrease calculation for combustor. In fact, pressure drop in combustor is necessary to ensure the fluid flow from compressor outlet to HPT inlet for cooling. In case of no pressure difference, fluid flow can not be guaranteed and turbine cooling may be unstable. Correspondingly, turbine blade life can be severely shortened.

$$P_4 = P_{31} * PR_{\text{Combustor,DP}} \tag{55}$$

3.3.6. Bleed In

There are four main cooling bleeds in a 2 spool turboshaft engine, NGV and Rotor cooling airs for both turbines. Some applications do not need to cool down PT. However, developed software has the capability to represent this effect. In case of uncooled PT configuration, it's mass flow fraction can be determined as zero. Bleed In element is required for cooling

calculations when needed. It is used for determining the station enthalpy and mass flow rate after a cooling bleed input.

The combustion product at the downstream of combustor is extremely hot. NGV blades are exposed to that extreme temperatures. Due to this reason, cooling effect is especially critical for performance calculation in this station. Mass flow rate, $\dot{W}_{41}$ should be calculated first, as shown in equation (56), to be used as an input in enthalpy balance, equation (57).

$$\dot{W}_{41} = \dot{W}_{4} + \dot{W}_{cooling,HPTNGV} \tag{56}$$

$$H_{41} = \frac{H_4 * \dot{W}_{4} + H_{cooling,HPTNGV} * \dot{W}_{cooling,HPTNGV}}{\dot{W}_{41}} \tag{57}$$

Same procedure applies to all cooling stations as given in Equations (58) to (63).

$$\dot{W}_{44} = \dot{W}_{43} + \dot{W}_{cooling,HPTRotor} \tag{58}$$

$$H_{44} = \frac{H_{43} * \dot{W}_{43} + H_{cooling,HPTRotor} * \dot{W}_{cooling,HPTRotor}}{\dot{W}_{44}} \tag{59}$$

$$\dot{W}_{45} = \dot{W}_{44} + \dot{W}_{cooling,PTNGV} \tag{60}$$

$$H_{45} = \frac{H_{44} * \dot{W}_{44} + H_{cooling,PTNGV} * \dot{W}_{cooling,PTNGV}}{\dot{W}_{PT,NGV}} \tag{61}$$

$$\dot{W}_{5} = \dot{W}_{49} + \dot{W}_{cooling,PTRotor} \tag{62}$$

$$H_{5} = \frac{H_{49} * \dot{W}_{49} + H_{cooling,PTRotor} * \dot{W}_{cooling,PTRotor}}{\dot{W}_{5}} \tag{63}$$

3.3.7. High Pressure Turbine

Similar to compressor outlet (station 3) and combustor inlet (station 31), there is a difference between combustor outlet (station 4) and HPT rotor inlet (station 41). As previously stated, there is a cooling bleed input between these stations and mass flow rate and enthalpy differences are given with equations (56) and (57), respectively. As equation (64) states,

minor pressure increase is neglected.

$$P_{41} = P_4 \tag{64}$$

After defining the inlet parameters, calculations can be performed for HPT. Isentropic efficiency of HPT is known as a cycle design input, but pressure/expansion ratio is still unknown. To calculate the HPT outlet parameters, compressor power will be used. Cycle design point is a steady-state working condition. consequently, there should be a balance between power generated by HPT and power consumed by compressor. The inlet mass flow rate and enthalpy are known for HPT. By using the required power generation and inlet conditions of HPT, working pressure ratio can be calculated. Required HPT power can be calculated by equation (65).

$$Power_{HPT} = \frac{Power_{comp} + POT}{\eta_{Mech_{HPShaft,DP}}} \tag{65}$$

Next, HPT outlet enthalpy can be calculated by using obtained power value as given in equation (66).

$$H_{43} = H_{41} - \frac{Power_{HPT}}{\dot{W}_{41}} \tag{66}$$

Outlet temperature T_{43} also can be calculated after obtaining H_{43} as shown with equation (67).

$$T_{43} = h2t(H_{43}, FAR_{41}) \tag{67}$$

Isentropic HPT efficiency is an input for design point calculations. Isentropic outlet enthalpy and temperature can be found by using $\eta_{HPT,isen}$ as given in equations (68) and (69).

$$H_{43,isen} = H_{41} - \frac{H_{41} - H_{43}}{\eta_{HPT,isen}} \tag{68}$$

$$T_{43,isen} = h2t(H_{43,isen}, FAR_{41}) \tag{69}$$

After obtaining isentropic outlet temperature $T_{43,isen}$, outlet pressure P_{43} can be calculated by using SP2T function as given with equation (70), since the isentropic expansion will not

increase the entropy.

$$P_{43} = st2p(s_{41}, T_{43,isen}, FAR_{41}) \tag{70}$$

PR_{HPT} is given with equation (71).

$$PR_{HPT} = \frac{P_{41}}{P_{43}} \tag{71}$$

3.3.8. Low Pressure Turbine (Power Turbine)

PT component is not different from HPT. The same calculations are still valid for PT. However, there is a discrepancy needs to be clarified for PT. In HPT component, there is a consistency between produced power by HPT and consumed power by compressor. For PT module, there is no such power balance. Yet, PT outlet pressure (P_{49}=P_5) is predefined because exhaust pressure ratio ($(P_8/P_{amb})_{DP}$) is a cycle design input parameter. In other words, P_8 is known as it can be seen from equation (72). Additionally, exhaust duct pressure ratio (NPR_{DP}) is another design parameter and it is used to determine PT outlet pressure as shown in equation (73).

$$P_8 = (\frac{P_8}{P_{amb}})_{DP} * P_{amb} \tag{72}$$

$$P_{49} = P_5 = \frac{P_8}{NPR_{DP}} \tag{73}$$

After finding P_{49}, PT pressure/expansion ratio, PR_{PT}, can be calculated as given in equation (74).

$$PR_{PT} = \frac{P_{45}}{P_{49}} \tag{74}$$

Isentropic outlet temperature can be found by using SP2T utility function as shown in equation (75), since the outlet entropy S_{49} will be equal to inlet entropy S_{45} for an isentropic turbine operation.

$$T_{49,isen} = sp2t(s_{45}, P_{49}, FAR_{49}) \tag{75}$$

Isentropic outlet enthalpy, which will be used together with isentropic efficiency to calculate actual outlet enthalpy, is calculated by equation (76).

$$H_{49,isen} = H(T_{49,isen}, FAR_{49}) \tag{76}$$

Actual outlet enthalpy and therefore actual outlet temperature are now explicit as shown with equations (77) and (78).

$$H_{49} = H_{45} - \eta_{PT,isen} * (H_{45} - H_{49,isen}) \tag{77}$$

$$T_{49} = h2t(H_{49}, FAR_{49}) \tag{78}$$

After finding inlet and outlet properties, power can be calculated as given in equation (79). It should be noted that, as shown in equation (80), produced power ($Power_{PT}$) and delivered power ($PWSD$) differs due to low pressure spool mechanical efficiency ($\eta_{Mech_{LPShaft,DP}}$).

$$Power_{PT} = W_{45} * (H_{45} - H_{49}) \tag{79}$$

$$PWSD = Power_{PT} * \eta_{Mech_{LPShaft,DP}} \tag{80}$$

3.3.9. Nozzle

Nozzle (or exhaust) component behaves similarly with 'Duct' element for design point calculations. It is assumed to be adiabatic as can be seen in equations (81) and (82). Only change happens in pressure value, due to friction losses. Before this element, P8 and P5 are already calculated with equations (72) and (73), respectively.

$$T_8 = T_5 \tag{81}$$

$$H_8 = H_5 \tag{82}$$

Fuel to air ratio at Nozzle exit is calculated with equation (83) to be used in entropy calculation.

$$FAR_8 = \frac{\dot{W}_{fuel}}{W_8} \tag{83}$$

Outlet entropy S_8 can be calculated with equation (84), since T_8, P_8 and FAR_8 are known.

$$S_8 = S(T_8, P_8, FAR_8) \tag{84}$$

Static outlet pressure is equal to ambient pressure for a turboshaft engine as can be seen in equation (85). For a turbojet or a turbofan engine this condition can be changed and should be investigated. There may be over-expanded or under-expanded cases for thrust engines with convergent-divergent nozzles.

$$Ps_8 = P_{amb} \tag{85}$$

Static outlet temperature can be found by using SP2T utility function with S_8, Ps_8 and FAR_8 inputs in equation (86).

$$Ts_8 = sp2t(S_8, Ps_8, FAR_8) \tag{86}$$

Then, density is calculated with equation (87) to be used in area calculation.

$$\rho_8 = \frac{P_{amb}}{R(FAR8) * Ts_8} \tag{87}$$

Nozzle exit area is defined with equation (88) for design point. Area is fixed for off design conditions for a turboshaft engine.

$$A_8 = \frac{\dot{W}_8}{\rho_8 * V_8} \tag{88}$$

3.4. Off Design Calculations

In Off Design mode the engine geometry is fixed (if there is not any moving guide vanes or other structures). Engine cycle design and geometry changes are completed and investigating

point is the engine behavior outside of the design point. Performance characteristics of a fixed engine geometry at part speeds is the main focus area.

Before performing the calculations, one concept should be clarified. In design mode, calculations were made in order. No iterations were needed for finding component performance characteristics. In other words; compressor pressure ratio, as an example, was a design parameter and input. However, in off design mode, compressor pressure ratio is an unknown parameter for a part speed. In a similar manner, all the other performance parameters are unknown at the beginning like T_4, η_{HPT}, and η_{PT}.

To find all the performance parameters, a method called "Component Matching Method" is most commonly used. In [3] and [6] the details of Buckingham PI theorem and non-dimensional behavior of engines can be found. As it is explained in these sources, fixing the value of a non-dimensional parameter also fixes other non-dimensional parameters for an engine operating with choked turbine or nozzle. As a result, engine follows a unique operating line in component performance maps. Finding that unique point for each shaft speed is an iterative process and the details of this procedure will be given in Section 3.4.3.

Because this working conditions is a steady-state condition, all the components should behave in a manner that their inputs and outputs are balanced. Mass flow rates through components are conserved, power generation and extraction is in balance. There is only one unique point which ensures these balances and "matches" the components with each other at that specific shaft speed. Before moving on with the details of iteration scheme, it is needed to understand basic usage of component performance maps.

3.4.1. Component Performance Maps

3.4.1.1. Compressor Performance Maps Compressor maps play a major role in high quality gas turbine performance calculations [36]. Usually detailed geometry is not open to a researcher or a gas turbine user. In such case, open literature can provide a performance map for a similar configuration turbomachinery and it can be scaled or tweaked to be used

in specific applications [3]. A compressor map generally reflects the corresponding pressure ratio versus corrected mass flow rate. Efficiency islands can both be given as contours in the background or as a separate chart for each corrected speed line.

Corrected mass flow rate represents the axial Mach number, M_{ax}, and corrected shaft speed represents circumferential Mach number, M_U. A velocity triangle analysis as given in Figure 3.6 hides the underlying information of a compressor performance map. At a very high incidence angle flow may not be following the blade profile. Thus, there may some separations and efficiency decreases in such case. Another option is lower incidence angle values than expected. In such case, M_{ax} increases and reaches its maximum, and passage chokes. Performance map reflects all these effects and an example performance map is given in Figure 3.7.

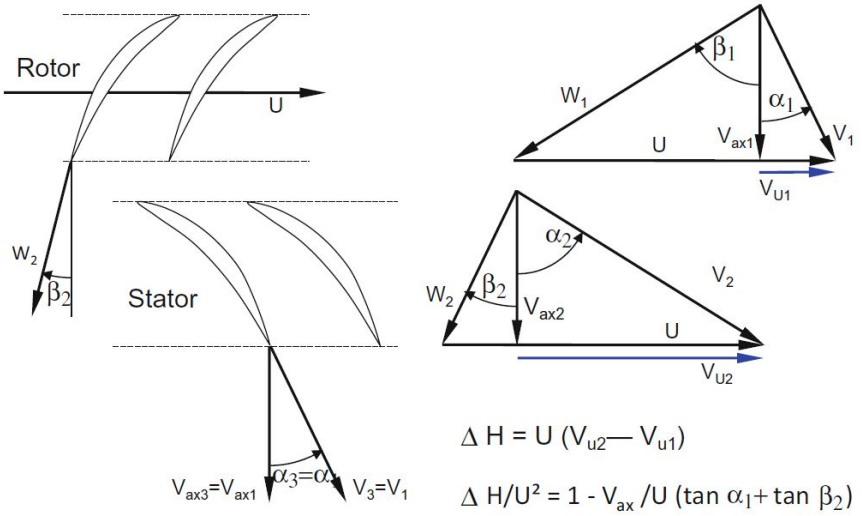

Figure 3.6 Velocity Triangle Analysis for Compressor [3]

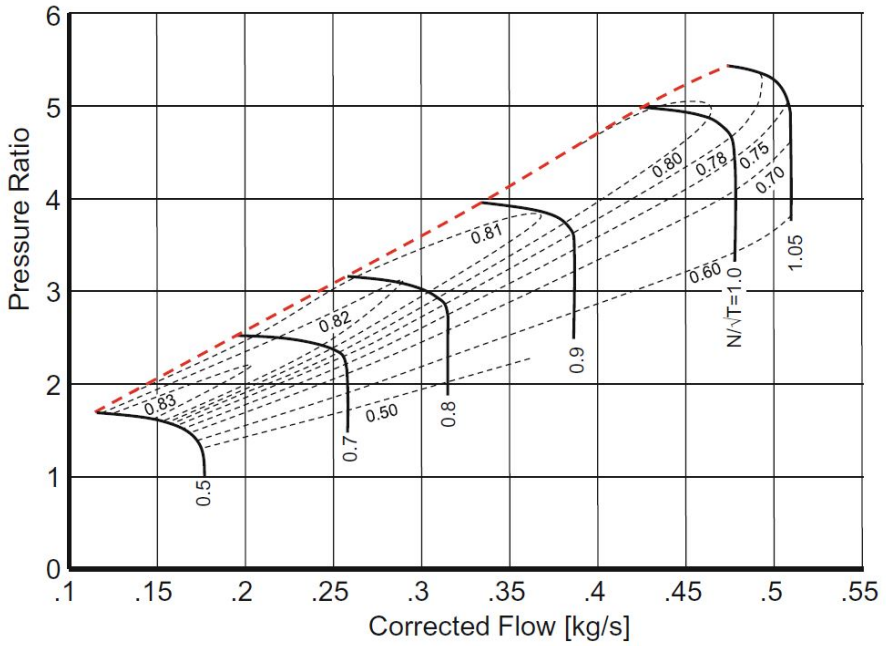

Figure 3.7 Sample map of a high-speed centrifugal compressor [5]

As it can be seen from Figure 3.7, almost for each speed line there is a choked region and mass flow does not increase after a certain point, with decreasing pressure ratio. If corrected speed line and corrected mass flow rate parameters are selected to read pressure ratio and efficiency properties from a map, it causes a problem in choked region due to multiple available solution. Similarly, a speed line shape may bend and involve lower pressure ratios after a peak. That means for the same pressure ratio, there might be two corresponding corrected mass flow rate values at a speed line as can be seen in Figure 3.8.

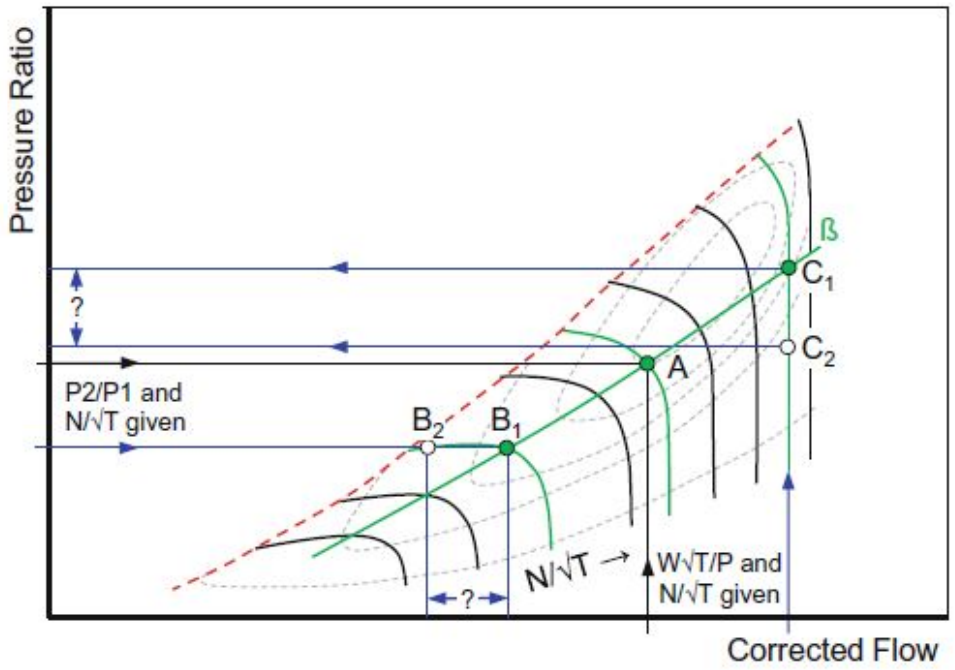

Figure 3.8 The compressor map reading problem [3]

To overcome this complicated situation, an arbitrary "β" number is introduced as given in Figure 3.9. β lines can be linear or parabolic lines which are parallel to the surge line and should cover the highest and lowest pressure ratio values for each speed line. β=0 and β=1 lines can be seen in Figure 3.9. They are arbitrary values, do not represent any physical property and equally spaced lines. There may be 20-30 equally spaced β lines for a proper above-idle compressor performance map. For extension purposes, 50 β lines are recommended [17].

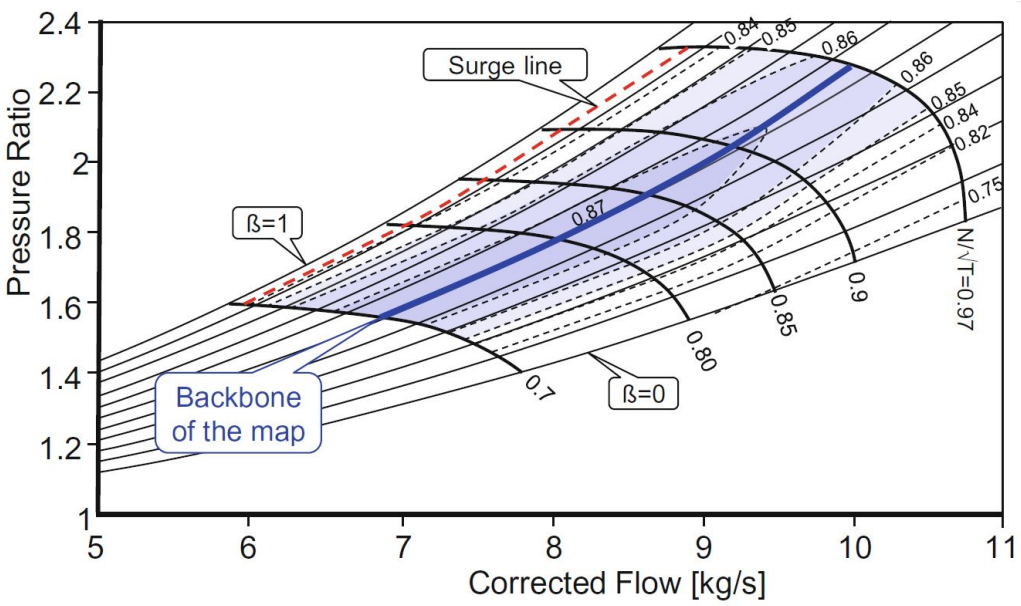

Figure 3.9 β -lines in the compressor map[3]

After introducing beta lines, compressor map can be represented with tables as it is given in Figure 3.10. 2-D look-up tables represent the compressor performance by using corrected speed lines and β numbers. As it is mentioned before, for a specific corrected speed, compressor will operate in a specific point in the compressor map. β for compressor map ($\beta_{compressor}$) will be an iteration guess.

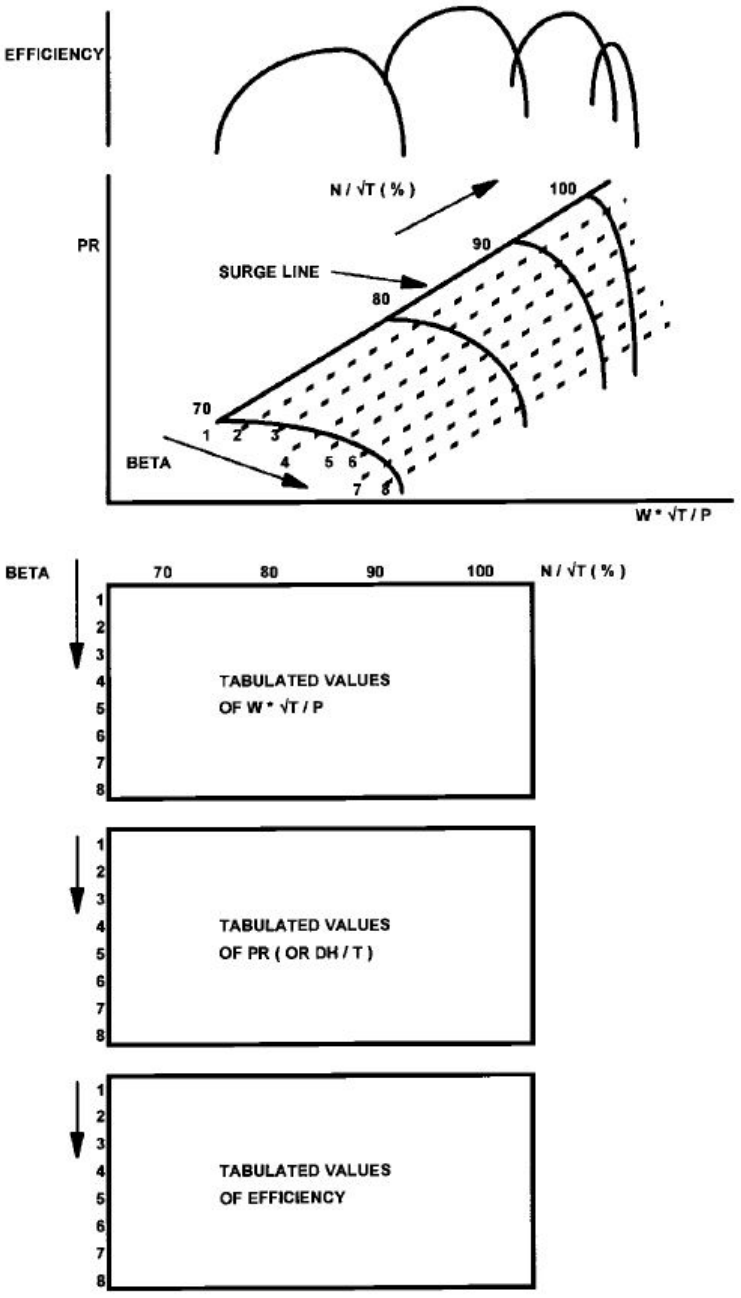

Figure 3.10 Tabulated compressor map [6]

3.4.1.2. Turbine Performance Maps Turbine map is not substantially different from a compressor map. Main difference comes from its operational behavior. Turbines are generally working under choked conditions. Due to this reason, all speed lines collapse to the choking corrected mass flow rate. In order to clearly represent a turbine's performance,

turbine maps generally use "*corrected mass flow*corrected speed*" as an axis, instead of only *"corrected mass flow rate"* as it is given in Figure 3.11.

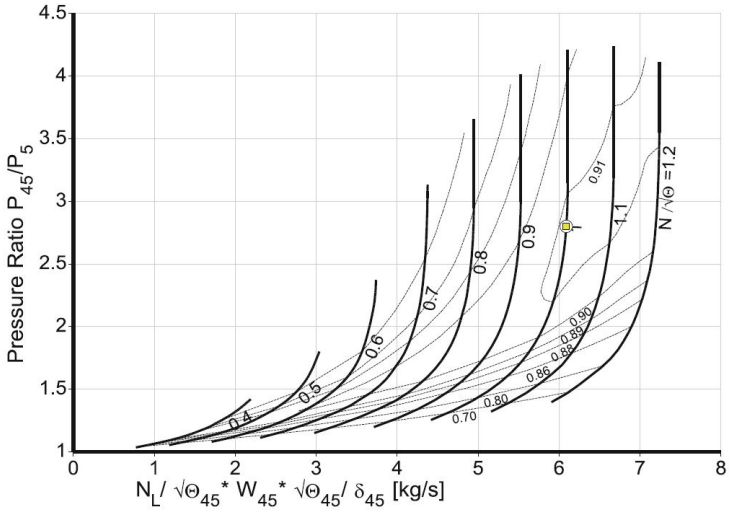

Figure 3.11 Turbine map with pressure ratio and the product of corrected speed and flow as axes[3]

Additionally, a choked turbine's map does not play a major role on the quality of a gas turbine performance simulation. Because, a choked turbine does not operate in a wide range. Pressure ratio can be accepted as constant and efficiency changes generally occur due to tip clearance. If the turbine is not operating under choked conditions (like a PT), it's off design performance characteristic should be investigated. In a turboshaft or turboprop configuration, PT generally operates with a fixed mechanical speed. However, corrected PT speed will not be constant due to varying inlet temperature conditions. Due to this reason, shape of the map matters for a non-choked turbine[3].

As already stated, off design performance prediction is an iterative process. At the beginning, a guess for operating point may be performed for each component in the engine. After completing the calculation there will be some incompatibilities between components. Guessed compressor outlet mass flow rate may be different than the HPT inlet mass flow rate. HPT power may be insufficient or excessive to drive compressor. Investigating these errors will reveal the solution.

3.4.2. Element Structure

Element structure in off design mode is very similar to the explained structure in design mode, with slight modifications.

Duct element calculates pressure ratio, pressure loss in other words, by taking design pressure ratio and design corrected mass flow rate values into account as given with equation (89). This is also valid for combustor pressure ratio calculations.

$$\frac{1-\frac{P_{out}}{P_{in}}}{\left(1-\frac{P_{out}}{P_{in}}\right)_{DP}} = \left(\frac{\frac{W*\sqrt{R*T}}{P}}{\left(\frac{W*\sqrt{R*T}}{P}\right)_{DP}}\right)^2 \tag{89}$$

$\eta_{combustor}$ is another parameter that should be considered. In off design mode, it is not a straight input. To be able to calculate combustor efficiency for any off design point, combustor loading (Ω) should be calculated with equation (90).

$$\Omega = \frac{\dot{W}_{31}}{P_3^{1.8} * e^{T_3/300K} * V_{Combustor}} \tag{90}$$

After calculating combustor loading, another constant (a) should be calculated as given with equation (91) by using $\eta_{combustor,DP}$, as well.

$$a = \log(1-\eta_{Combustor,DP}) \tag{91}$$

Finally, off design combustor efficiency can be calculated by equation (92).

$$\log(1-\eta_{combustor}) = a + b * \log(\frac{\Omega}{\Omega_{DP}}) \tag{92}$$

3.4.3. Iterations

Section 3.4.1. provides an overview on component performance maps. Making a guess for a component at the beginning of iteration process is actually means picking a point

on performance map. After one full calculation loop as in design mode, errors will be calculated. Then, Newton-Raphson algorithm will help in order to modify first guesses to reduce errors. By using this algorithm, slight modifications will be applied for each guess and corresponding effect on errors will be observed. Partial derivatives of errors according to each guess will create a matrix, which is called *Jacobi matrix*. Gauss Elimination method will be put to service to find out how to modify the guesses to find a solution. In each loop, errors will be smaller and a better set of guesses will be obtained. A generalized iteration scheme for Newton-Raphson is given in Figure 3.12 Details of the process will be explained in Subsection 3.4.3.1.

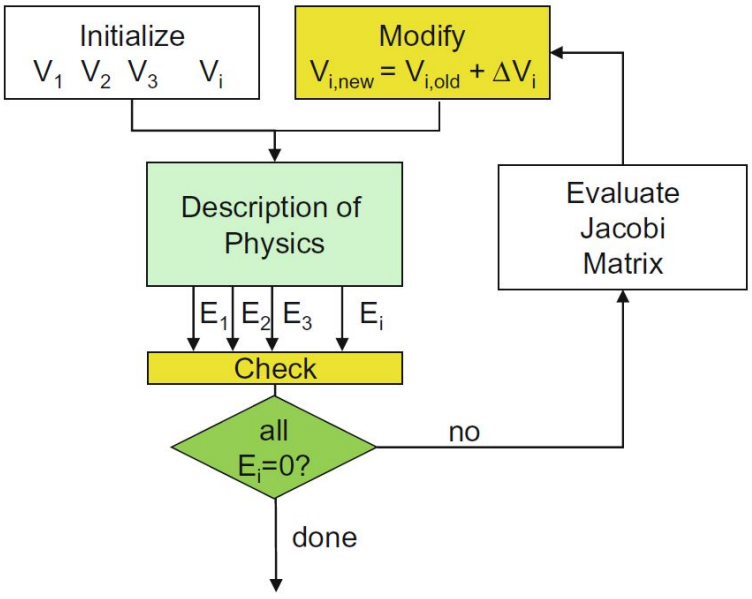

Figure 3.12 Generalized Newton-Raphson Iteration [3]

3.4.3.1. Iteration Process GasTurb13's User's Manual [4] has a clear numerical example for the described iteration process. Let there be a set of 2 equations for E_1 and E_2 with variables V_1 and V_2 as given in equations (93) and (94).

$$E_1 = 5 * V_1 + 3 * V_2 + 4 \tag{93}$$

$$E_2 = -3 * V_1 + 7 * V_2 + 24 \tag{94}$$

At the beginning of the iteration process, V_1 and V_2 are unknown. Let the first pick for V_1 to be 3, and for V_2 to be 7. In this case E_1 will be 40 and E_2 will be 64. Aim is to find values of V_1 and V_2 which makes E_1 and E_2 zero, simultaneously. To do that, effect of a small change of each variable $(\frac{\partial E_i}{\partial V_j})$ to the result should be observed. This is called as influence coefficient and the matrix which is formed by them is called *Jacobian Matrix*. It will be used to obtain required amount of change to each guess of variables V_1 and V_2.

$$\frac{\partial E_1}{\partial V_1} * \Delta V_1 + \frac{\partial E_1}{\partial V_2} * \Delta V_2 = -E_1$$
$$\frac{\partial E_2}{\partial V_1} * \Delta V_1 + \frac{\partial E_2}{\partial V_2} * \Delta V_2 = -E_2$$

Coefficiencts of influence for this example can be calculated as given below:

$$\frac{\partial E_1}{\partial V_1} = 5 \qquad \frac{\partial E_1}{\partial V_2} = 3$$
$$\frac{\partial E_2}{\partial V_1} = -3 \qquad \frac{\partial E_2}{\partial V_2} = 7$$

Final system of linear equations:

$$5 * \Delta V_1 + 3 * \Delta V_2 = -40$$
$$-3 * \Delta V_1 + 7 * \Delta V_2 = -64$$

Here, ΔV_1 and ΔV_2 can be found as -2 and -10, respectively. Finally, $V_1 = 3 - 2 = 1$ and $V_2 = 7 - 10 = -3$. These values will make E_1 and $E - 2$ zero, as expected. However, an off design iteration will not be this simple. It may require more than hundred iterations, depending on initial guesses. Yet, the calculation procedure is as given in this section.

3.4.3.2. Guesses and Errors Number of iteration variables and errors depends on the engine configuration and number of components. In this part, a 2 spool turboshaft engine will be explained by comparing it to a turbojet configuration from time to time. Figure 3.13 shows the guesses and errors for a 2 spool turboshaft engine.

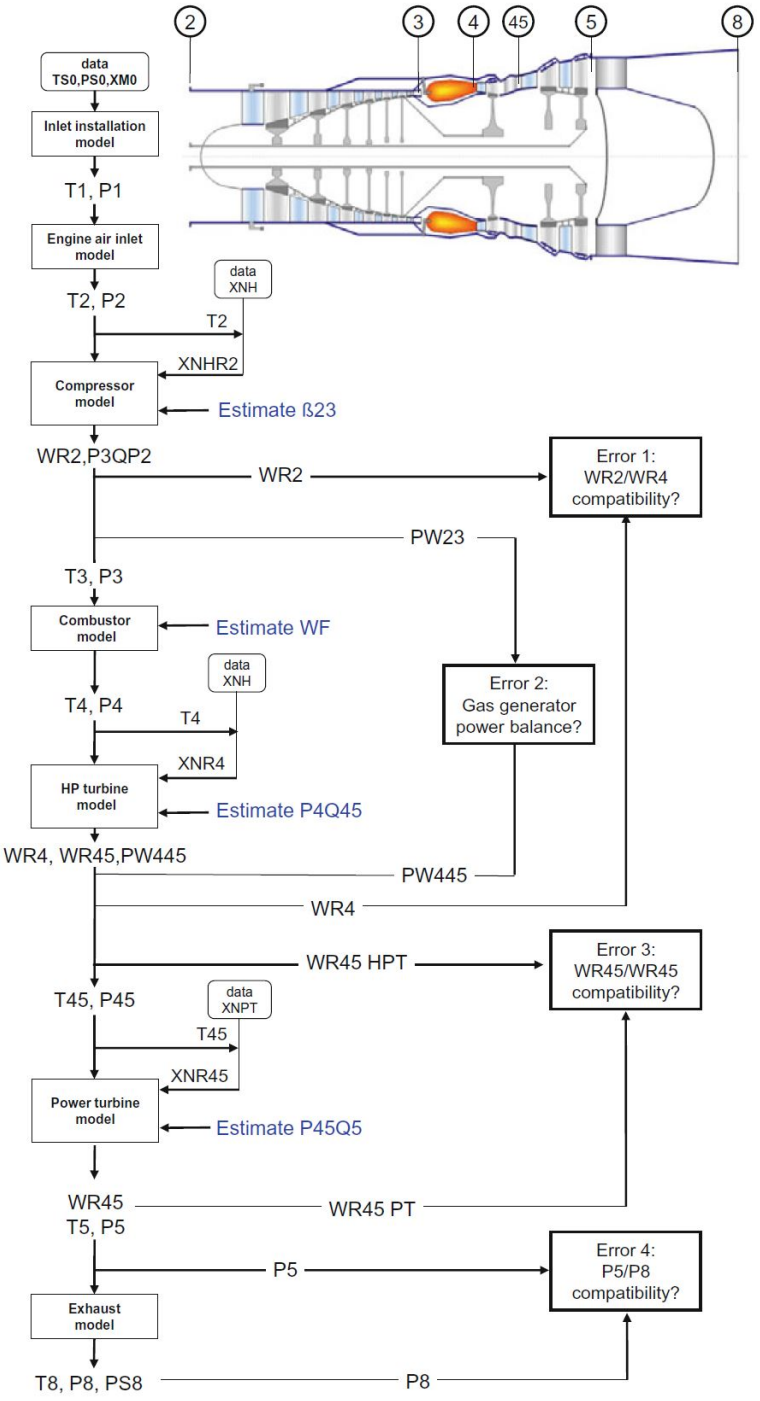

Figure 3.13 Newton-Raphson Approach for a 2 Spool Turboshaft Engine [3]

As it can be seen here, $\beta_{Compressor}$ is the first guess. This guess picks an operating point for compressor on the map which means the mass flow rate, pressure ratio and efficiency of the compressor is now defined. The second guess is fuel mass flow rate, $\dot{W}_{fuel}$. This guess sets

T_4 and FAR. With considering cooling bleeds, HPT inlet conditions are now defined. $\dot{W}_{41}$ can be calculated by using actual mass flow rate, station temperature and pressure. β_{HPT} is the third guess. Correspondingly, the turbine generated power can be calculated. Compressor power and turbine power inconsistency is the second error. $\dot{W}_{41}$ can be read from turbine map, as well. Incompatibility between two $\dot{W}_{41}$ sources brings the third error. Last guess is β_{PT}. After, required $\frac{P_8}{P_{amb}}$ to pass the flow can be calculated. This requires P_5 to have a specific value. Initial β_{PT} will not provide that specific value. Fourth error reveals itself at here, as required total pressure $P_{8,req}$ and P_8 calculated in iteration difference.

After founding all the errors, Newton-Raphson algorithm modifies all iteration variables as mentioned before, until the convergence criteria is met. GasTurb13 uses $\Sigma Error^2 > 10^{-8}$ as convergence criteria and that is accepted as it is for the developed software.

3.5. Transient Operation

In transient mode, $\dot{W}_{fuel}$ is not a guess, but an input. One iteration variable diminishes. Accordingly, one error should also be cancelled out. Transient operation differs from steady-state operation in power balance between compressor and HPT. There is not such a balance in transient operation and in fact, there should not be for acceleration or deceleration manoeuvres. Difference between HPT generated power and compressor consumed power is named as "Unbalanced Power" and required for transient operation. Unbalanced power/torque reveals due to the excessive/insufficienct fuel feed. If the fuel flow is more than steady-state fuel flow, T4 and T41 will increase. Consequently, HPT will begin to produce more power than demanded by compressor. At each time step, unbalanced power can be calculated with equation (95).

$$UnbalancedPower = Power_{HPT} * \eta_{mech} - (Power_{Compressor} + POT) \tag{95}$$

This unbalanced power will speed up high pressure spool. For insufficienct flow case, opposite will happen and high pressure spool will slow down because HPT will not produce required amount of power to keep the compressor operating at same speed. Acceleration or

deceleration rate is calculated by using unbalanced power, polar moment of inertia and shaft speed as given in equation (96) for each time step.

$$\frac{dn}{dt} = \frac{UnbalancedPower}{(\pi * 2/60)^2 * Inertia * ShaftSpeed} \tag{96}$$

As the spool speed increases, unbalanced power will decrease if the fuel flow kept constant. A step fuel increase can be given as an example. At the beginning, required fuel flow for steady-state operation for current shaft speed and transient fuel flow input is far from each other. So, the excessive fuel flow is dominant at beginning and it will accelerate the spool, rapidly. As the speed increases, delta between required fuel flow for steady-state operation and transient fuel flow input will decrease and as a result, the unbalanced power will decrease. After a certain amount of time the acceleration will stop and engine will operate under steady-state conditions. In other words, transient fuel flow input will be equal to a higher shaft speed's steady-state fuel flow rate and engine will operate at that specific shaft speed, in case of a higher constant fuel flow input. Until reaching the steady-state conditions, engine shaft speed for each time step will be calculated by equation (97). While making these calculations, all other thermodynamic performance properties are being calculated for each time step, as well.

$$NG = NG_{previous} + \frac{dn}{dt} * timestep \tag{97}$$

Usually, engine control systems and fuel pumps have a minor delay. Instant fuel flow increase or a step fuel flow increase can not be reached in practice. An ordinary relation, given in equation (98) [6], can model this behavior and provide actual flow rate by using intended fuel flow input and combustor time constant. This time constant holds the heat release delay like movement of fuel metering device and the needed time for fuel evaporation [4].

$$LaggedValue = \frac{PreviousValue * TimeStep + TargetValue * CombustorTimeConstant}{TimeStep + CombustorTimeConstant} \tag{98}$$

This approach helps to calculate fuel input for each time step. For comparison and validation purpose, time constant value of 0.01 is accepted for 2 Spool Demo Turboshaft model. It could be argued that this is a more realistic version of a step fuel increase.

3.5.1. Heat Sink Model

In steady-state operation of a gas turbine engine there is negligible level of heat transfer between the gas path and the engine carcass. During transient acceleration manoeuvres, metallic parts absorb some energy from hot gas. All off the fuel energy is not used to heat the flow, some part of it is soaked by the metal. While deceleration, opposite is valid. This effect can be taken into account for all stations. However, it is most dominant in HPT inlet due to the largest temperature gradients. Convective heat transfer from the gas to the metal parts, given with equation (99), is proportional to the heat transfer coefficient h, the surface area A_m and the difference between the gas and metal temperature ($T_{g,i} - T_m(t)$).

$$Q = h * A_m * (T_{g,i} - T_m(t)) \tag{99}$$

Equation (100) shows the relation between metal temperature change due to temperature difference between the gas and metal temperatures.

$$c_{p,m} * M * \frac{dT_m}{dt} = h * A_m * (T_{g,i} - T_m) \tag{100}$$

Owing to the conservation of energy, absorbed heat by the metal should be equal to the transferred energy from gas flow. Gas temperature change due to the heat sink effect can be seen in equation (101).

$$c_{p,g} * \dot{W}_g * (T_{g,i} - T_{g,o}) = c_{p,m} * M * \frac{dT_m}{dt} \tag{101}$$

Ballin's work includes the heat sink model provided by GE for T700-GE-700 engine. It calculates the ratio of T41 with heat sink effect and without heat sink effect ($T41_{ns}$) and given with equation (102).

$$\frac{T_{g,o}}{T_{g,i}} = \frac{T_{41}}{T_{41,ns}} = \frac{(\frac{M*c_{p,m}}{h*A_m} - \frac{M*c_{p,m}}{W_g*c_{p,g}}) * s + 1}{\frac{M*c_{p,m}}{h*A_m}) * s + 1} \tag{102}$$

The time constant $\frac{M*c_{p,m}}{h*A_m}$ function is given with equation (103). Here, TC_{T41} is an empirically determined constant which is equal to 0.29.

$$\frac{M * c_{p,m}}{h * A_m} = TC_{T41} * \frac{\sqrt{T41_{ns}}}{\dot{W}_{41}^{4/5}} \tag{103}$$

Additionally, value of $\frac{M*c_{p,m}}{c_{p,g}}$, which also named as $T41_{sgn}$ or heat sink constant, is represented as a function of corrected HP shaft spool speed as can be seen from equation (104). This function can be seen from Figure 3.14.

$$T41_{sgn} = f(NG_C) \tag{104}$$

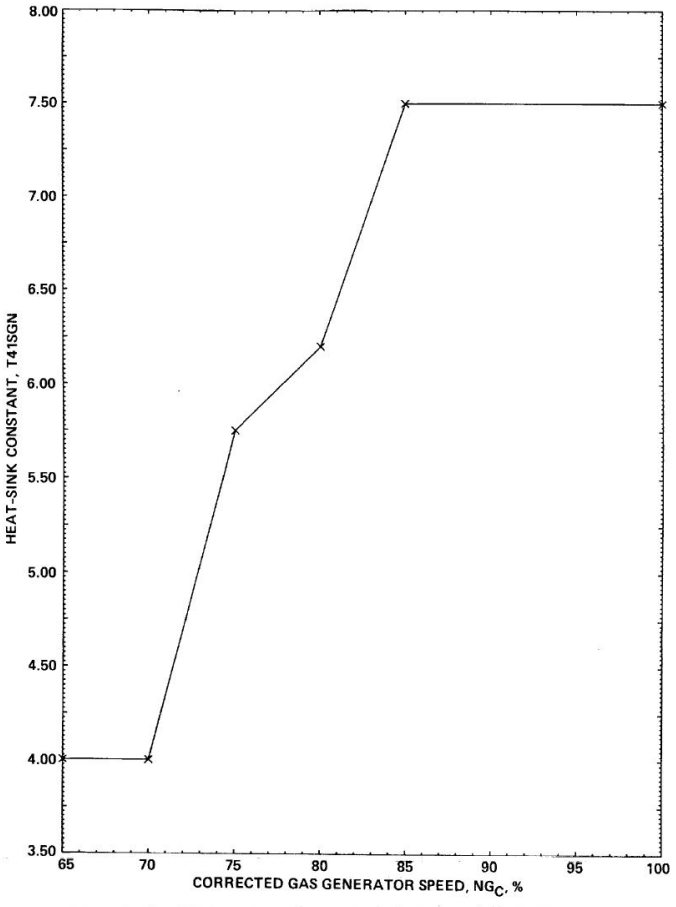

Figure 3.14 T700-GE-700 $T41_{sgn}$, station 41 heat sink constant [7]

Unknown part of the equation (102) now can be found by equation (105).

$$\frac{M * c_{p,m}}{W_g * c_{p,g}} = \frac{T41_{sgn}}{\dot{W}_{41}} \tag{105}$$

Developed software calculates T41 value both with and without heat sink effect for T700-GE-700 model in transient mode. 2 Spool Demo Turboshaft model does not include heat soakage modelling.

3.6. Starting Simulation

During an engine development process, using engine performance models broadly helps in terms of budget and time schedule. One part of the operational range of an engine is called starting. Starting can be summarized as the transient process between the pilot or operator command and stabilisation at idle speed and it is one of the toughest gas turbine performance topics [6]. It may involve dry cranking, purging, light off, acceleration to idle and stabilisation phases at idle speed. However, for starting part, physics based performance models are difficult to be created since having component characteristics at sub-idle region is quite difficult [8]. In order to model the sub-idle region, Yepifanov and Sirenko [8] narrates there are two methods. One of them extrapolates components' above-idle performance maps to the sub-idle region and another one approximates the experimental data with various polynomials. Also, Asgari et al. suggests, performance models can be grouped into two categories as white-box and black-box models according to knowledge about system physics [37]. White-box models utilizes complex equations, thermodynamic properties, energy balance and coupled equations belong to the system, while black-box models are used for the cases which detailed information is not accessible. In this study, thermodynamic relations are taken as basis and a component-matching based performance simulation tool was developed. Available component performance characteristics in above-idle region should be extended to lower speeds in order to use the same tool for starting modeling.

For a successful starting attempt, air mass flow rate and pressure in combustion chamber is critical. In order to fulfill these two requirements, a starter mechanism cranks the HP

spool and increases the shaft speed. This phase is named as ”dry” cranking, since no fuel flow is introduced to the combustor at this particular phase. In Figure 3.15, Stage 1 can be accepted as dry cranking, since there is no fuel introduced to combustor and HPT does not generate noteworthy power. At the highest shaft speed reachable by dry cranking, there may be a purging step. Purging helps to dispose unburnt fuel if there are any from previous unsuccessful start attempts to prevent any possible damage. Then, in the light off phase, fuel is introduced to combustor for the first time and igniters are activated. Next, HPT will start to produce power, additional to the starter assistance, and total engine resistance will decrease. Stage 2 in Figure 3.15 shows the effect of fuel on HPT power. HPT cannot produce sufficient power solely both to overcome engine resistances like bearing and windage losses, auxiliary equipment and to supply compressor operation until a certain point, which is called self-sustainable speed. Theoretically, engine can operate by itself after self-sustainable speed, without starter assistance. However, in practice, this is not a steady operable point due to poor combustor exit temperature profiles which can be harmful for turbine life. So, engine continues to accelerate to idle speed, which completes Stage 3 and starting process at the same time. In larger engines, there may be stabilisation or thermal soakage phase to ensure thermal balance along the engine.

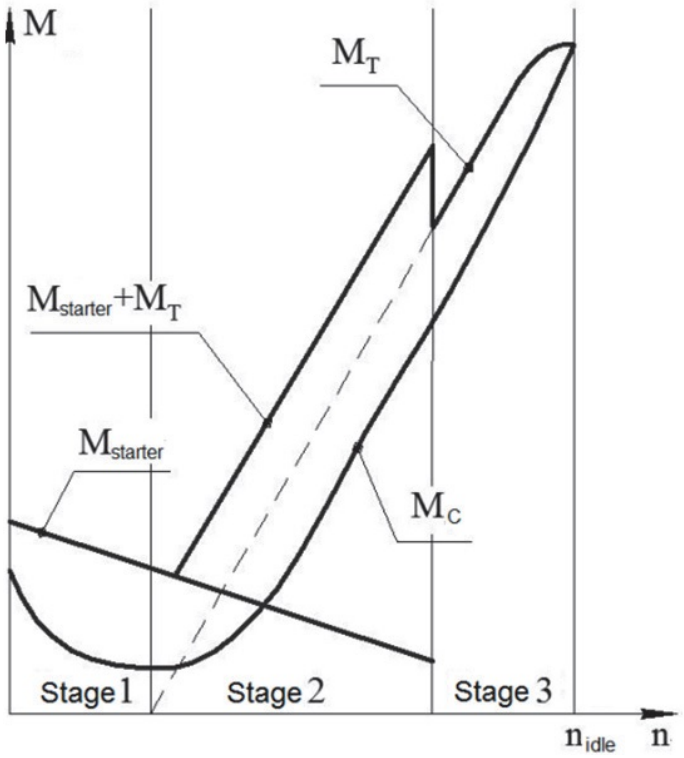

Figure 3.15 Compressor, Starter and Turbine Torque During Engine Start [8]

3.6.1. Starter Characteristics

A more detailed sample chart for starting phase is given in Figure 3.16 from Ref. [6]. Here, engine assistance/resistance curve and starter assistance curves can be seen. Normally, resistance is shown by negative numbers and assistance is shown by positive numbers. However, in this figure starter assistance is shown with negative numbers in order to see the net unbalanced torque or power on HP spool shaft, easily. It can be seen that dry cranking increases the HP spool speed until around 20%. Engine resistance increases with shaft speed, almost linearly. At 20% HP spool speed, light off occasion takes place. Obviously, with light off engine resistance reduces but still engine causes a resistance instead of assistance. With increasing fuel flow and shaft speed, HPT begins to produce power and around 25% shaft speed, engine resistance and assistance becomes equal. As it is previously explained, in theory, hereupon engine can manage to hold the shaft speed steadily. Although, it is not the case in reality. After a while, during engine acceleration, starter power is cutout and HPT

solely increases the shaft speed until idle. Example given in Figure 3.16 marks this point around 33-34% shaft speed. In reality, it depends on engine application. The lower chart in the same figure shows the torque version of the same occasion. It should be noted that maximum starter torque is applied just after the starting while maximum starter power is around the light off.

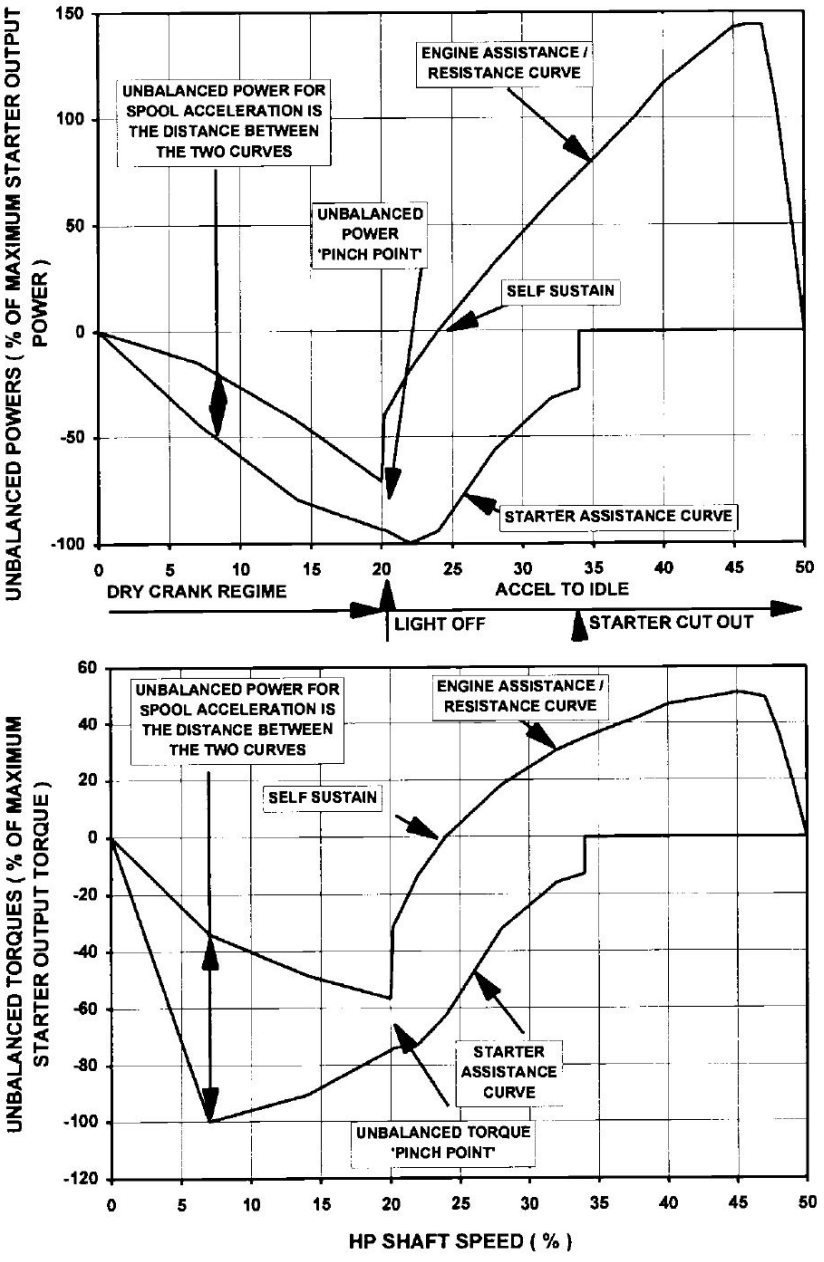

Figure 3.16 Torque and Power on the HP spool during starting [6]

Ref. [9] provides the engine starting characteristics for T700-GE-700 engine as given in Figure 3.17. In case of a light off failure, it shows how the engine resistance continues to increase after light off speed range. It also indicates how engine resistance decreases through warmer ambient temperatures, for all shaft speeds. Additionally, it declares light off and starter cutout speed ranges, minimum required and maximum allowable starter torques for T700-GE-700 engine.

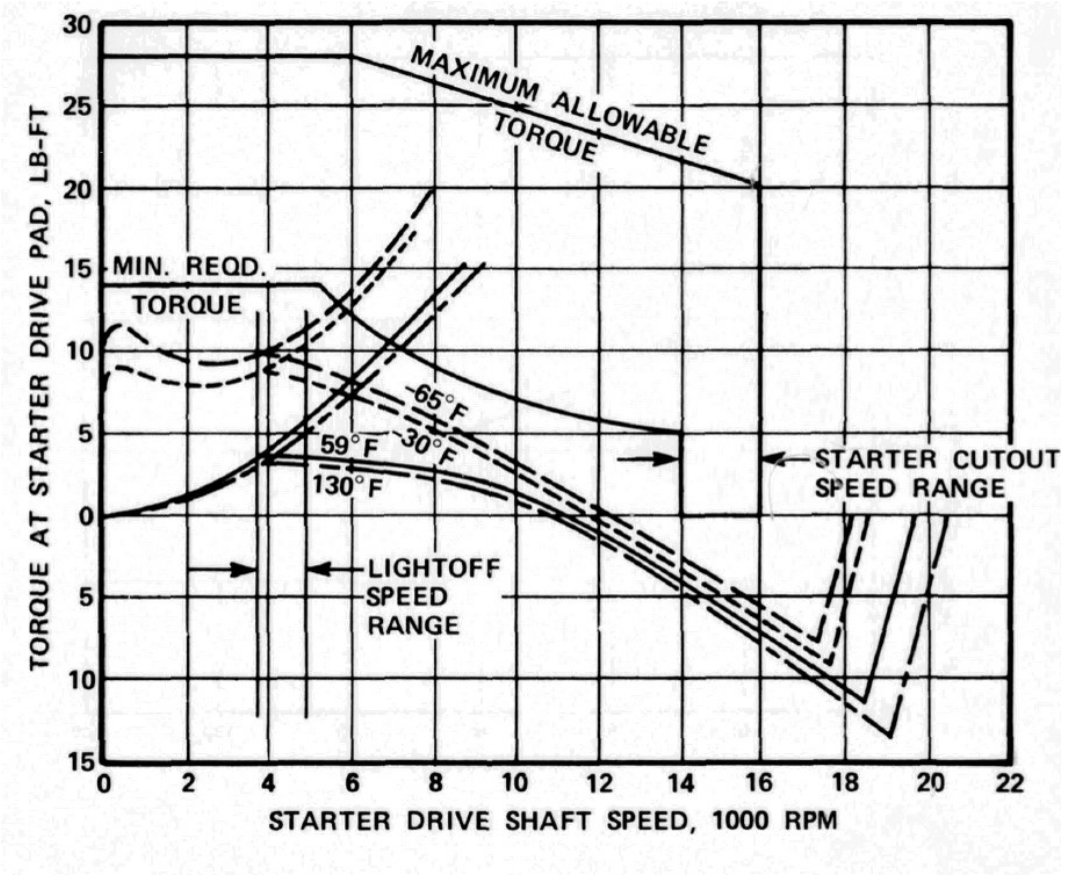

Figure 3.17 Starting torque and speed requirements,SLS conditions, T700-GE-700 engine [9]

Ref. [9] also provides the required time to starter cutout and idle speeds with the engine drag and starter torque characteristics specifically at -25°F (-31.67°C & 241.5K) ambient temperature, which are given in Figure 3.18. It is stated that with this behaviour, starter cutout speed is reached in 8.8 seconds and engine idle is reached in 16.2 seconds. However, fuel schedule information for reaching these values is missing.

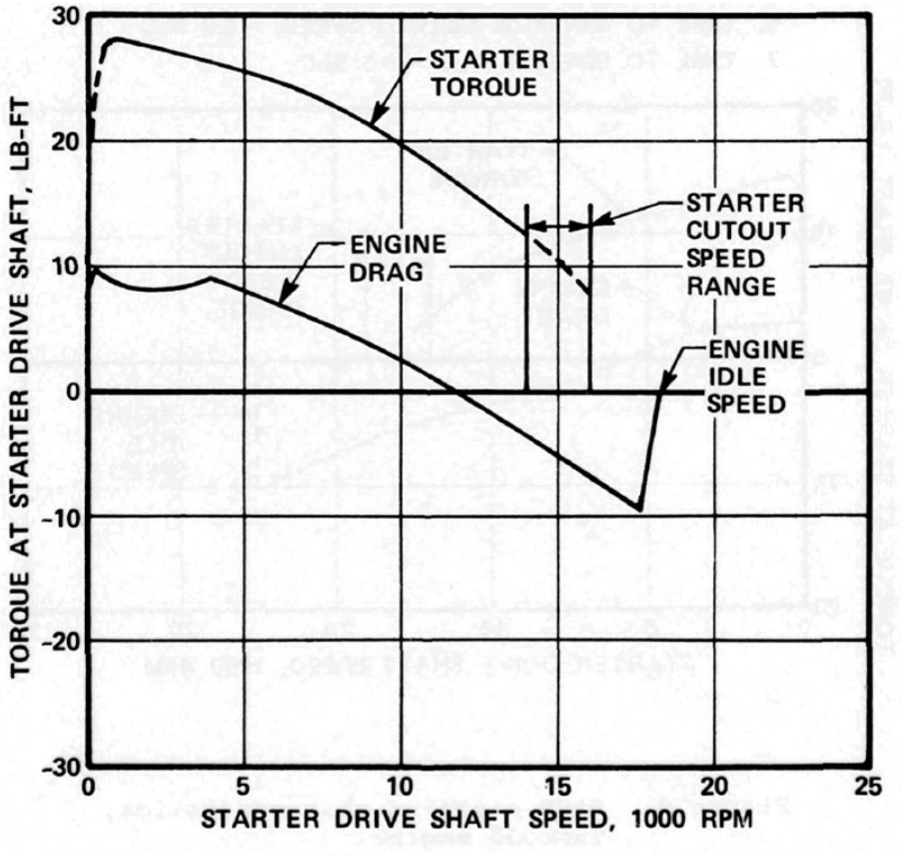

Figure 3.18 Starter Characteristic at SLS conditions -25°F, T700-GE-700 engine [9]

In Figure 3.18, engine idle speed is marked around 18350 rpm at starter drive shaft and engine idle is accepted around 60% HP spool speed ($0.6 * 44700 = 26820rpm$). So, the gear ratio between starter pad and HP spool is around 1.47 ($26820/18350$). By using this gear ratio, starter drive pad speed is converted to HP spool speed. Starter torque (converted to Nm and given in below part of Figure 3.19) and speed is used to calculate starter power. Starter power as a function of HP spool speed is an appropriate performance model input and given in above part of Figure 3.19.

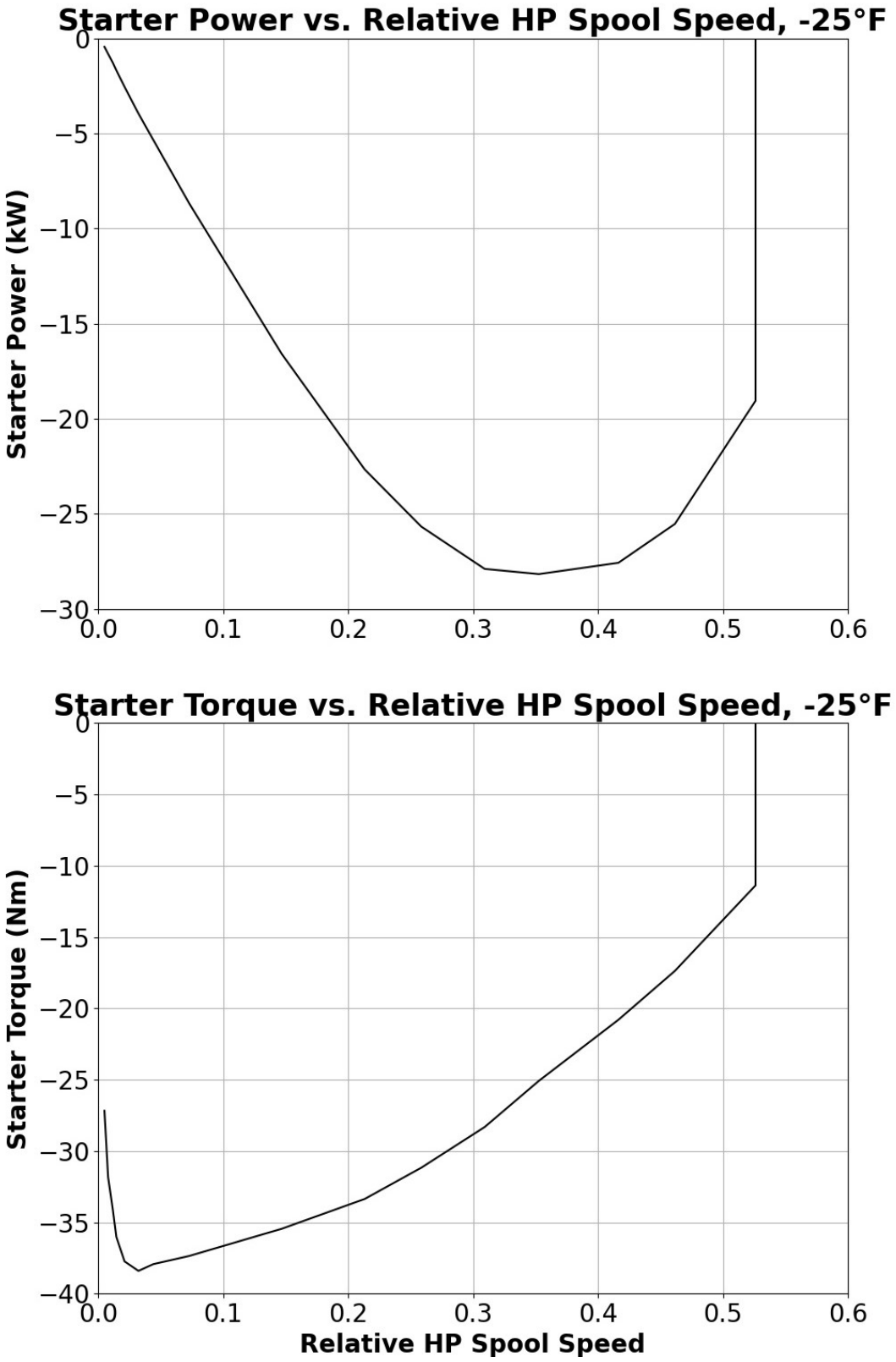

Figure 3.19 Power on the T700-GE-700 HP spool during starting

Moreover, minimum and maximum starter cutout speeds are given as 14000 and 15000 rpm starter drive shaft speed which corresponds to 46 and 52% HP spool speeds, respectively. By using the same gear ratio, light-off speed range is also guessed between 3800 and 4500 rpm of starter drive shaft. Figure 3.18, shows around 4000 starter drive shaft rpm, engine drag starts to decrease. This point, which corresponds to ≈13% (≈6000rpm) of HP Spool speed, is selected as the light-off point.

To be able to create a performance model for starting and perform an analysis, after obtaining starter equipment characteristics, component characteristics should be obtained for sub-idle region. Details of the map extension study will be given in Subsection 3.6.2.

3.6.2. Map Entension Studies

Kurzke proposes a method to describe zero speed line and then interpolate other low speed lines between zero speed line and lowest available speed in performance map [10] [32]. Zero speed torque and pressure losses is derived from correlations in the map. After obtaining zero speed line characteristics, other speed lines are interpolated between zero speed line and available lowest speed line in the map by using correlations and limitations explained in this subsection. First of all, relationship between work and flow coefficients (Ψ and Φ) for a compressor stage which has symmetrical velocity triangles is given with equation (106). This relationship can be used if the leaving gas is following the trailing edge shape.

$$\Psi = 1 - \phi * (tan\alpha_1 + tan\beta_2) = 1 - c_1 * \Phi \tag{106}$$

Where

$$\Psi = \frac{H}{U^2} \quad and \quad \Phi = \frac{V_{ax}}{U} \tag{107}$$

and U, α_1 and β_2 can be seen from Figure 3.6 for a compressor stage.

As long as the leaving gas direction is determined by the blade geometry, the relation given with equation (106) is valid and independent from spool speed. However, in compressible flow region fluid density changes and causes a change in velocity and flow coefficient Φ, as

well. Kurzke examined numerous of component maps [38] and developed a density based correction method for related problem [10]. Flow coefficient can be corrected by $(\frac{\rho(N)}{\rho_{ref}})^{0.5}$ and equation (106) can be used independently from speed, mainly at low speed and Φ values.

Compressor power calculated by equation (50) can also be expressed as shown with equation (108) in terms of flow $\dot{W}$ and specific work H or angular speed ω and torque Trq.

$$Power_{Compressor} = \dot{W} * H = \omega * Trq \tag{108}$$

If equation (108) is rearranged and equation (106) included, equation (109) can be obtained with insignificant constants.

$$\frac{Trq}{\dot{W}^2} = c_2 * \frac{H}{U^2} * \frac{U}{\dot{W}} = c_2 * \frac{1 - c_1 * \Phi}{\Phi} = c_2 * \frac{1}{\Phi} - c_1 * c_2 \tag{109}$$

This results in equation (110) and shows $\frac{Trq}{\dot{W}}$ is a function of rotational speed U and mass flow rate $\dot{W}$.

$$\frac{Trq}{\dot{W}} = c_3 * U - c_4 * \dot{W} \tag{110}$$

Equation (110) implies there is a linear relationship between $\frac{Trq}{\dot{W}}$ and $\dot{W}$ for incompressible part of each shaft speed. This relationship is also valid for zero-speed line. It should be noted that the slope between $\frac{Trq}{\dot{W}}$ and $\dot{W}$ is constant for each speed and can be seen from Figure 3.20. After a certain amount of Mach number for each speed, compressibility effect bends the speed line due to density and therefore the flow coefficient variation. Compressibility becomes less powerful with lower speeds and Mach numbers.

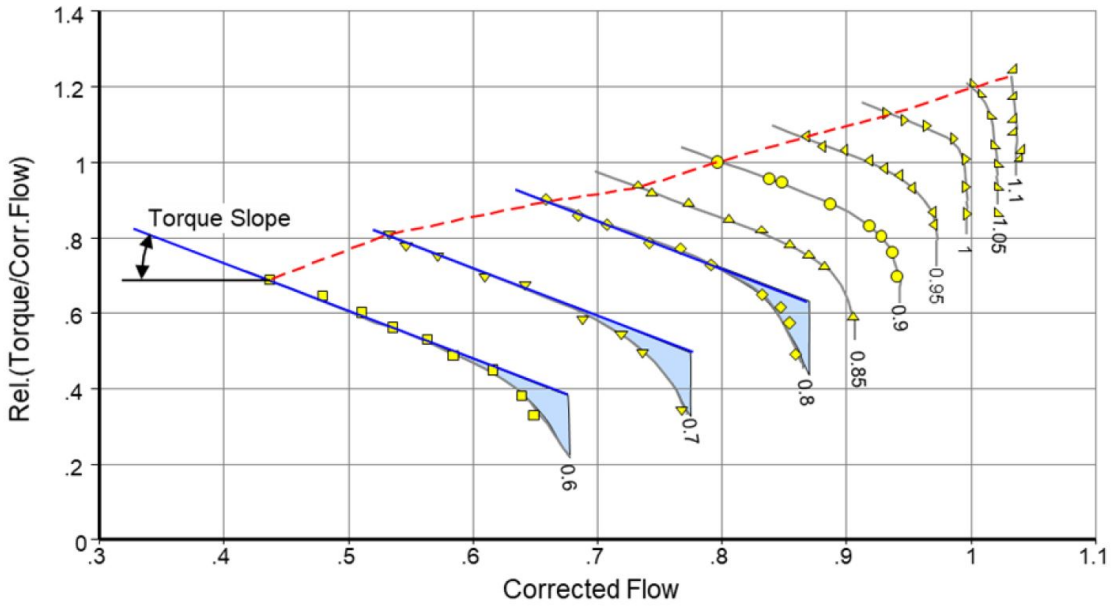

Figure 3.20 Torque/flow lines for a single stage fan [10]

Figure 3.21 shows the torque/flow and flow relationship for all speeds with a sample extended map from Ref. [10]. Here it is clear that the linearity between $\frac{Trq}{\dot{W}}$ and $\dot{W}$ is conserved for all speed lines, not just for above-idle speeds. Moreover, bending due to compressibility is almost neglected for lower speeds.

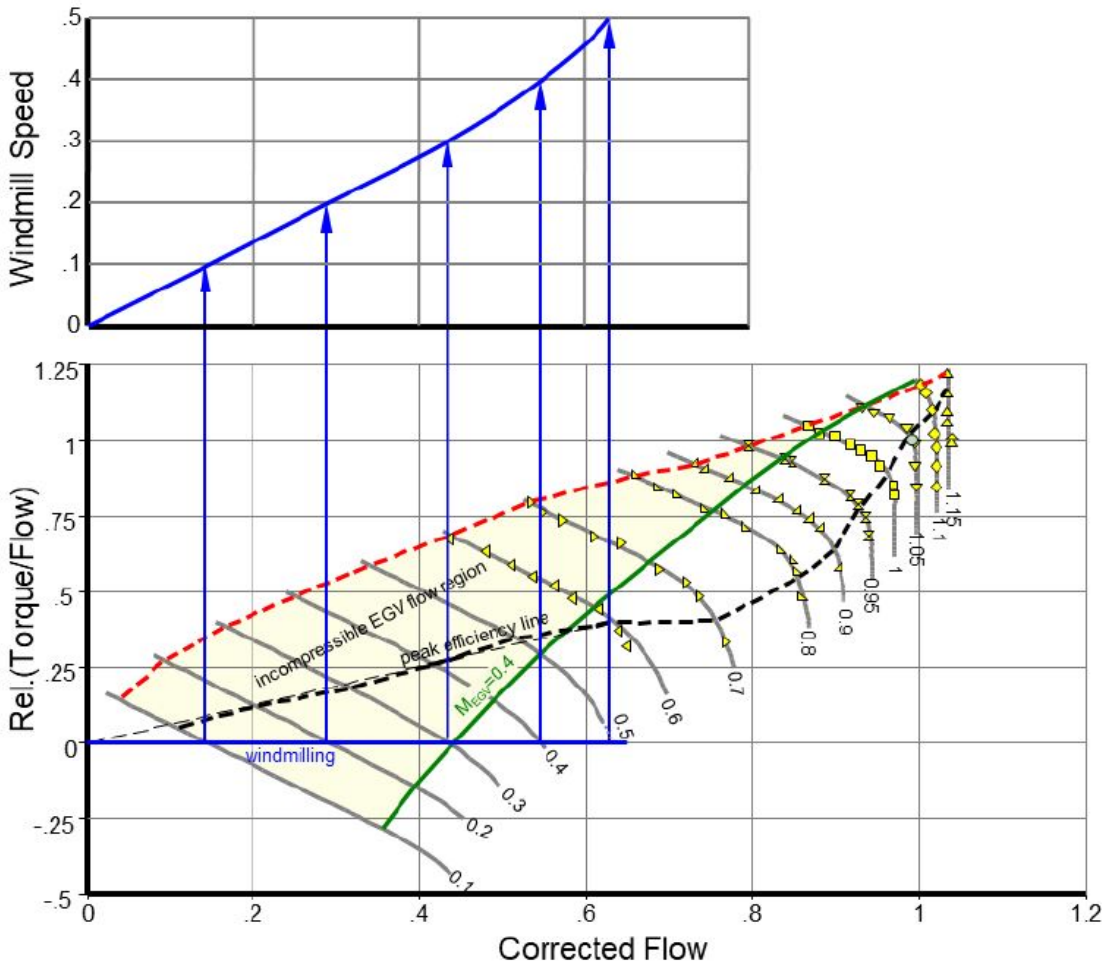

Figure 3.21 Sample extended map with windmilling information [10]

Hereby, T700-GE-700 model component maps are extended towards lower speeds and power pressure ratios considering the $\frac{Trq}{\dot{W}}$ and $\dot{W}$ relationship by using SmoothC [17] and SmoothT [18] software and given by Figures 3.22, 3.23 and 3.24 for compressor, HPT and PT, respectively. $\frac{Trq}{\dot{W}}$ and $\dot{W}$ relationship for extended compressor map can be seen from Figure 3.25

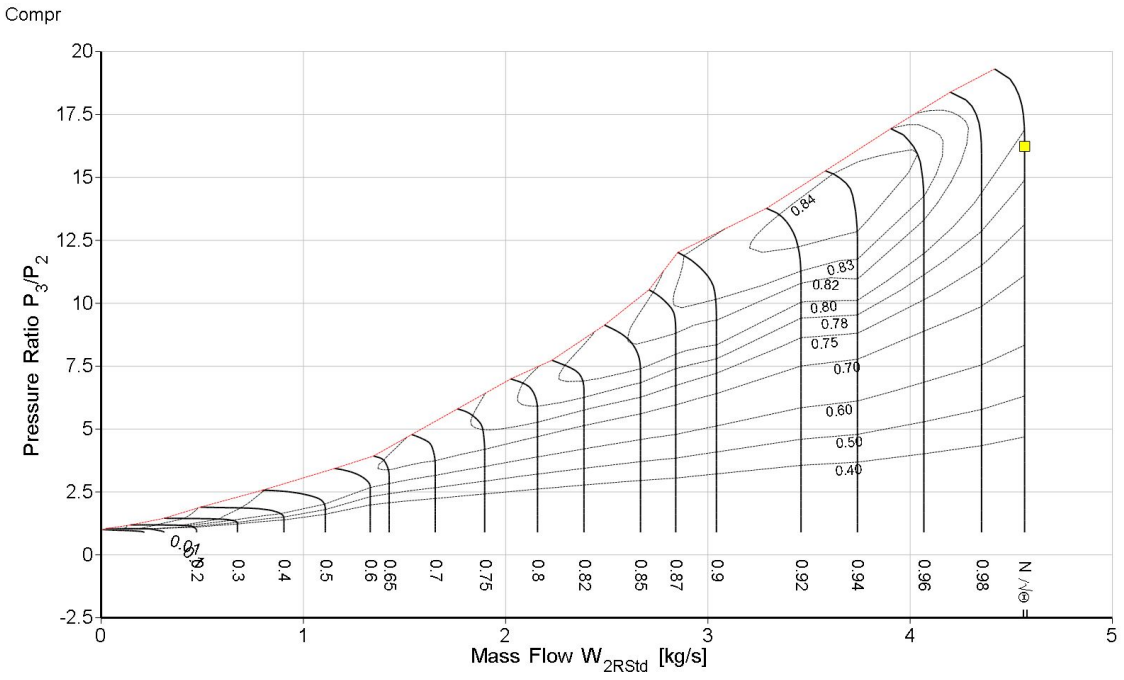

Figure 3.22 Extended T700-GE-700 Compressor Map

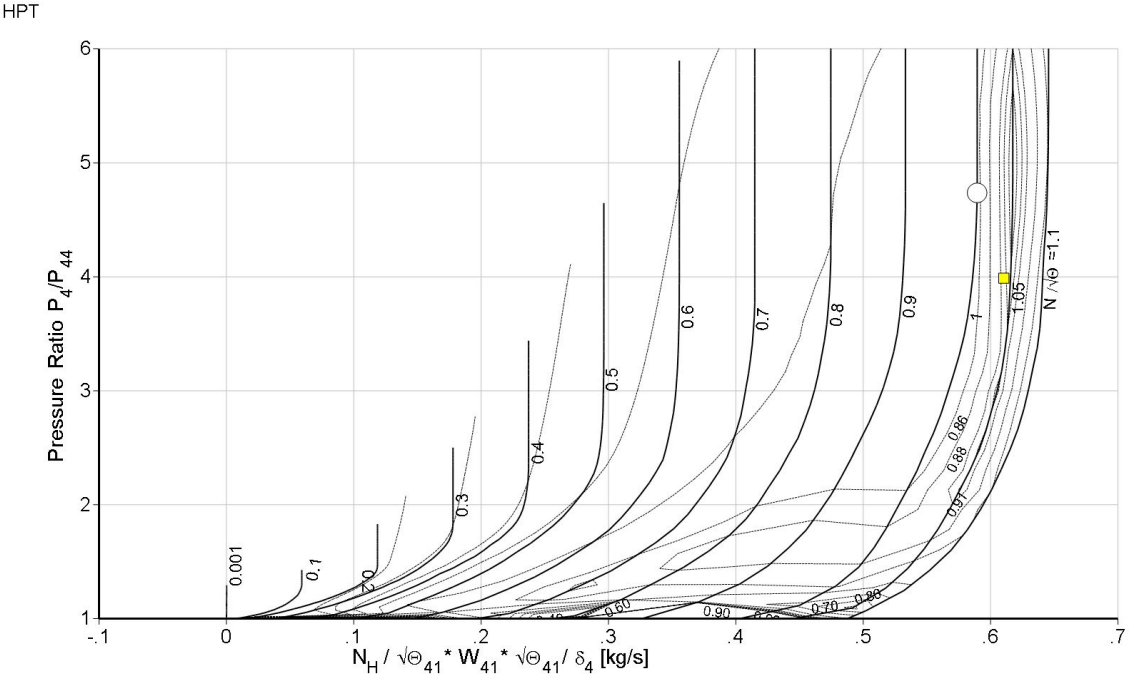

Figure 3.23 Extended Standard GasTurb HPT Map

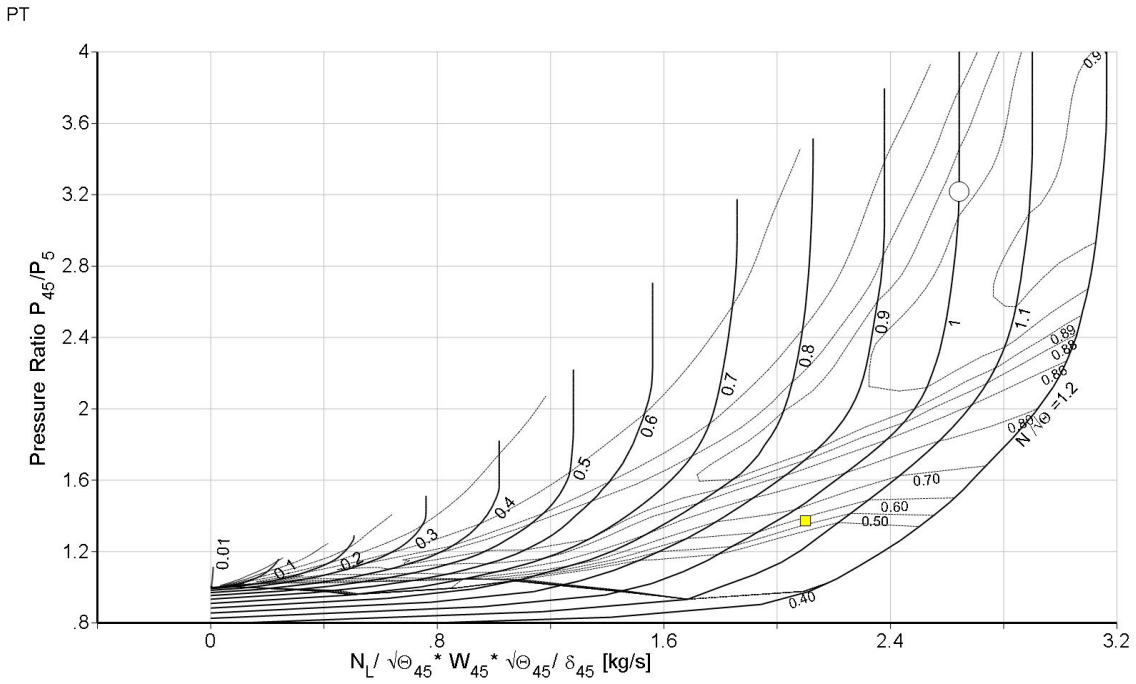

Figure 3.24 Extended Standard GasTurb PT Map

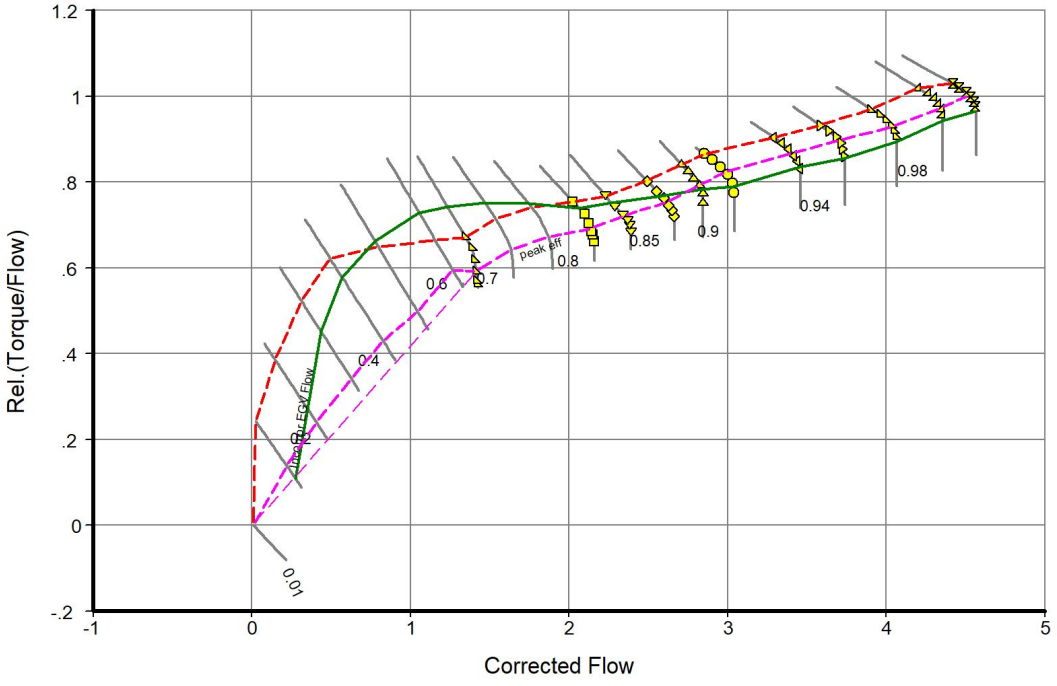

Figure 3.25 Extended T700-GE-700 Compressor Map, $\frac{Trq}{\dot{W}}$ and $\dot{W}$ relationship

Isentropic efficiency becomes negative in low speed region where the pressure ratio is below unity, as Figure 3.26 shows, due to the pressure drop while enthalpy is increasing. Compressor acts like a paddle or turbine and $H_{isentropic}$ becomes negative, when the pressure ratio drops below unity. Additionally, as it can be seen from the same figure, efficiency becomes infinite by definition when the effective/actual specific work H is zero. Efficiency should be replaced by corrected torque parameter in this region for more robust performance calculations [28] [36]. Details of torque usage instead of efficiency parameter will be given in Subsection 3.6.3.

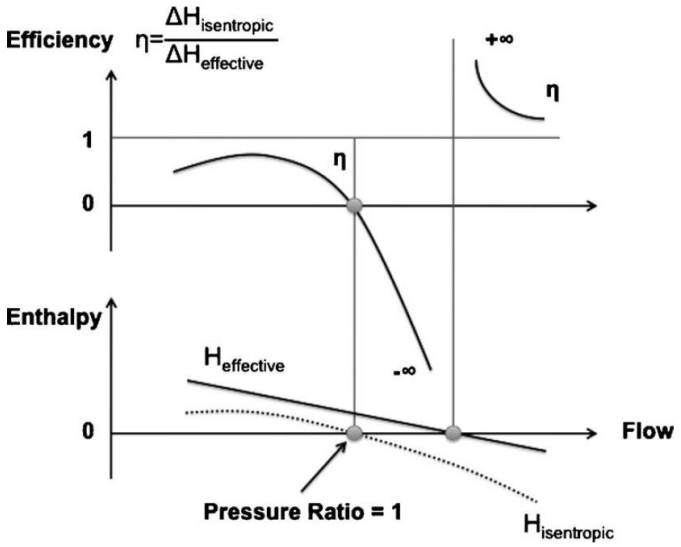

Figure 3.26 Efficiency and enthalpy at low speed conditions [11]

3.6.3. Torque Mode

SmoothC and SmoothT software show the plots including torque values but do not export torque values for speed lines. Moreover, as can be seen from Figure 3.26, efficiency values get extremely steep and not suitable for interpolation operation in lower speeds. Newton-Raphson process will be more robust with corrected torque parameter. Thus, corrected torque values should be calculated by using efficiency values for each β in sub-idle speeds in order to be used as a replacement for efficiency. Calculation showed with Equations from (111) to (118) is repeated for each point in performance map. Aim is to find the

corresponding torque value for each efficiency value in the map. After finding outlet pressure with equation (111), isentropic outlet temperature and enthalpy can be calculated with equations (112) and (113), respectively.

$$P_{out} = P_{in} * PR \tag{111}$$

$$T_{out,isen} = sp2t(s_{in}, P_{out}, FAR_{in}) \tag{112}$$

$$H_{out,isen} = H(T_{out,isen}, FAR_{in}) \tag{113}$$

Equation (114) shows the calculation of actual outlet enthalpy by using η read from performance map.

$$H_{out} = H_{in} + \frac{H_{out,isen} - H_{in}}{\eta_{map}} \tag{114}$$

Actual outlet enthalpy and inlet enthalpy are found. Mass flow rate should also be calculated to continue with Power and Torque calculations. Equation (115) introduces the actual mass flow rate calculation by using corrected mass flow rate read from performance map. Here, attention should be paid to the δ and θ definitions. If the performance map is obtained for reference conditions (SLS ISA), then the δ and θ will be equal to unity.

$$\dot{W}_{in} = \dot{W}_{in,corr} * \delta/\sqrt{\theta} \tag{115}$$

After having $\dot{W}_{in}$, corrected power can be calulated by equation (116).

$$Power_{corrected} = \dot{W}_{in} * (H_{out} - H_{in}) \tag{116}$$

Similar to $\dot{W}_{in}$, actual shaft speed should also be calculated by using corrected shaft speed and compressor inlet temperature as given with equation (117).

$$NG_{mechanical} = NG_{corrected} * \sqrt{\theta} \tag{117}$$

Finally, corrected torque values can be obtained with equation (118).

$$Trq_{corrected} = \frac{60}{2 * \pi} * \frac{Power_{corrected}}{NG_{mechanical} * \delta} \tag{118}$$

After constructing corrected torque map for a component, output will be corrected torque for each beta and speed value at sub-idle speeds. Then, for each point of interest, actual torque and power can be calculated by equations (119) and (120), respectively.

$$Trq = Trq_{corrected} * \frac{P_{in}}{101.325} \tag{119}$$

$$Power_{compressor} = \frac{Trq * 60}{2 * \pi} * NG_{mechanical} \tag{120}$$

After finding compressor power, compressor exit enthalpy can be found by equation (121) for each operating point of interest.

$$H_{exit} = H_{in} + \frac{Power_{compressor}}{\dot{W}_{in}} \tag{121}$$

Remaining calculations like T_{out} and s_{out} can be done after obtaining outlet enthalpy value without an issue.

4. RESULTS

4.1. Design Point Results

A sample design point calculation is performed with the developed software. For validation of the software, GasTurb®13's *Demo 2 Spool Turboshaft Design Point* inputs were used. These inputs are given in Table 4.1.

Table 4.1 Design Point Inputs

Group	Parameter	Value	Group	Parameter	Value
Ambient Conditions	Altitude	0 m	Secondary Air System Network	HPTNGV	0%$\dot{W}_2$
	ΔT from ISA	0 K		HPTROTOR	5%$\dot{W}_2$
	#Ma	0		PTNGV	0%$\dot{W}_2$
Turbomachinery Inputs	$W2_{corr,DP}$	3.5 kg/s		PTROTOR	1%$\dot{W}_2$
	$PR_{Inlet,DP}$	0.99		Overboard	0.5%$\dot{W}_2$
	$PR_{Compressor,DP}$	13		$H_{rel,overboard}$	1
	$\eta_{Compressor,DP}$	0.82		$H_{rel,coolingPTNGV}$	0.6
	$\eta_{HPT,DP}$	0.85		$H_{rel,coolingPTRotor}$	0.6
	$\eta_{PT,DP}$	0.89	Duct Inputs	$\Delta P_{Combustor,DP}$	3%
Combustor Inputs	$T4_{DP}$	1450 K		$PR_{InterTurbDuct,DP}$	0.975
	$\eta_{Combustor,DP}$	0.999		$PR_{ExhaustDuct,DP}$	0.98
	FHV	43.124 MJ/kg		$\frac{P8}{Pamb}$	1.03
	T_{ref}	288.15 K	Mechanical Inputs	POT	30 kW
	T_{fuel}	288.15 K		$\eta_{Mech_{HPShaft,DP}}$	0.998
	P_{fuel}	101.325 kPa		$\eta_{Mech_{LPShaft,DP}}$	0.978

Results can be seen in Table 4.2. All the station parameters are in consistency. Compressor outlet temperature (T_3) difference between two result is below 0.5 K. HPT outlet temperature

(T_{43}) difference is around 0.6 K. Temperature decrease between Station 43 and Station 44 is also in line. Present model predicted much the same amount of cooling with GasTurb13 for the same input. Calculated HPT and PT expansion ratios are also accurate. Power and fuel consumption consistency is remarkable.

Table 4.2 Design Point Result Comparison

	Software	**GasTurb**	**Present Model**	**GasTurb**	**Present Model**	**GasTurb**	**Present Model**
		Ẇ [kg/s]		**T [K]**		**P [kPa]**	
Station Number	**amb**	-	-	288.15	288.15	101.325	101.325
	1	3.465	3.465	288.15	288.15	101.325	101.325
	2	3.465	3.465	288.15	288.15	100.312	100.312
	3	3.430	3.430	657.99	658.45	1304.05	1304.05
	31	3.240	3.240	657.99	658.45	1304.05	1304.05
	4	3.314	3.314	1450	1450	1264.93	1264.93
	41	3.314	3.314	1450	1450	1264.93	1264.93
	43	3.314	3.314	1120.44	1121.06	332.922	333.171
	44	3.487	3.487	1099.22	1099.71	332.922	333.171
	45	3.487	3.487	1099.22	1099.71	324.599	324.842
	49	3.487	3.487	865.76	865.87	106.495	106.495
	5	3.521	3.522	862.51	862.63	106.495	106.495
	6	3.521	3.522	862.51	862.63	104.365	104.365
	8	3.521	3.522	862.51	862.63	104.365	104.365
		Power [kW]		**Fuel Flow Rate [kg/s]**		**PSFC [kg/(kW*h)]**	
	Result	934.9	935.2	0.07376	0.07383	0.28401	0.28420

As per results given with Table 4.2, Design Point mode is validated. Off Design mode results will be given in Subsection 4.2.

4.2. Off Design Results

In order to validate the off design mode of developed software, it is intended to create a demo performance model and compare the results with GasTurb13. To that end, GasTurb13's "*2 Spool Demo Turboshaft*" model is created with developed software. Inputs for this model and the results will be given in Subsection 4.2.1. Additionally, after validating the software by comparing the produced results to a commercial software, another performance model is created for T700-GE-700 engine. Many details for this engine was obtained from Ballin's work at Ref [7]. This part of the study aims to create a consistent engine performance model before extending the performance maps and create an engine starting model. Off Design study is the first leg for that purpose. Details and results for T700-GE-700 engine will be presented in Subsection 4.2.2.

4.2.1. 2 Spool Demo Turboshaft Results

After validating design point study for this demo model, a steady-state off design study has been performed. Component performance maps are taken from GasTurb13 and given below in Figures 4.1, 4.2 and 4.3 for compressor, HPT and PT, respectively.

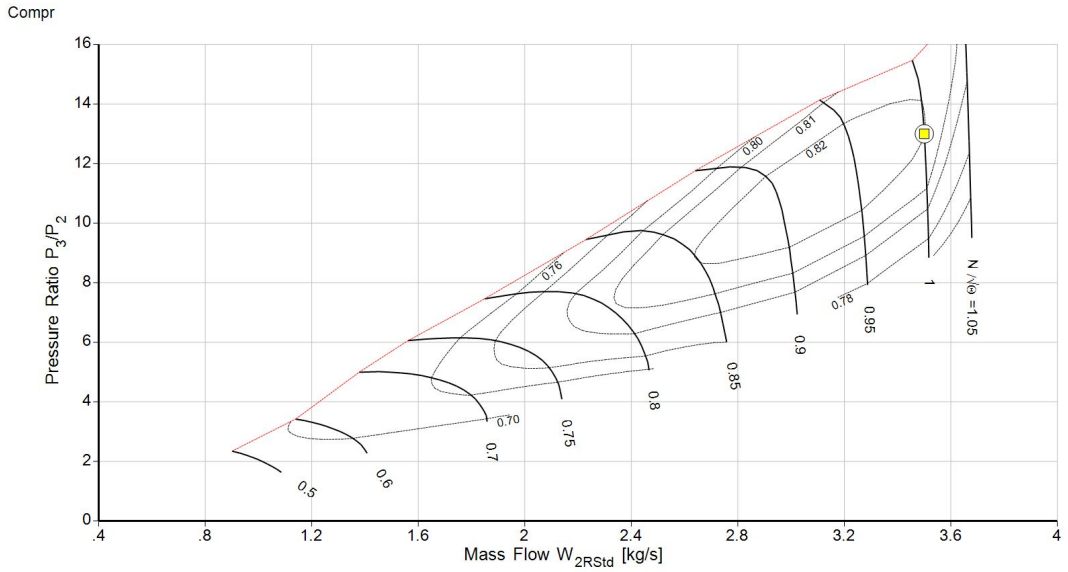

Figure 4.1 Standard Compressor Map from GasTurb

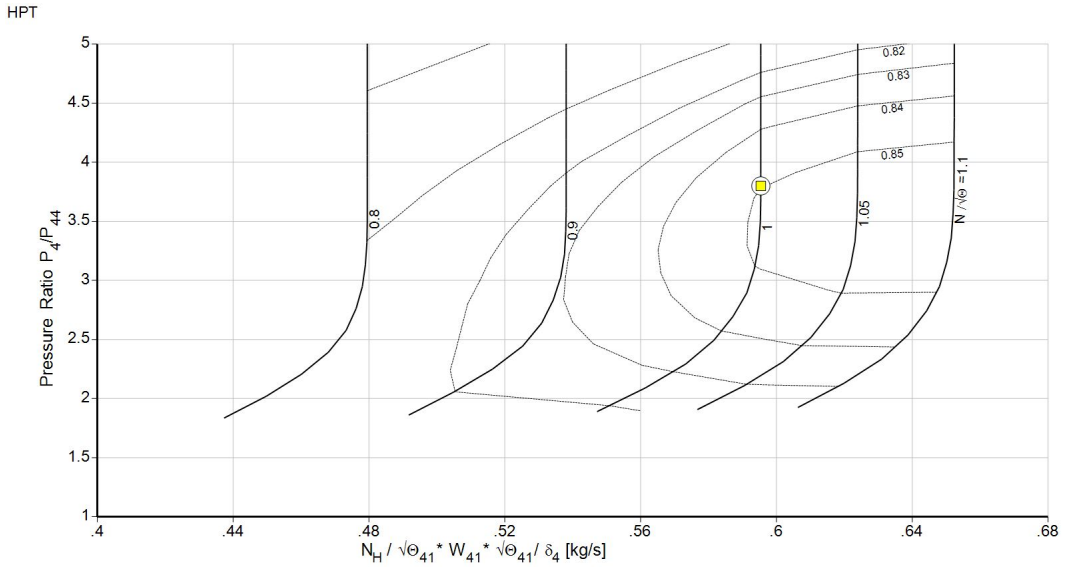

Figure 4.2 Standard HPT Map from GasTurb

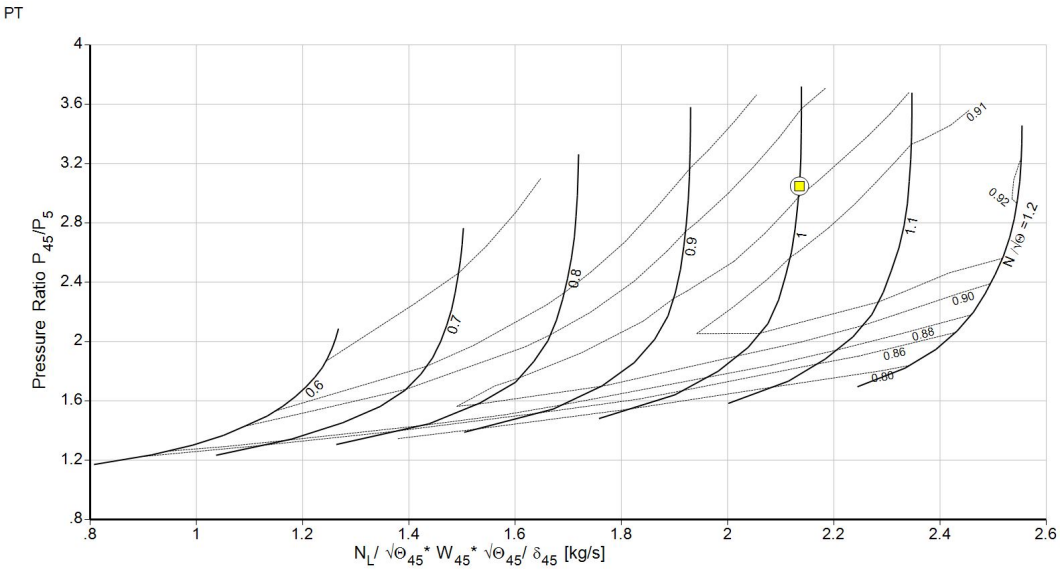

Figure 4.3 Standard PT Map from GasTurb

85% relative spool speed at sea level static conditions is selected as the comparison point. Table 4.3 presents the off design mode inputs for 2 Spool Demo Turboshaft model.

Table 4.3 2 Spool Demo Turboshaft Model Inputs for Off Design Condition

Group	Parameter	Value	Group	Parameter	Value
Ambient Conditions	Altitude	0 m	Secondary Air System Network	HPTNGV	$0\%\dot{W}_2$
	ΔT from ISA	0 K		HPTROTOR	$5\%\dot{W}_2$
	#Ma	0		PTNGV	$0\%\dot{W}_2$
Mechanical Inputs	POT	30 kW		PTROTOR	$1\%\dot{W}_2$
	$\eta_{Mech_{HPShaft}}$	0.998		Overboard	$0.5\%\dot{W}_2$
	$\eta_{Mech_{LPShaft}}$	0.978		$H_{rel,overboard}$	1
Combustor Inputs	$\eta_{Combustor,DP}$	0.999		$H_{rel,coolingPTNGV}$	0.6
	PartLoadConstant$_{Combustor}$	1		$H_{rel,coolingPTRotor}$	0.6
	FHV	43.124 MJ/kg	Duct Inputs	PR_{Inlet}	0.99
	T_{ref}	288.15 K		$PR_{InterTurbDuct,DP}$	0.975
	T_{fuel}	288.15 K		$PR_{ExhaustDuct,DP}$	0.98
	P_{fuel}	101.325 kPa		$\Delta P_{Combustor,DP}$	3%

Obtained results for 85% relative spool speed at sea level static conditions are given in Table 4.4 for GasTurb13 and developed software, respectively.

Table 4.4 2 Spool Demo Turboshaft Model Output @85% relative spool speed, SLS ISA

	Software	**GasTurb**	**Present Model**	**GasTurb**	**Present Model**	**GasTurb**	**Present Model**
		Ẇ [kg/s]		**T [K]**		**P [kPa]**	
Station Number	**amb**	-	-	288.15	288.15	101.325	101.325
	1	2.599	2.599	288.15	288.15	101.325	101.325
	2	2.599	2.599	288.15	288.15	100.312	100.312
	3	2.573	2.573	590.54	590.79	907.605	907.68
	31	2.430	2.430	590.54	590.79	907.605	907.68
	4	2.475	2.475	1264.78	1264.93	879.228	879.301
	41	2.475	2.475	1264.78	1264.93	879.228	879.301
	43	2.475	2.475	984.43	984.96	239.542	239.638
	44	2.605	2.605	965.93	966.55	239.542	239.638
	45	2.605	2.605	965.93	966.55	233.867	233.974
	49	2.605	2.605	806.63	807.19	104.037	104.039
	5	2.631	2.631	803.55	804.07	104.037	104.039
	6	2.631	2.631	803.55	804.07	102.903	102.904
	8	2.631	2.631	803.55	804.07	102.903	102.904
		Power [kW]		**Fuel Flow Rate [kg/s]**		**PSFC [kg/(kW*h)]**	
	Result	466.1	466.5	0.04541	0.04553	0.35072	0.35132

Off design results for part speed shows similar behavior to design mode results. All thermodynamic properties for all stations are consistent with GasTurb13 results. Maximum absolute percent error is below 0.07%. The biggest difference in prediction between two software is 0.62 K for temperature and 0.11 kPa for pressure. This results proves the developed software is successful from reading the component maps to match the components and calculate all thermodynamic properties. During off design calculations, effect of Reynolds number is included for all components as an addition to design mode. Moreover, duct pressure loss calculations and combustor efficiency calculation were slightly different as mentioned in Subsection 3.4.2.

To check the validity of the code for a comprehensive spectrum, the same comparison was performed for an operating line. A wide range of shaft speeds were scanned and compatibility between present model's results and GasTurb13's outputs was checked. Fuel flow rate, combustor outlet temperature, specific fuel consumption , compressor temperature ratio (T_3/T_2) and compressor surge margin parameters were selected as control parameters. Results can be seen from Figures 4.4 to 4.8. All parameters seem to be in harmony. No problems were detected for steady-state demo model as can be seen from these figures.

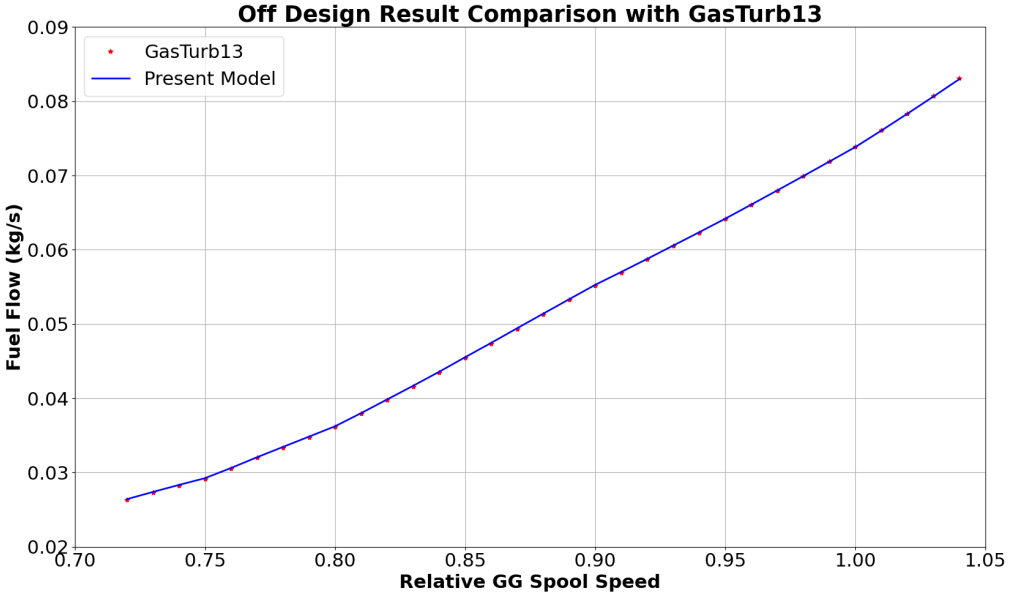

Figure 4.4 2 Spool Demo Turboshaft Fuel Flow vs. Relative Shaft Speed @SLS ISA

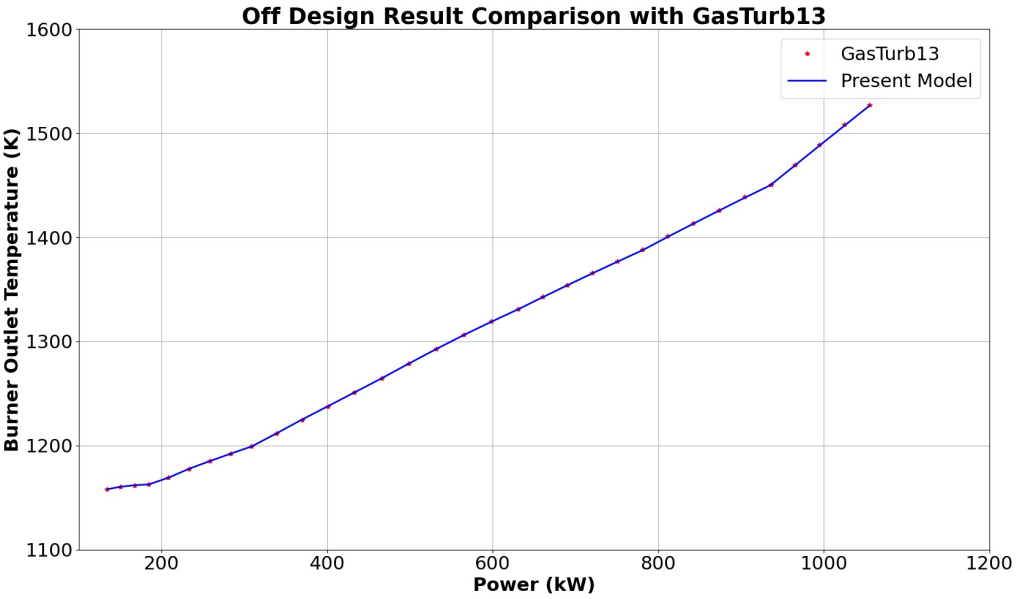

Figure 4.5 2 Spool Demo Turboshaft T4 vs. Power @SLS ISA

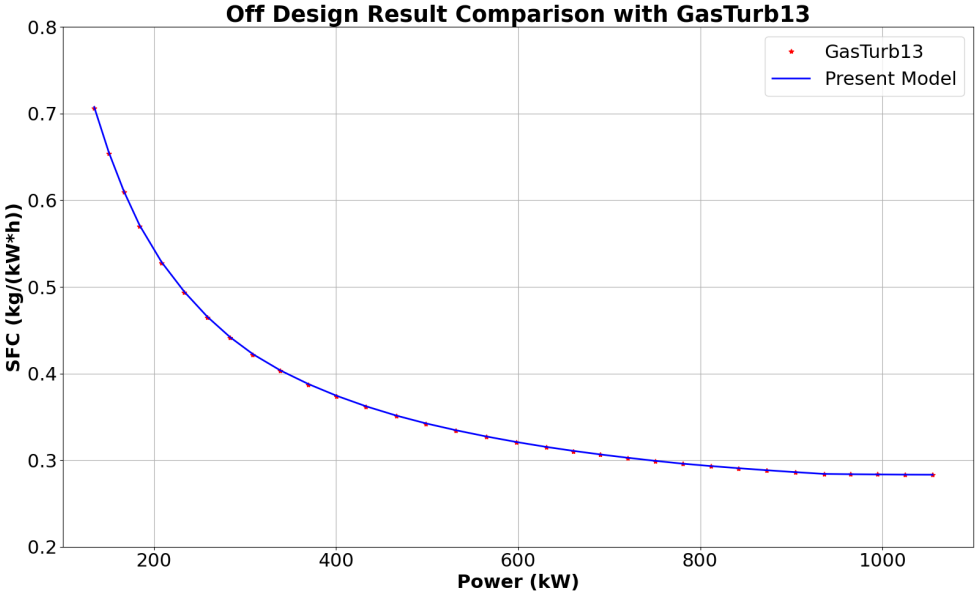

Figure 4.6 2 Spool Demo Turboshaft PSFC vs. Power @SLS ISA

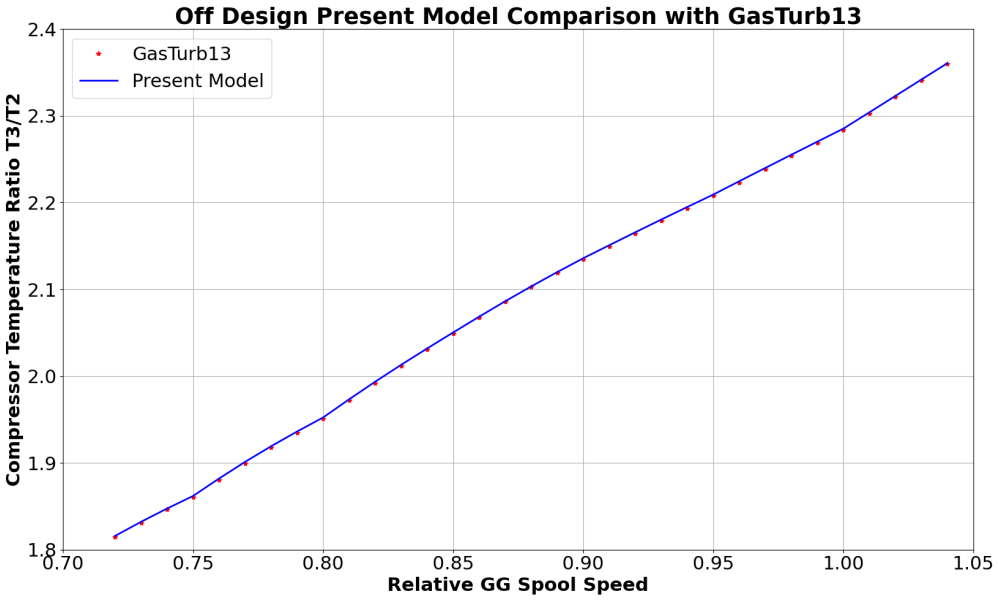

Figure 4.7 2 Spool Demo Turboshaft T3/T2 vs. Relative Shaft Speed @SLS ISA

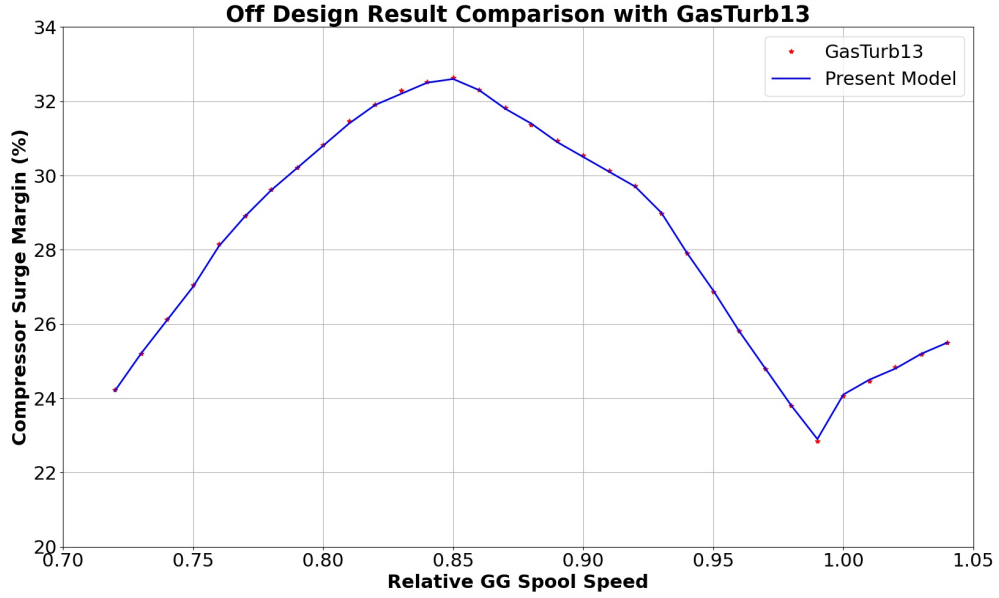

Figure 4.8 2 Spool Demo Turboshaft Surge Margin vs. Relative Shaft Speed @SLS ISA

4.2.2. T700-GE-700 Results

Mark G. Ballin's work [7] is widely used in this study to create a performance model for T700-GE-700 engine. His work basically focused on developing a real time engine performance model and provided the results by comparing them to reference software results which are provided by GE. Ballin uses basic correlations in order to speed up the process and make it a usable software for engine controlling. Additional to these specific correlations, compressor map is also provided in this study and given in Figure 4.9.

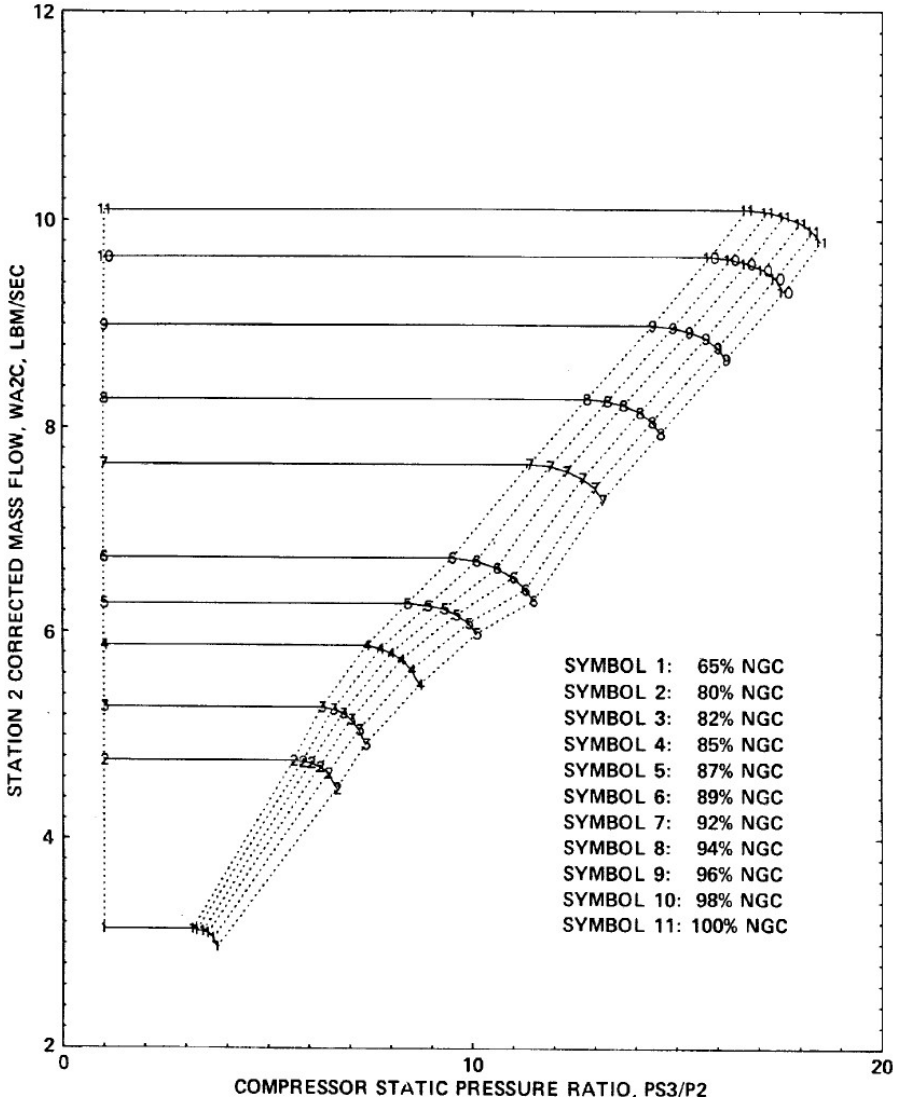

Figure 4.9 T700-GE-700 Compressor Performance Map [7]

Ballin also provided other information like bleed air fraction for cooling and pressurizing purposes, constant $\eta_{combustor}$ of 0.985, exhaust pressure ratio (P_{49}/P_{amb}) as a function of corrected spool speed. All details are not presented in here to avoid confusion. However, all the necessary information is taken from that source.

For validation of his real-time model, Ballin used 2 different models (Unbalanced Torque Model and Status-81 Model) which are provided by GE. Comparison of present model's results, Ballin's real-time model and other 2 models by GE can be seen in Figure 4.10, Figure 4.11 and Figure 4.12. Results coincides with each other for most of speeds. However, in lower speeds there can be seen a little discrepancy. As it is mentioned in Section 3.4.1.2., HPTs generally work under choked conditions, but not in such lower speeds in some cases. Using standard GasTurb HPT map does not cause any harm in choked region but in such a low speed, actual T700-GE-700 HPT map would be more appropriate to obtain better results. Same small incompatibility can be observed in all 3 figures.

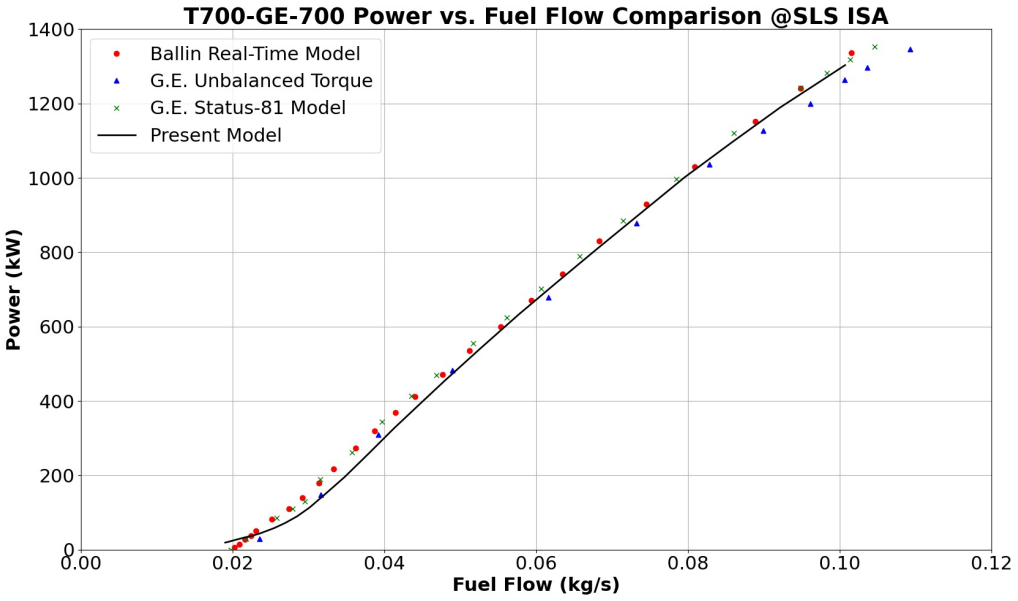

Figure 4.10 T700-GE-700 Power vs. Fuel Flow Comparison @SLS ISA

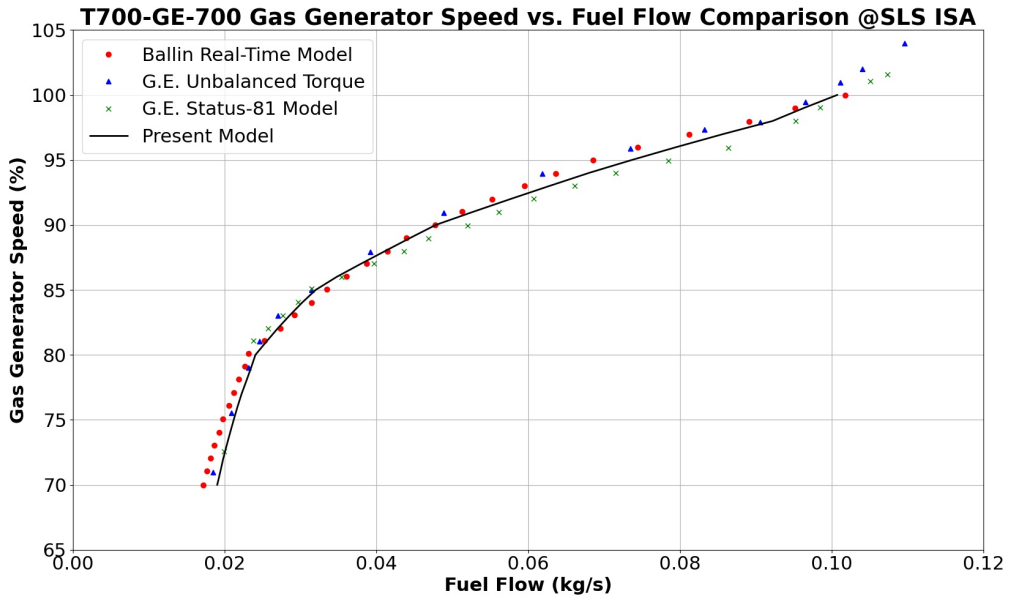

Figure 4.11 T700-GE-700 Gas Generator Speed vs. Fuel Flow Comparison @SLS ISA

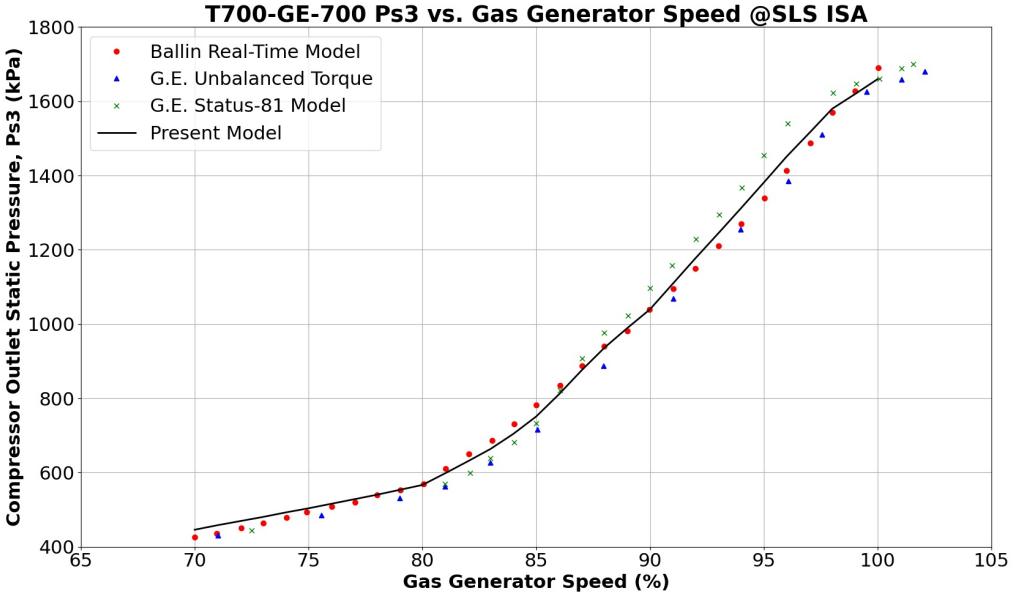

Figure 4.12 T700-GE-700 Compressor Outlet Static Pressure vs. Gas Generator Speed Comparison @SLS ISA

4.3. Transient Operation Results

4.3.1. 2 Spool Demo Turboshaft Results

Inputs for transient manoeuvre are given in Table 4.5. Input fuel schedule calculated by using equation (98) and inputs from Table 4.5 for each time step are given in Figure 4.13. Time step is selected as 0.01 seconds.

Table 4.5 2 Spool Demo Turboshaft Model Inputs for Transient Manoeuvre

Group	Parameter	Value	Group	Parameter	Value
Ambient Conditions	Altitude	0 m	Secondary Air System Network		
	ΔT from ISA	0 K		HPTNGV	0%$\dot{W}_2$
	#Ma	0		HPTROTOR	5%$\dot{W}_2$
Mechanical Inputs	POT	30 kW		PTNGV	0%$\dot{W}_2$
	$I_{HPShaft}$	0.0314785 kg*m^2		PTROTOR	1%$\dot{W}_2$
	$\eta_{Mech_{HPShaft}}$	0.998		Overboard	0.5%$\dot{W}_2$
	$\eta_{Mech_{LPShaft}}$	0.978		$H_{rel,overboard}$	1
Combustor Inputs	$\eta_{Combustor,DP}$	0.999		$H_{rel,coolingPTNGV}$	0.6
	PartLoadConstant$_{Combustor}$	1		$H_{rel,coolingPTRotor}$	0.6
	FHV	43.124 MJ/kg			
	T_{ref}	288.15 K	Duct Inputs		
	T_{fuel}	288.15 K		PR_{Inlet}	0.99
	P_{fuel}	101.325 kPa		$PR_{InterTurbDuct,DP}$	0.975
	$\dot{W}_{fuel,beginning}$	39.8 g/s		$PR_{ExhaustDuct,DP}$	0.98
	$\dot{W}_{fuel,target}$	70 g/s		$\Delta P_{Combustor,DP}$	3%
	$BurnerTimeConstant$	10^{-2}			

Consistency between GasTurb13 and present model fuel flow calculation in each step is exquisite and can be seen in Figure 4.13 for each time step.

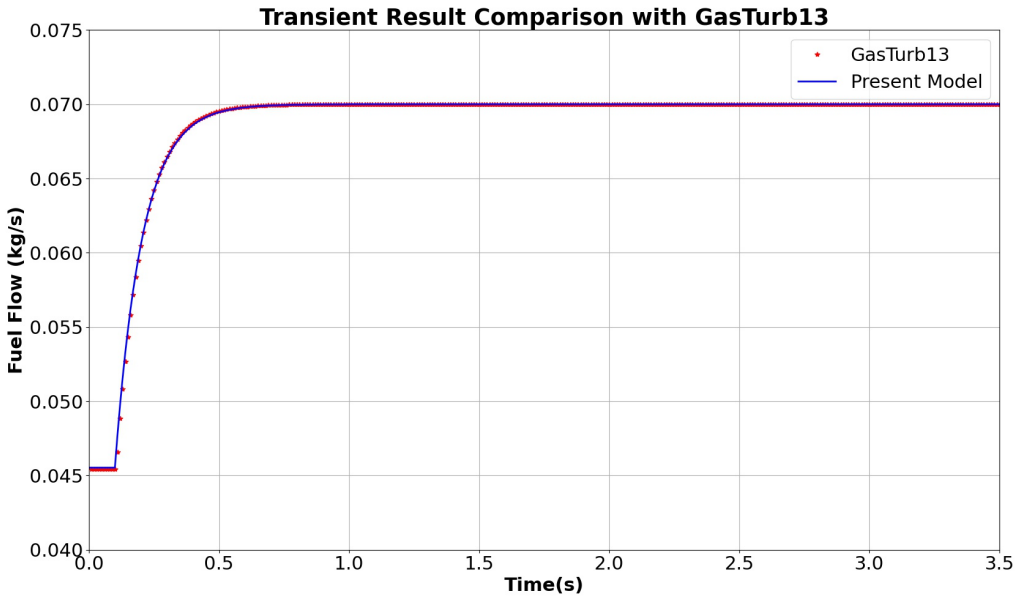

Figure 4.13 2 Spool Demo Turboshaft Acceleration Fuel Flow Input @SLS ISA

For each time step, unbalanced power calculated and presented in Figure 4.14. Maximum unbalanced power during this manoeuvre seems to be around 90 kilowatts. After reaching the maximum value, it starts to decrease immediately. After approximately 3 seconds, it reaches a balance and it can be said that engine starts to operate in steady-state condition.

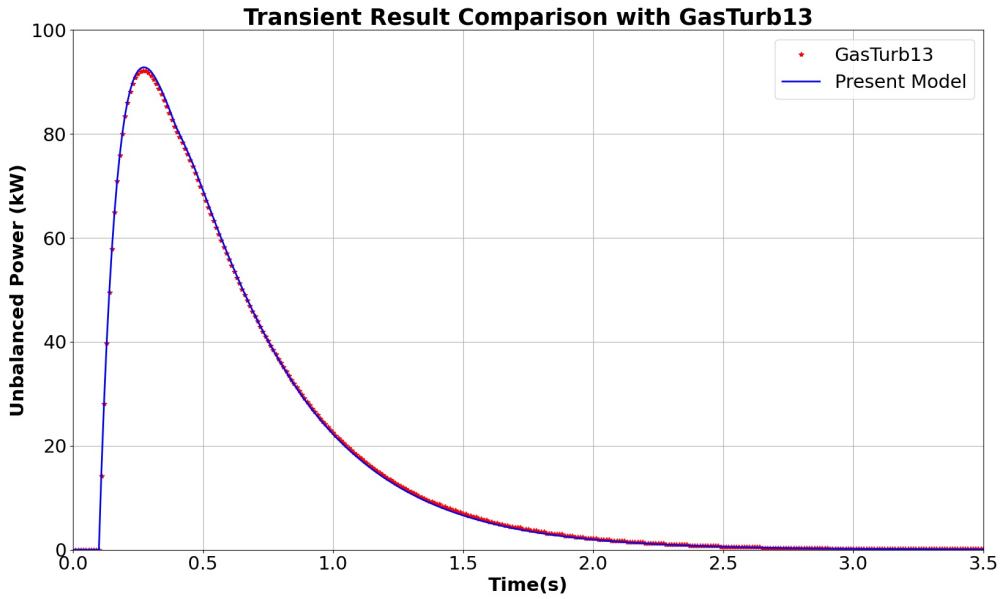

Figure 4.14 2 Spool Demo Turboshaft Unbalanced Power @SLS ISA

Acceleration rate, dn/dt, is a linear function of Unbalanced Power, polar moment of inertia and shaft speed. As a consequence, it behaves in a similar way to Unbalanced Power. Figure 4.15 shows the acceleration rate and Figure 4.16 shows the shaft speed of 2 Spool Demo Model for this manoeuvre. Polar moment of inertia for HP Spool is taken from GasTurb13's default as 0.0314785 $kg * m^2$.

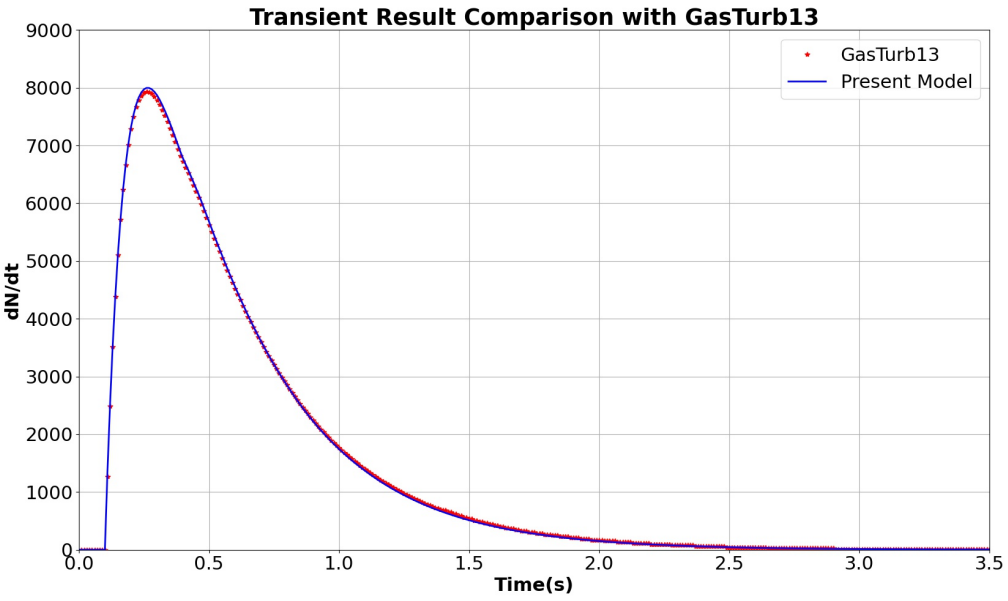

Figure 4.15 2 Spool Demo Turboshaft Acceleration Rate @SLS ISA @SLS ISA

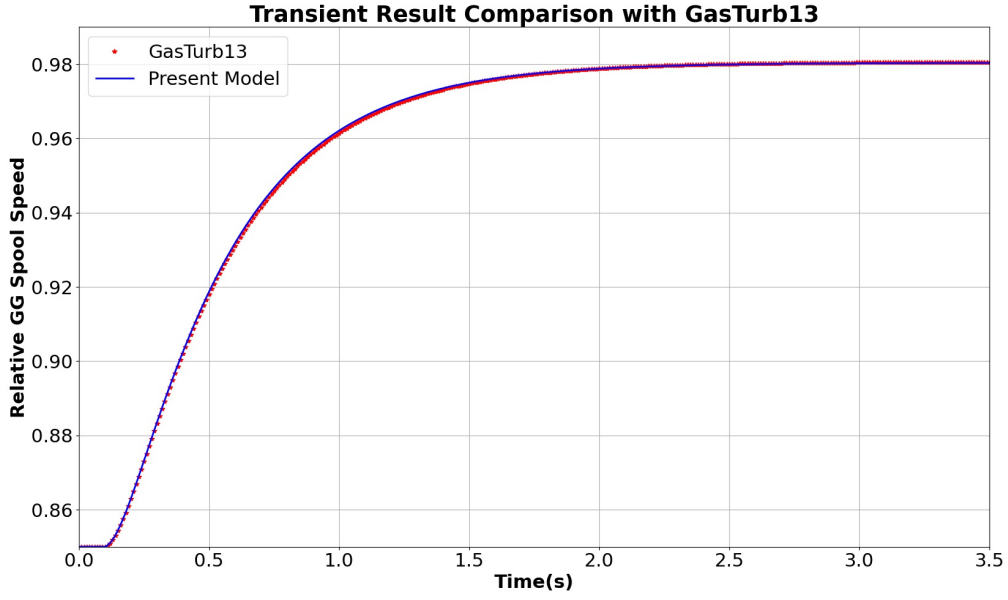

Figure 4.16 2 Spool Demo Turboshaft Shaft Speed @SLS ISA

Combustor outlet temperature and PT inlet temperature are shown in 4.17 and 4.18, respectively. It should be noted that temperature graphs has peak values. So, during transient manoeuvres, there can be a limitation for temperature and fuel schedule may be modified to avoid limit temperature values. Fuel delay smoothens the temperature graphs. In case of excluding fuel delay, T4 and T45 values will jump steeply. Additionally, T700-GE-700

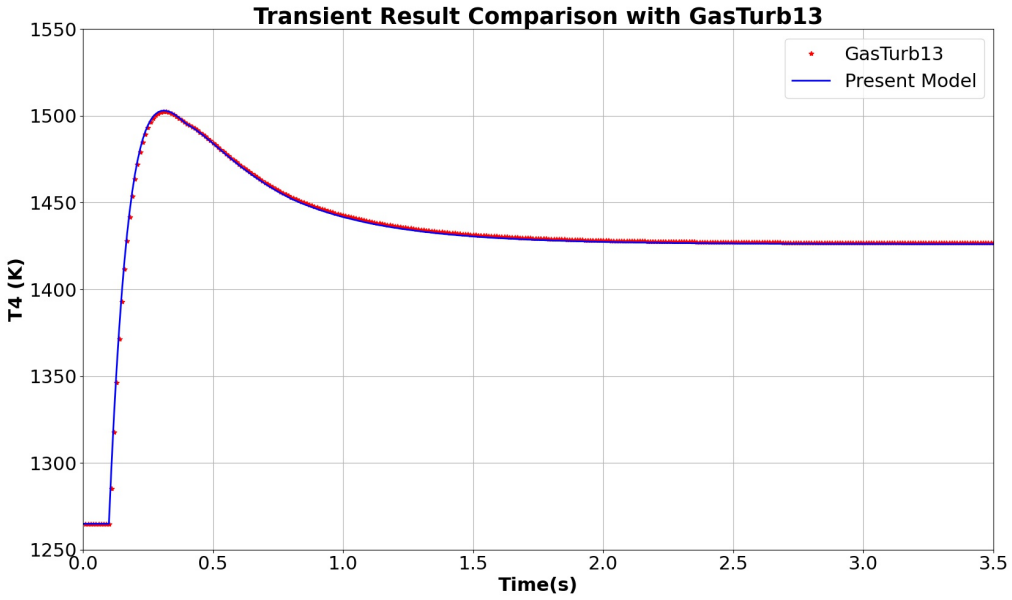

Figure 4.17 2 Spool Demo Turboshaft Combustor Outlet Temperature @SLS ISA

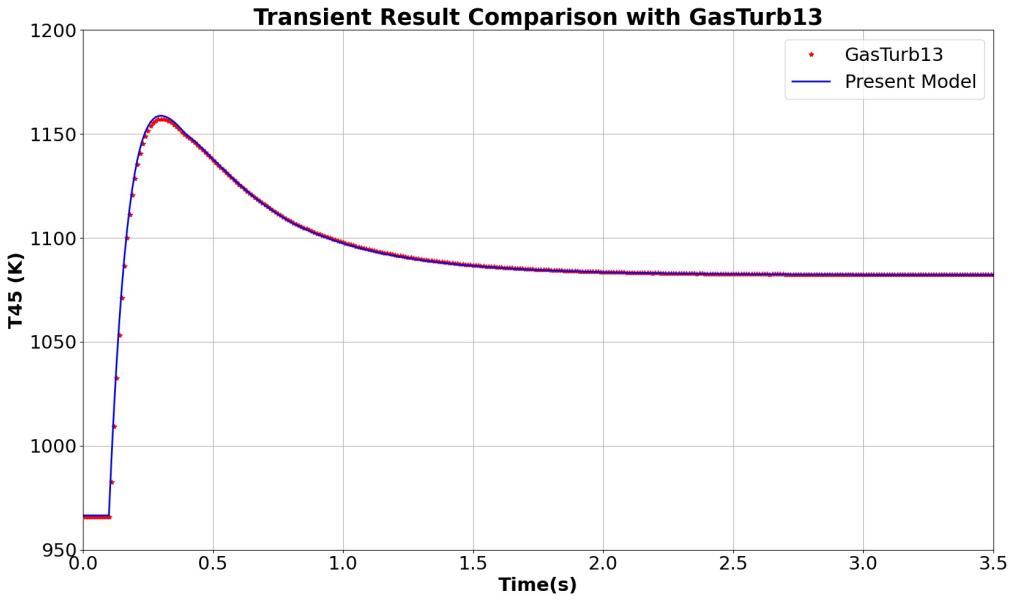

Figure 4.18 2 Spool Demo Turboshaft PT Inlet Temperature @SLS ISA

All figures prove present model produces highly accurate results during for transient operation. Fuel delay, unbalanced power, acceleration rate, shaft speed and station temperatures predicted accurately, with the same inputs and same component maps. This proves the code performing calculations properly.

4.3.2. T700-GE-700 Results

As it is mentioned in Subsection 4.2.2., T700-GE-700 compressor performance map is taken from Ballin's work [7] and presented in Figure 4.9. Turbine maps are taken from GasTurb13's 2 Spool Demo Turboshaft model and they are also presented in Figures 4.2 and 4.3, respectively for HPT and PT. Polar moment of inertia also comes from Ballin's study as 0.0462302 $kg * m^2$. Figure 4.19 shows the results for a given acceleration fuel step input. This model does not include fuel delay in order to make a reasonable comparison. Results with heat sink effect shows substantially matched results, especially for T41 and T45 temperatures. Torque values seem to have a slight offset during acceleration.

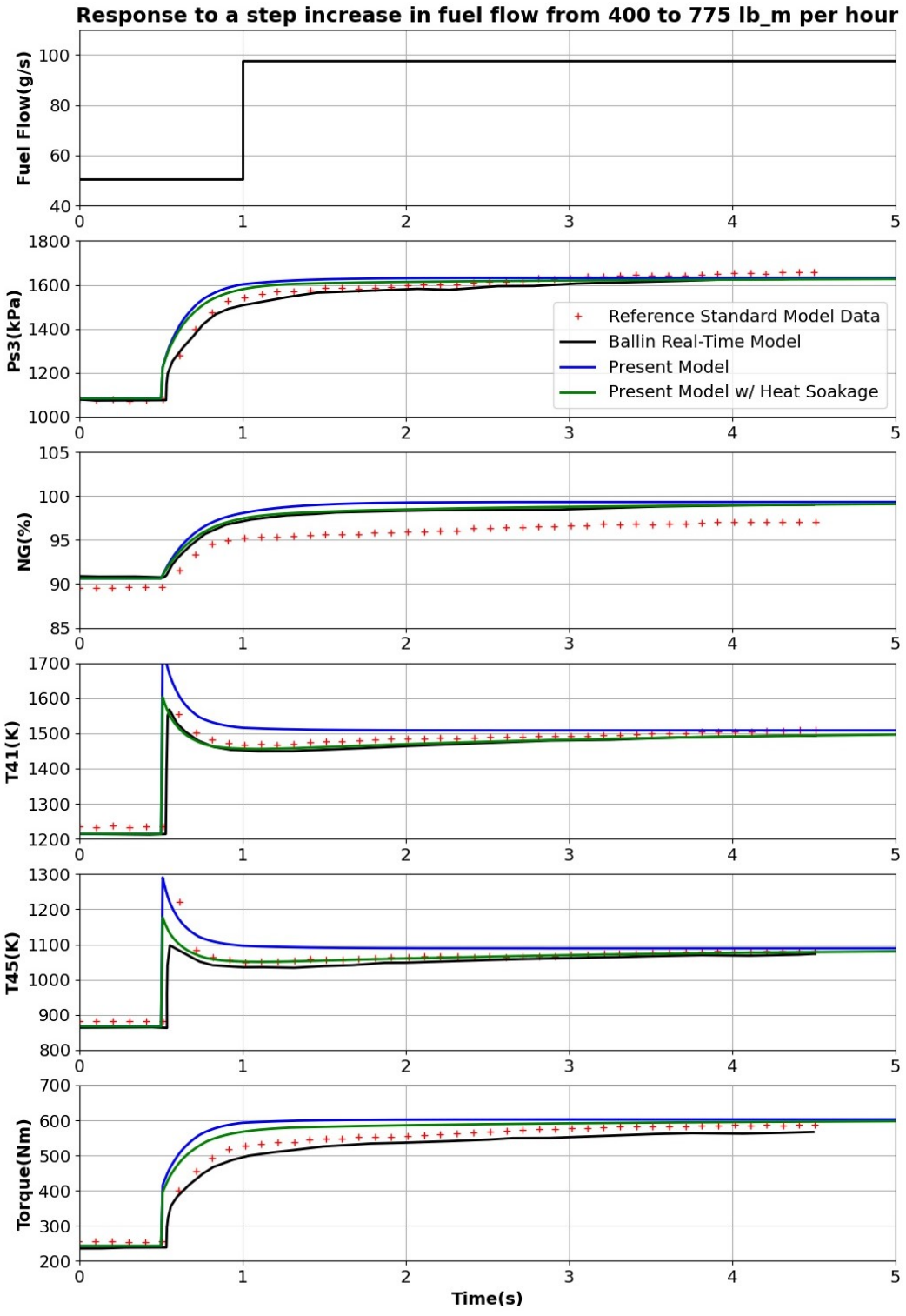

Figure 4.19 T700-GE-700 Response to a step increase in fuel flow from 400 to 775 pph @SLS ISA

As it is previously mentioned in Subsection 4.2.2., using standard GasTurb13 turbine maps causes this differentiation. Actual T700-GE-700 PT map would be more appropriate to obtain better torque results. It should also be noted, Ballin's real time model results are not in 100% consistency with Reference Standard Model Data in Torque graph.

4.4. Starting Simulation Results

During starting phase, PT speed is controlled by a controller. Thermal power generated by core engine (gas generator spool) and helicopter rotor load affects the PT speed during starting [31]. However, for T700-GE-700 engine the PT speed information during starting is missing. To be able to perform a calculation, PT spool speed is selected parallel to the NG speed. Additionally, Ref [31] shows a couple of PT loading alternatives during starting and its effect on gas generator spool acceleration is negligible.

Defined fuel schedule input is given with Figure 4.20.

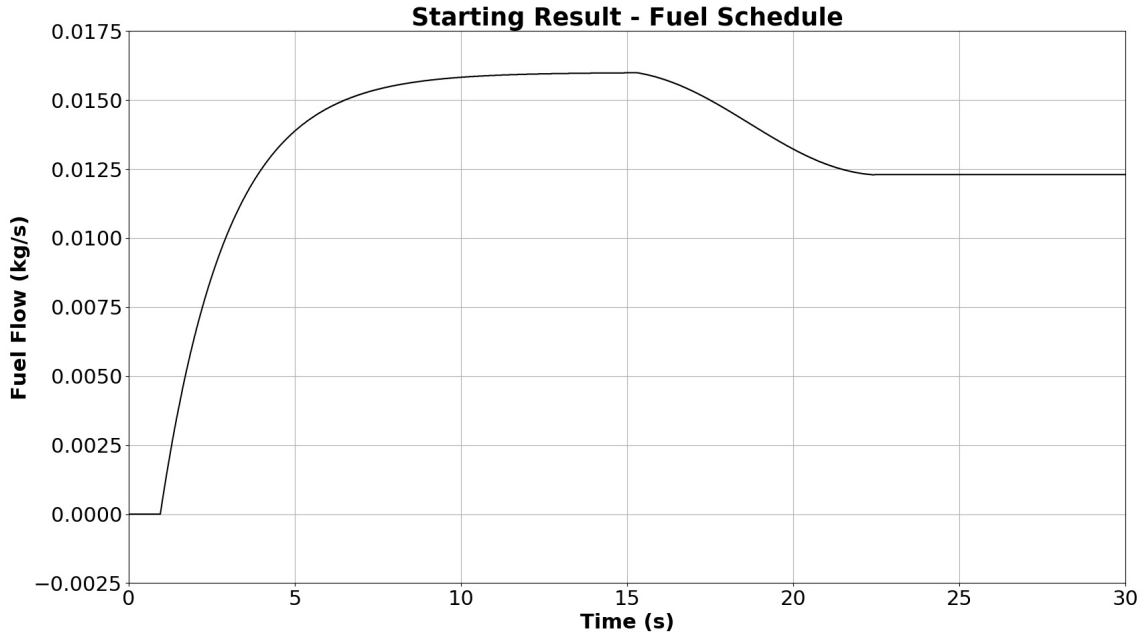

Figure 4.20 T700-GE-700 Starting Code Input, Fuel Schedule

At the beginning, around a second, there is no fuel flow input for cranking phase. Next, fuel flow started to be increased. For a faster acceleration to starter cutout and idle speeds, more fuel than required for idle speed is fed to the engine at the top level. After 15 seconds, it is reduced to the idle fuel level ($\approx 12.5g/s$) and kept constant. Outputs for given fuel schedule are presented with Figure 4.21 for Combustor Outlet Temperature T_4 and Figure 4.22 for HP Spool Speed.

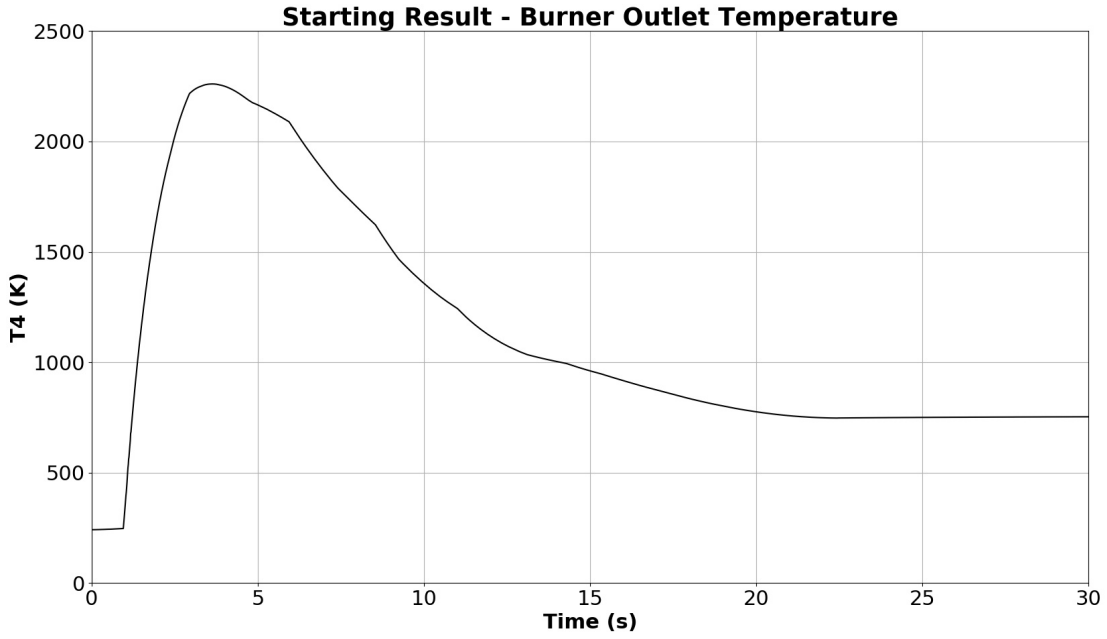

Figure 4.21 T700-GE-700 Starting Code Result, Combustor Outlet Temperature vs Time

Since component characteristics are not fine tuned for sub-idle region, obtained combustor outlet temperature behavior is not as smooth as it is for above-idle runs. Cranking phase can be noticed in all figures in the beginning. Higher fuel flow can start the engine and reach the starter cutout or idle speeds faster than obtained results. However, as Figure 4.21 shows, Combustor Outlet Temperature T_4 reached to $\approx 2250K$. Feeding more fuel will increase this value even more. That scenario may significantly lower the turbine blade life.

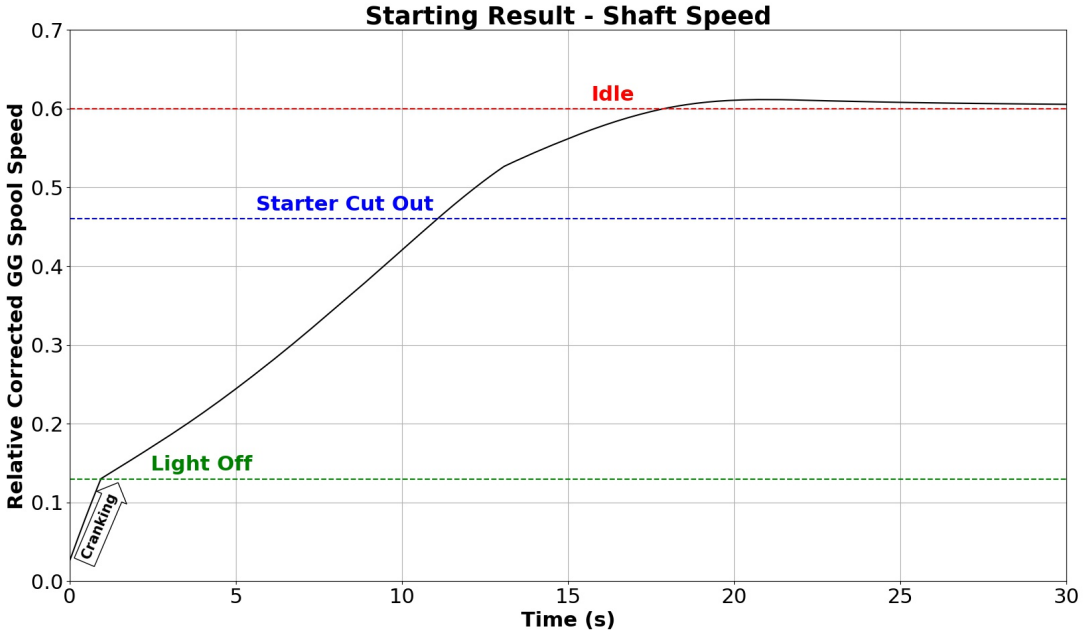

Figure 4.22 T700-GE-700 Starting Code Result, Relative HP Spool Speed vs Time

As Figure 4.22 shows 8.8 seconds starter cutout time and 16.2 seconds idle times could not be reached. Component characteristics' severe uncertainty in sub-idle region may result in failure to reach starter cutout idle times. Also, gear ratio between starter pad and HP spool and starting fuel schedule are estimated. Yet, the results are not significantly over the specified time values in Ref. [9]. Minor modifications can help to reach target times. Map extension and torque mode usage at least provides a starting model to observe engine performance trends and can be helpful for optimization studies. Fuel schedule can be optimized by having a performance model before the actual and expensive engine tests or effect of accessories can be observed with the model.

5. CONCLUSION

Sub-idle engine performance and especially starting/restarting capability are substantial certification subjects for gas turbine engines. Modeling capability provides a vast flexibility to predict the thermodynamic parameters before going into costly engine tests. By having this chance, starting sequence can be optimized and engine components can be preserved from excessive temperature, starting time can be shortened, altitude relight capability can be increased with minimizing the risk. Also, starter equipment characteristic can be evaluated, size can be determined and also the starter torque/power can be adjusted due to mechanical concerns. To that end, this thesis aims to develop a computer software in order to simulate starting phase of a gas turbine engine. A generic component-matching based gas turbine performance simulation tool is developed with element structure, in accordance with this purpose. One can create models for different gas turbine configurations with minor modifications to the code. Developed tool has the design mode, steady-state off design mode, transient acceleration/deceleration and starting simulation capabilities.

In order to validate the study, commercially available gas turbine performance simulation software GasTurb13 was taken as the reference. GasTurb13's 2 Spool Demo Turboshaft model was selected to be modeled and compared to. Component performance maps and other inputs were taken as they are from GasTurb13 model. Present model's results were compared to GasTurb13 results for design point, at first. Design mode study found to be successful due to prediction of all performance related parameters with a terrific accuracy. Next, steady-state off design point comparison was made at 85% relative spool speed. Similarly to the design mode, off design calculation showed great compatibility with commercially available software results. In addition to that single point, a whole operating line comparison was performed from a low speed to over 100% relative shaft speed. Performance wise critical parameters like fuel flow, combustor outlet temperature, compressor surge margin and some other were selected and compared. Present model results along the operating line are in exquisite consistency with GasTurb13 results. After completion of steady-state mode validation, a transient step fuel input was given to the both

software. Fuel delay simulation capability is also included in developed software. Engine response to an instant fuel flow change was observed with two software. Developed software predicted all performance parameters for each time step with a terrific accuracy. Unbalanced power, acceleration rate, shaft speed and internal station temperatures are monitored during the transient manoeuvre. Obtained results are completely in agreement. Validity of the developed software is completed for above-idle speeds.

For starting and sub-idle operation, GasTurb13 does not have a modeling capability. Literature found data is required to validate starting study. T700-GE-700 engine is selected to be modeled, since open literature provides a compressor performance map, steady-state and transient performance behavior and also a starting time information. Mark G. Ballin's work [7] is widely used during this study. By using the compressor map and other details provided in Ref. [7] and standard GasTurb13 turbine maps, a performance model was created for T700-GE-700 engine. To check the validity of the created model for above-idle speeds, Ballin's results were taken as reference. Ballin provided 3 different engine performance chart for steady-state operation. Same figures were obtained with created performance model. Slight discrepancies observed in lower speeds. Primary reason for that may be the standard GasTurb turbine maps, since in such lower speeds high pressure turbines do not operate under choked conditions and their performance characteristics matter. Apart from mentioned minor lower speed characteristic inconsistency, steady-state results are utterly in line with literature data. Afterward, a transient study was performed with created performance model. Since Ballin's study include heat soakage effect for transient simulation, that capability was also included in performance model. For a given step fuel increase, present model provided highly consistent results for compressor outlet pressure, shaft speed and especially for combustor outlet and power turbine inlet temperatures. Nonetheless, a minor discrepancy was observed for torque value. Again, using standard GasTurb power turbine map causes a minor incompatibility but the gap is in acceptable tolerances. These results concluded that the used component maps for T700-GE-700 model can be accepted as base maps and extended for sub-idle studies.

To create a physics related starting model, component characteristics should be obtained for

a component-matching based performance simulation tool. CFD solvers and test rigs do not provide reliable results due to complex component behavior in such lower speeds. In order to obtain component characteristics for such low speeds, a physics concerned map extension technique proposed by Kurkze [10] [32] was selected and available above-idle information for all components were used as basis. By conserving the $\frac{Trq}{\dot{W}}$ relation, component maps were extended until zero-speed line and a torque map was created in order to get rid of interpolation problems where the efficiency lines behave abnormally. Additionally, Ref. [9] provides starter equipment characteristics and corresponding acceleration times for T700-GE-700 engine. In order to perform a starting simulation, an arbitrary fuel schedule is determined. After obtaining all the necessary ingredients, a starting simulation was performed. Mentioned time values for reaching starter cutout and idle speed in Ref. [9] could not be reached exactly, but the results are pretty close.

In addition to using standard GasTurb turbine maps, map extension process brings extra uncertainties. Different engineers can obtain different results for sub-idle behavior by using the same method since the process is not framed by certain rules. Moreover, other components from compressor and turbines also behave differently in sub-idle region. Combustor efficiency, duct pressure losses and accessory power offtake can alter, as well. Having experimental data in this region can contribute to obtain a more representative performance model for starting and sub-idle region. Missing fuel schedule information is also vital. Having internal station temperature or pressure trends, secondary air system network behavior, combustor behavior for starting phase would be extremely beneficial.

All in all, this study shows developed component-matching based performance simulation tool can be used to simulate a gas turbine engine starting phase. Developed tool showed great consistency both with commercially available GasTurb13 software and literature data for T700-GE-700 engine. Having access to component behavior with locked-rotor (zero-speed) condition, starting fuel schedule and other engine characteristics can improve the quality of starting model.

REFERENCES

[1] Society of Automotive Engineers Inc. Aircraft propulsion system performance station designation, as755f, **2014**.

[2] Eshwarprasad Thirunavukarasu. *Modeling and simulation study of a dynamic gas turbine system in a virtual test bed environment*. Master's thesis, University of South Carolina, **2013**.

[3] Joachim Kurzke and Ian Halliwell. *Propulsion and power: an exploration of gas turbine performance modeling*. Springer, **2018**.

[4] Joachim Kurzke. Gasturb 13, user manual, **2018**.

[5] Hiroshi Uchida, Mutsuo Shiraki, Akinobu Bessho, and Yoichi Yagi. *Development of centrifugal compressor for 100 kW automotive ceramic gas turbine*, volume 78842. American Society of Mechanical Engineers, **1994**.

[6] Philip P Walsh and Paul Fletcher. *Gas turbine performance*. John Wiley & Sons, **2004**.

[7] Mark G Ballin. A high fidelity real-time simulation of a small turboshaft engine. Technical report, **1988**.

[8] Sergiy Yepifanov and Feliks Sirenko. Turbine engine starting simulation. In *Modeling of Turbomachines for Control and Diagnostic Applications*. IntechOpen, **2020**.

[9] JA Rhoden. Evaluation of a pressurized air start system for advanced army helicopters. Technical report, AIRESEARCH MFG CO OF ARIZONA PHOENIX, **1977**.

[10] J Kurzke. Generating compressor maps to simulate starting and windmilling. *ISABE 2019*, **2019**.

[11] Joachim Kurzke. How to get component maps for aircraft gas turbine performance calculations. In *Turbo Expo: Power for Land, Sea, and Air*, volume 78767, page V005T16A001. American Society of Mechanical Engineers, **1996**.

[12] Vivek Sanghi, BK Lakshmanan, and V Sundararajan. Survey of advancements in jet-engine thermodynamic simulation. *Journal of Propulsion and Power*, 16(5):797–807, **2000**.

[13] YG Li. Performance-analysis-based gas turbine diagnostics: A review. *Proceedings of the Institution of Mechanical Engineers, Part A: Journal of Power and Energy*, 216(5):363–377, **2002**.

[14] Janitha Kanishka Suraweera. *Off-design performance prediction of gas turbines without the use of compressor or turbine characteristics*. Master's thesis, Carleton University, **2012**.

[15] Herbert IH Saravanamuttoo, Gordon Frederick Crichton Rogers, and Henry Cohen. *Gas turbine theory*. Pearson Education, **2001**.

[16] Joachim Kurzke. Advanced user-friendly gas turbine performance calculations on a personal computer. In *Turbo Expo: Power for Land, Sea, and Air*, volume 78828, page V005T16A003. American Society of Mechanical Engineers, **1995**.

[17] GasTurb GmbH. Smoothc 9, user manual, **2021**.

[18] GasTurb GmbH. Smootht 9, user manual, **2021**.

[19] Russell Claus, AUSTIN EVANS, and GREGORY FOLLEN. Multidisciplinary propulsion simulation using npss. In *4th Symposium on Multidisciplinary Analysis and Optimization*, page 4709.

[20] John K. Lytle. The numerical propulsion system simulation: An overview. **2000**.

[21] Wilfried PJ Visser and Michael J Broomhead. Gsp a generic object-oriented gas turbine simulation environment. **2000**.

[22] Wilfired PJ Visser. *Generic Analysis Methods for Gas Turbine Engine Performance: The development of the gas turbine simulation program GSP*. Ph.D. thesis, **2015**.

[23] MA Chappell and PW McLaughlin. Approach of modeling continuous turbine engine operation from startup to shutdown. *Journal of Propulsion and Power*, 9(3):466–471, **1993**.

[24] RK Agrawal and M Yunis. A generalized mathematical model to estimate gas turbine starting characteristics. In *Turbo Expo: Power for Land, Sea, and Air*, volume 79610, page V001T01A011. American Society of Mechanical Engineers, **1981**.

[25] Wayne Randolph Sexton. *A method to control turbofan engine starting by varying compressor surge valve bleed*. Master's thesis, Virginia Tech, **2001**.

[26] Shaun R Gaudet and JE Donald Gauthier. A simple sub-idle component map extrapolation method. In *Turbo Expo: Power for Land, Sea, and Air*, volume 4790, pages 29–37. **2007**.

[27] Claus Riegler, Michael Bauer, and Joachim Kurzke. Some aspects of modeling compressor behavior in gas turbine performance calculations. *J. Turbomach.*, 123(2):372–378, **2001**.

[28] Pavlos K Zachos, Ioanna Aslanidou, Vassilios Pachidis, and Riti Singh. A sub-idle compressor characteristic generation method with enhanced physical background. *Journal of engineering for gas turbines and power*, 133(8), **2011**.

[29] Linyuan Jia and Yuchun Chen. Validation of a physically enhanced sub idle compressor map extrapolation method. In *16th International Symposium on Transport Phenomena and Dynamics of Rotating Machinery*. **2016**.

[30] J Honle, M Kerler, H Nachtingall, W Erhard, and H Kau. Experimental validation of a sub-idle compressor map extrapolation. *ISABE 2013*, **2013**.

[31] Catana Razvan Marius, Grigore Cican, and Gabriel Dediu. Gas turbine engine starting applicated on tv2-117 turboshaft. *Engineering, Technology Applied Science Research*, 7, **2017**. doi:10.48084/etasr.1315.

[32] Kurzke Joachim. Turbine map extension-theoretical considerations and practical advice. *Journal of the Global Power and Propulsion Society*, 4:176–189, **2020**.

[33] Ahmet Duyar, Zhen Gu, and Jonathan S Litt. A simplified dynamic model of the t700 turboshaft engine. *Journal of the American Helicopter Society*, 40(4):62–70, **1995**.

[34] OĞUZ UZOL. A new high-fidelity transient aerothermal model for real-time simulations of the t700 helicopter turboshaft engine. *Isı Bilimi ve Tekniği Dergisi*, 31(1):37–44, **2011**.

[35] Yunus A Cengel, Michael A Boles, and Mehmet Kanoğlu. *Thermodynamics: an engineering approach*, volume 5. McGraw-hill New York, **2011**.

[36] Joachim Kurzke. Correlations hidden in compressor maps. In *Turbo Expo: Power for Land, Sea, and Air*, volume 54617, pages 161–170. **2011**.

[37] Hamid Asgari, XiaoQi Chen, Raazesh Sainudiin, Mirko Morini, Michele Pinelli, Pier Ruggero Spina, and Mauro Venturini. Modeling and simulation of the start-up operation of a heavy-duty gas turbine by using narx models. In *Turbo Expo: Power for Land, Sea, and Air*, volume 45653, page V03AT21A003. American Society of Mechanical Engineers, **2014**.

[38] Joachim Kurzke. Compressor and turbine maps for gas turbine performance computer programs–issue 3. *GasTurb GmbH: Aachen, Germany*, **2013**.